Mitochondrial Redox Adaptations Enable Alternative Aspartate Synthesis in SDH-Deficient Cells

Madeleine Louisa Hart

A dissertation

submitted in partial fulfillment of the

requirement for the degree of

Doctor of Philosophy

University of Washington

2023

Reading Committee:

Lucas Sullivan, Chair

Yasemin Sancak

David Hockenbery

Program Authorized to Offer Degree:

Molecular Medicine & Mechanisms of Disease

University of Washington

Abstract

Mitochondrial Redox Adaptations Enable Alternative Aspartate Synthesis in SDH-Deficient Cells

Madeleine Louisa Hart

Chair of the Supervisory Committee:

Lucas B. Sullivan

Department of Biochemistry

The oxidative tricarboxylic acid (TCA) cycle is a central mitochondrial pathway integrating catabolic conversions of NAD+ to NADH and anabolic production of aspartate, a key amino acid for cell proliferation. Several TCA cycle components are implicated in tumorigenesis, including loss of function mutations in subunits of succinate dehydrogenase (SDH), also known as complex II of the electron transport chain (ETC). Mechanistic understanding of how proliferating cells tolerate the metabolic defects of SDH loss is still lacking. Here, we identify that SDH supports cell proliferation through aspartate synthesis but, unlike other ETC impairments, SDH inhibition is not ameliorated by electron acceptor supplementation. Interestingly, we find aspartate production and cell proliferation are restored to SDH-impaired cells by concomitant inhibition of ETC complex I. We determine that the benefits of complex I inhibition in this

context depend on decreasing mitochondrial NAD+/NADH, which drives SDH-independent aspartate production. We also find that genetic loss or restoration of SDH selects for cells with concordant complex I activity, establishing distinct modalities of mitochondrial metabolism for maintaining aspartate synthesis. Collectively, these data identify a metabolically beneficial mechanism for complex I loss in proliferating cells and reveal that compartmentalized redox changes can impact cellular fitness.

Table of Contents

List of Figures

List of Tables

Acknowledgements

I have so many people to thank for their constant support and love during this chapter of my life. First and foremost, I need to thank my advisor and fearless leader, Lucas Sullivan. Thank you for spending countless hours talking about metabolism and science and all of the guidance and support. I know it must have been a lot of work, and I truly appreciate everything you've done for me. Thank you for being one of the most genuine, caring, empathetic and supportive people I have ever met and immediately accepting me for who I am.

Thank you to the members of my supervisory committee consisting of Drs. Yasemin Sancak, David Hockenbery, Michael Metzger, and David Macpherson for providing constructive feedback on this project since its infancy. I would also like to thank my previous mentors including David Bernlohr, Amy Hauck, and Jon Gottesman at the University of Minnesota, who played an integral role in my success today. My biochemistry professor from Beloit College, Ted Gries, deserves enormous thanks. Your methods for teaching metabolism made it so fascinating and led to my passion for the field. You inspired me to want to be able to teach concepts in metabolism in a way that gets people excited. Next, I'd like to thank my mentors during my post-baccalaureate fellowship at the University of Washington. These include Michael Lagunoff and Daniel Holmes: both of you helped me prepare for graduate school and taught me so much, and your guidance will not be forgotten. During my time in the Lagunoff Lab, I also met my best friend and partner-in-crime, Hannah Lewis. You are such an important person in my life, and I don't think I could have gotten through grad school without you. Next, I'd like to thank my cohort mates, Nandita Kumar and Kurt Berckmueller. The M3D PhD program

has some of the best and weirdest people I've ever met and going through this chapter of lives together will always have a special place in my heart. There are so many wonderful people I have met during graduate school, and I want to thank all of them, including the past and present members of the Sullivan Lab who made it such a great place to work. A special shout out goes to Ian Engstrom and Anna-Lena Vigil who always kept the good vibes rolling and the lab running smoothly. I would also like to acknowledge my undergraduates Ayaha Itokawa and Abby Parrish. You both brought a renewed joy to the lab that I desperately needed after the pandemic. I know you'll both go on to do great things in science and medicine and I'm honored to have played a small role in your current and future accomplishments.

I'd also like to acknowledge Ben Wiggins and my STEP-UP cohort, a teaching program I participated in during my 5th year. Designing a 10-week course from scratch helped solidify everything I had learned about metabolism and frame it in new and interesting ways. That was instrumental when writing the introduction to this thesis, and I had a great time tying everything together.

In my life outside of science, I have many people to acknowledge as well. I'd like to thank everyone in the bluegrass community of Seattle for welcoming me with open arms and creating such an invigorating, tight-knit space for me to hang out in and get away from the scientists for a while. I'd especially like to thank my friends and bandmates, Todd Gray, Dave Kiyak, DJ Gibson, Ryan Jochim, and Shannon Murray, for providing space for my creative outlet. You will always be family to me.

Lastly, I'd like to thank my family: especially my parents Maria and Dave, my brother Noah, and my sister-in-law Kelsey for your never-ending love and support. Thank

you for listening to me rant about science even when you thought I was speaking a different language. I love you all so much! And of course, thank you to my cat, Winston, for being the most purrfect friend throughout grad school.

For my parents, Maria and David.

Chapter 1. Introduction

1.1 Cell Metabolism

Cellular metabolism encompasses the network of biochemical reactions critical to carry out the basic functions of life. On the organismal level, metabolism defines the unique ways that our cells consume, utilize, and generate fuel in the form of nutrients. Described as one of the criteria for living entities, the countess metabolic pathways across species can shift flux, change directions, and respond to stimuli. Metabolism is broadly defined as the conversion of nutrients into building block molecules that fuel catabolic (generating chemical energy) or anabolic (synthesizing biomolecules) processes. These catabolic and anabolic pathways are tightly coordinated through gene regulation systems and cell signaling pathways to specifically control cellular metabolism, which is dependent on cell identity. While many prokaryotes regulate their metabolism autonomously, multicellular organisms also rely on cell-cell communication to control energy processing for growth and development. Indeed, metabolic pathway activation and repression depend on a variety of factors including hormone action and signal transduction to support cell function and prevent needless expenditures. Metabolic demands of cells are contingent on cell specialization and nutritional state, and metabolic genes are dynamically regulated across cell types, which require collective cooperation to ensure organismal health. In conclusion, understanding the specific metabolic pathways in every cell type and how dysregulated metabolism affects cell behavior in disease states is critical to understand a variety of human health conditions.

1.2 Redox Metabolism

Biochemically speaking, cellular energy is stored in the molecular bonds between atoms in macronutrients such as carbohydrates, fats, and proteins. This energy is extracted through a series of tightly controlled electron transfer mechanisms know as redox (reduction/oxidation) reactions. Oxidation refers to a loss of electrons while reduction refers to a gain of electrons. Redox reactions are central to a variety of energy transfer mechanisms including the generation of heat and energy from natural gas or wood, charging of lithium batteries, photosynthesis, and much of the metabolic processes in our bodies.

Enzymes are the protein subset responsible for catalyzing the biochemical reactions that make up metabolism. While there are several classifications of metabolic enzymes, an important cluster is the oxidoreductase or redox enzyme family. This group of enzymes catalyzes the (often) reversible transfer of electrons between reactants and products. However, in physiological contexts, most redox enzymes thermodynamically favor one direction over the other, which can be influenced by the redox state of the cell. Electrons are transferred from the reduced molecule, or electron donor and are received by the oxidized molecule, or electron acceptor. Specific cofactors, often metallic ions or organic molecules are required for redox enzymes to function, and many cofactor molecules are derived from vitamins in our diet.

Under the umbrella of redox enzymes, the majority belong to the dehydrogenase family, which are classified by the oxidation of the substrate by means of reducing an electron acceptor or reducing the substrate by oxidizing an electron donor. These enzymes often require the specific cofactors nicotinamide adenine dinucleotide (NADH) or nicotinamide adenine dinucleotide phosphate (NADPH) to catalyze their reactions. NADH and NADPH are core components of metabolism that perform diverse functions made possible by their divergent roles in catabolism and anabolism. Many mammalian enzymes exclusively use either NADH or NADPH, even though NADP(H) only differs from NAD(H) by a single phosphate group on the 2′ position of the adenosine ribose (Cracan et al., 2017). Typically, the reduced form of NADPH is maintained in cells to drive anabolism, while NADH pools are sustained mostly in the oxidized state (NAD+) to catalyze catabolic reactions. The preference of NADPH in biosynthetic processes and NADH in energy-producing processes is a key strategy of cellular metabolism that enables concurrent yet thermodynamically incompatible reactions to occur (Cracan et al., 2017). While adenosine triphosphate (ATP) is classically known as the cellular currency, NADP(H) is referred to as the 'second' currency due to its important role in anabolism.

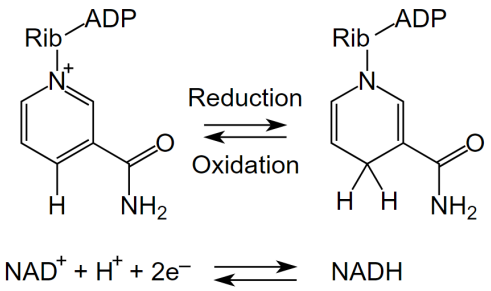

Figure 1.1. Reduction and oxidation of NAD+ and NADH.

Additionally, redundancy in metabolic enzymes that preferentially use NAD(H) or NADP(H), often in different cellular compartments, is an important design that allows us to be metabolically flexible and adapt to various nutritional states. For example, there are three isoforms of malic enzyme encoded by different genes, all of which interconvert

malate and pyruvate: ME1, in the cytosol which uses NADP(H); ME2, in the mitochondria which uses NAD(H); and ME3, also in the mitochondria but uses NADP(H). There are several other redundant enzyme networks throughout cellular compartments that all play critical roles in biomass synthesis and antioxidant defense systems (Ciccarese & Ciminale, 2017).

1.3 Mitochondria and Metabolism

1.3.1 Origin of Mitochondria

Found in most eukaryotic cells, mitochondria are double membrane-bound organelles that contain their own circular DNA (resembling bacteria), which has led to the general acceptance of endosymbiotic theory to explain their origin. Endosymbiosis, first postulated by Dr. Lynn Margulis, dictates that mitochondria spurred from an evolutionary symbiotic merger event between ancient archaea and chemiosmotic bacteria about two billion years ago following the Great Oxidation Event (GOE) (Gray, 2017; Sagan, 1967; Zimorski et al., 2019). The GOE, or the surplus of molecular oxygen on Earth was theorized to have caused the first mass extinction from an overpopulation of photosynthesizing cyanobacteria (Zimorski et al., 2019). The accumulation of oxygen and therefore displacement of the greenhouse gases methane and carbon dioxide was toxic to Earth and caused global glaciation since a primary role of greenhouse gases is to trap heat from sunlight to warm the planet. This near extinction of anerobic life is theorized to be a catalyst for endosymbiosis and the development of oxygen utilization as an energy source to sustain life. Then, natural selection favored cells that established this symbiotic

relationship, and these ancient eukaryotes continued evolving for the next billion years into “modern” mitochondria, cultivating the diverse set of species that we appreciate today.

1.3.2 Mitochondrial Structure

Organized by several layers, mitochondria fulfill a variety of specialized functions including cell signaling, differentiation, programmed cell death, cell cycle maintenance, and cell growth (Murphy et al., 2016; Osellame et al., 2012; Sherratt, 1991). The outer mitochondrial membrane (OMM) is porous, allowing molecules to flow from the cytosol into the intermembrane space (IMS) or vice versa, while the inner mitochondrial membrane is tightly controlled and is impermeable even to protons (H^+). Any molecule that needs to pass through the IMM requires specific transport proteins. The IMM folds to form cristae that allow for greater surface area within the OMM, efficiently maximizing space for energy production. The inner compartment of the mitochondrion is called the matrix, conventionally a viscous, oxidizing environment to catabolize and extract energy from glucose, amino acids, and fatty acids. The mitochondrial matrix also houses mitochondrial DNA (mtDNA), a small circular ~16.5kb genome separate from the nuclear genome in mammals. Indeed, mtDNA is conserved across eukaryotic organisms due to their important role in mitochondrial metabolism; however, the mitochondrial genome is more prone to replication error due to less efficient DNA repair mechanisms compared to that of nuclear DNA (Arnold et al., 2022). mtDNA only encodes 37 genes, including 22 transfer RNAs, two ribosomal RNAs, and 13 protein subunits, all of which are involved in oxidative phosphorylation (OXPHOS) (Dimauro & Davidzon, 2005).

1.3.3 Oxidative Phosphorylation

OXPHOS is a central, multi-compartmental amphibolic process, meaning it encompasses both anabolic and catabolic pathways. It is primarily associated with metabolism of carbohydrates, which are broken down to form the simple sugar glucose during digestion. From the small intestine, glucose travels through the blood, resulting in insulin secretion from the pancreas, which signals cells to take up glucose throughout the body (Cori, 1931). Once glucose has been transported into the cytoplasm, it undergoes a 10-step process called glycolysis, resulting in two molecules of adenosine triphosphate (ATP) and two pyruvate molecules, which are transported into the mitochondrial matrix and converted to acetyl Co-A before continuing through the tricarboxylic acid (TCA) cycle.

The TCA cycle begins by condensing oxaloacetate (OAA) and acetyl Co-A to create citrate via the enzyme citrate synthase (CS). Next, aconitase (ACO) converts citrate to isocitrate, which is a reversible isomerization process that occurs in both the cytosol (ACO1) and the mitochondria (ACO2). Isocitrate then undergoes two dehydrogenase reactions: the conversion to a-ketoglutarate (AKG) by isocitrate dehydrogenase (IDH) and then by a-ketoglutarate dehydrogenase (a-KGDH) which yields succinyl Co-A. Both of these reactions are redox linked, but IDH encompasses three isoforms; IDH1, which is cytosolic and uses NADP+; IDH2, which is mitochondrial and uses NADP+; and IDH3, which is mitochondrial and uses NAD+. a-KGDH is a large enzyme complex only expressed in the mitochondria and utilizes NAD+. Next, succinyl Co-A synthetase, housed in the mitochondria, generates succinate from succinyl Co-A, generating either guanosine triphosphate (GTP) or ATP. The conversion of succinate to

fumarate by succinate dehydrogenase (SDH) is next, which will be discussed thoroughly in subsequent sections of this manuscript. After the SDH step is fumarate hydratase (FH) which converts fumarate to malate, releasing an H_2O molecule in the process. Closing out the TCA cycle, is malate dehydrogenase (MDH) which uses NAD+ to catalyze the reaction of malate to OAA. This enzyme contains two isoforms with MDH1 in the cytosol and MDH2 localized to the mitochondria. This broadly conserved metabolic cycle generates NADH molecules in the mitochondria but does not consume oxygen; instead, the TCA cycle is linked to oxygen consumption through the electron transport chain (ETC) (Arnold & Finley, 2022). The TCA cycle, amphibolic in nature, is often described through a catabolic lens as described above, but it also supplies several universal metabolites (acetyl Co-A, aKG, succinate, and OAA) for macromolecule synthesis, which include glucose, lipids, nucleic acids, proteins, and cofactors (Arnold & Finley, 2022).

This metabolic sequence of energy transfer via redox reactions coupled to chemiosmosis for ATP production, or the ETC, is comprised of four protein complexes embedded in the IMM. Complex I, or 'NADH: ubiquinone oxidoreductase,' the largest transmembrane protein complex of the ETC, is encoded by 46 genes from both the nuclear and mitochondrial genomes. Complex I plays a critical role in the redox ecosystem of the mitochondrial matrix because it consumes NADH generated by the TCA cycle to pass electrons down the ETC, in turn yielding NAD+, which keeps the TCA cycle flowing.

The holoenzyme complex II, or 'succinate dehydrogenase,' is tightly bound to the cofactor flavin adenine dinucleotide (FAD), which accepts electrons transferred from succinate in the TCA cycle. Both complex I and II independently transfer electrons from

their substrates to ubiquinone (Coenzyme Q), meaning that complexes I and II do not rely on one another for electron transfer.

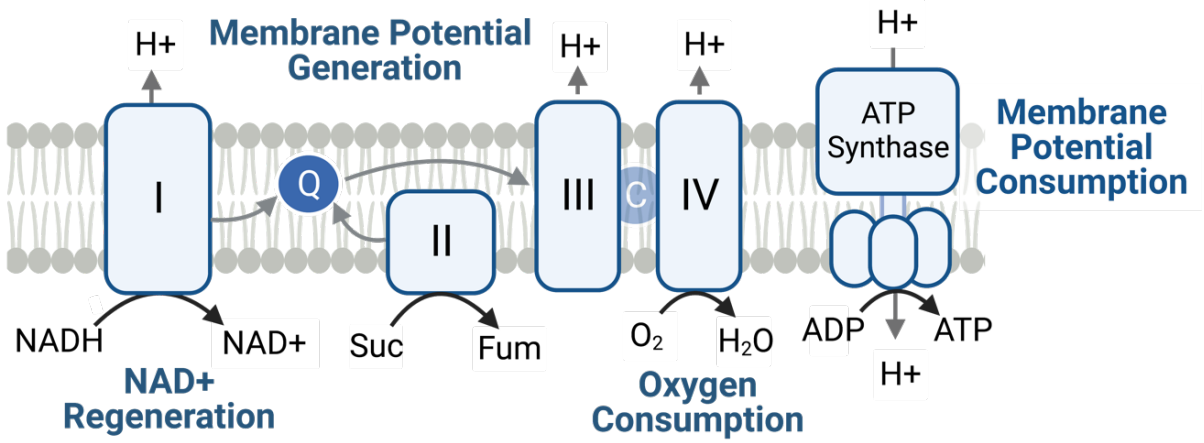

Figure 1.2. The electron transport chain and associated functions. Complexes I and II independently pass electrons from NADH and succinate, respectively, to Coenzyme Q, which then shuttles them to complexes III and IV, where molecular oxygen is the terminal electron acceptor. Complex I regenerates NAD+ and complex II converts succinate to fumarate, and both of these processes drive TCA cycling. Additionally, complexes I, III, and IV pump protons across the inner mitochondrial membrane (IMM) which generate a membrane potential, powering ATP synthase by proton-motive force.

Once electrons reduce the pool of ubiquinone to ubiquinol, these electrons flow through the transmembrane complexes III and IV, also known as 'ubiquinol: cytochrome c oxidoreductase 'and 'cytochrome c oxidase,' respectively. Complex IV catalyzes the ultimate redox reaction where protons and the transferred electrons are terminally consumed by molecular oxygen (O_2) to generate water (H_2O) in the mitochondrial matrix. In addition, complexes I, III, and IV pump protons across the IMM to generate an electrochemical gradient which then powers F_1F_0 adenosine triphosphate synthase (ATP synthase). This complex synthesizes about 36 molecules of ATP, the main molecular form of cellular energy, per glucose molecule, whereas glycolysis only synthesizes two ATP molecules per glucose molecule. ATP hydrolysis is thermodynamically favorable ($-\Delta G$) which is often coupled to unfavorable reactions ($+\Delta G$) to promote anabolism.

Therefore, ATP is described as cellular currency since cells often must “spend” ATP to synthesize biomolecules. Because of this, the mitochondria, which houses ATP synthase, is known as the ‘powerhouse’ of the cell, but it requires O_2 to function. In hypoxic conditions, where oxygen is low, this ‘powerhouse’ shuts down, and cells rely on glycolysis for their energetic requirements. For this reason, anaerobic glycolysis functions as a ‘backup generator’ for the cell, because it is a fast yet inefficient way to synthesize ATP. In summary, OXPHOS, or the entire process of glucose oxidation to generate ATP, is also commonly called cellular respiration and is summarized by this combustion equation ($C_6H_{12}O_6 + 6O_2 \rightarrow 6CO_2 + 6H_2O$).

1.4 Altered Glucose Metabolism in Cancer Cells

Cancer is a disease characterized by uncontrolled cell proliferation. Rising incidences of cancer in the early 20th century sparked monumental scientific progress in the field of biology. At that time, one prominent German scientist named Otto Warburg was studying cellular respiration during the development of sea urchin eggs. Warburg observed that sea urchin eggs consumed more oxygen upon fertilization, which made sense at the time because more oxygen meant more energy for the cells to grow, divide, and develop (Warburg, 1925). Eager for scientific fame, Warburg turned to studying respiration in tumor cells to understand how the disease manifests. He anticipated the same phenomenon for cancer cells, which are constantly dividing. However, Warburg measured no substantial changes in the oxygen consumption of cancer cells when compared to healthy cells of the same tissue (Weinhouse, 1956). Instead, he made a

monumental observation that tumor cells uptake much larger quantities of glucose compared to normal cells. The tumor cells then burn though that extra glucose through glycolysis to generate pyruvate, but shockingly, the cells then convert the pyruvate to lactate via lactate dehydrogenase (LDH), which was then excreted from the cells (Hardie, 2022). This pathway known as fermentation or anerobic glycolysis, was associated with hypoxia, only to be used as the backup generator for the cell when O_2 was sparse. Warburg (incorrectly) hypothesized that the reason why tumor cells were undergoing fermentation, was because they c*ouldn't* respire, and therefore concluded that damaged cellular respiration caused cancer (Weinhouse, 1956). Despite Warburg's prolific scientific career, where he made many seminal contributions in metabolism such as discovering complex IV, elucidating that cofactors are required for respiratory enzymes, and determining that NADH is a cofactor for complex I, he was overconfidently mistaken about how cancer forms (Hardie, 2022; Krebs, 1972; Warburg, 1925, 1928).

Warburg's conclusion on the origin of cancer has now been proven wrong, as he never actually showed a decrease in O_2 consumption; nonetheless, his initial observation remains a salient feature of cancer cell metabolism (Liberti & Locasale, 2016; Potter et al., 2016). There are many hypotheses describing how and why the now called 'Warburg Effect' is a hallmark of nearly every cancer cell (Hanahan & Weinberg, 2011). For example, similar to the redox link between the TCA cycle and the ETC, fermentation regenerates cytosolic NAD+, which is consumed during the glyceraldehyde-3-phosphate dehydrogenase (GADPH) step of glycolysis. Therefore, driving pyruvate towards lactate in turn supplies the power to drive glycolysis, synthesizing plenty of ATP for the cancer cell, as long as ample glucose is available (Liberti & Locasale, 2016; Luengo et al., 2021).

Moreover, cellular signaling cascades triggered by both oncogene activation and tumor suppressor gene inactivation act on metabolic targets, increasing expression of glucose transporters, glycolytic enzymes, and LDH. These discoveries in part explain the constitutive requirement for aerobic glycolysis in cancer cells (Dang, 2007).

Great scientific exploits are often followed by long valleys of silence, and the field of cancer metabolism is now recirculating many old ideas. Today in 2023, exactly 100 years after Otto Warburg published his paper on aerobic glycolysis of tumor cells, the field of cancer metabolism is flourishing due to a series of discoveries around the turn of the century highlighting the roles that mitochondria play in dysregulated cancer metabolism (Vander Heiden & DeBerardinis, 2017). With more robust methods to measure oxygen consumption, the development of tissue culture practices, and the discoveries of dysregulated amino acid metabolism in cancer, researchers determined that most cancer cells consume oxygen readily and have active mitochondrial metabolism. Now, the mitochondria are appreciated beyond their role in cellular respiration and ATP production. In noncancerous cells, mitochondria, in addition to their ’powerhouse’ responsibility, are sites of amino acid and lipid synthesis; ketogenesis; redox exchange, calcium, antioxidant, and reactive oxygen species (ROS) signaling; heme and porphyrin synthesis; and many more (Murphy et al., 2016; Osellame et al., 2012). Therefore, the role of the mitochondria in rapidly proliferating cells shifts to that a biosynthetic hub, rather than a ‘powerhouse’ (Ahn & Metallo, 2015).

1.5 Altered Amino Acid Metabolism in Cancer Cells

While the Warburg Effect is the most famous example of altered cell metabolism in cancer, glucose is not the only nutrient that proliferating cells depend upon. Harry Eagle identified that HeLa (ovarian cancer) cells also require high concentrations of glutamine in the media compared to other amino acids (Eagle, 1955). Additionally, research in the past two decades has identified many more dysregulated metabolic pathways in cancer cells. The anabolic demands of proliferating cells are high in addition to their catabolic demands, which are largely met by aerobic glycolysis (Pavlova et al., 2022). For every division, a cell must completely replicate their genome and biomass (nucleotides, proteins, lipids, etc.). Amino acids are the building blocks of protein, and many are precursors for other amino acids and nucleotides, which are essential for all DNA and RNA macromolecule synthesis. Amino acids are classified as essential or non-essential: eukaryotic cells cannot synthesize essential amino acids (EAA) and are therefore dependent on consuming these molecules from diet. Cells can synthesize non-essential amino acids (NEAA) through various pathways in the cytoplasm or mitochondria.

Essential Amino Acids (EAAs)	Non-essential Amino Acids (NEAAs)
Arginine	**Alanine**
Isoleucine	**Arginine**
Leucine	**Aspartate**
Lysine	**Asparagine**
Histidine	Cysteine
Methionine	**Glutamine**
Phenylalanine	**Glutamate**
Threonine	**Glycine**
Tryptophan	Proline
Valine	**Serine**
	Tyrosine

Table 1. Table of amino acids humans must acquire from diet (essential) and amino acids that human cells are capable of synthesizing (non-essential). Bolded amino acids are discussed in this manuscript.

The importance of amino acid metabolism in cancer followed the discoveries that highlighted the connection between genetics and metabolic changes. In fact, the

oncogenic transcription factor *c-MYC*, a master regulator of cell growth and metabolism, is often overexpressed in cancer cells (Yancopoulos et al., 1985). In the late 1990s, researchers found that dramatic increases in c-*MYC* lead to activation of target genes involving glycolysis, mitochondrial biogenesis, and glutaminolysis (Shim et al., 1997; Stine et al., 2015). Since most glucose is converted to lactate in cancer cells, glutamine fulfilled the TCA cycle requirements for cellular anabolism. Glutaminolysis is the breakdown of glutamine for energy, highlighting how protein metabolism can overlap with carbohydrate metabolism when needed. Glutamine is hydrolyzed to glutamate through glutaminase (GLS), a process that generates ATP in the process. Glutamate is then canonically transaminated to AKG by glutamate dehydrogenase (GDH) which uses NAD+, and feeds into the TCA cycle, a process known as anaplerosis. Essentially all cancer cells are glutamine auxotrophs in culture, meaning they require this specific nutrient that noncancerous cells are not reliant on (Wise et al., 2008). Indeed, glutamine concentration in the serum is the highest of all amino acids and is readily taken up by cancer cells (Hensley et al., 2013). Therefore, while glucose is important for energy production in the cytosol, cancer genetics has shown that mitochondrial metabolism is also crucial for cancer cells (Ahn & Metallo, 2015; Stine et al., 2015).

Although cancer cells require glutamine for catabolic and anaplerotic purposes, recent studies have shown that many amino acids themselves are limiting for cancer cell proliferation. Studies have shown that macropinocytosis of protein, or the endocytic process by which extracellular content is delivered to the cell for nutrient recycling, is a feature of Ras-transformed cells and hypoxic pancreatic cancer cells (Commisso et al., 2013; Garcia-Bermudez et al., 2022; Recouvreux & Commisso, 2017). Protein

macropinocytosis, which was shown to be driven by oncogenic transformation, provides additional amino acids for rapidly dividing cells, even when cells can synthesize their own.

For example, *de novo* serine synthesis branches off from the glycolytic intermediate 3-phosphoglycerate, highlighting how many metabolic pathways are complex webs rather than direct pathways. The enzyme phosphoglycerate dehydrogenase (PHGDH) which begins serine synthesis is often amplified in tumors, and has been shown to contribute to oncogenesis (Locasale et al., 2011; Yang & Vousden, 2016). A downstream step of PHGDH is serine hydroxymethyltransferase (SHMT) which reversibly catalyzes serine to glycine, highlighting another important anabolic role for aerobic glycolysis (Diehl et al., 2019). Serine and glycine both are important precursors for purine and thymidine synthesis, which are important for cancer cell proliferation (McBride et al. 2023; Sullivan et al., 2019). Interestingly, although certain cancers increase the biosynthetic demand for serine and glycine biosynthesis, many require exogenous serine for optimal proliferation (Maddocks et al., 2017). Cancer cells in culture respond to serine starvation by upregulating genes for glucose-derived serine biosynthesis by activating transcription factor 4 (*ATF4*) which senses withdrawal of several amino acids. Conversely, in mouse models of cancer*, de novo* serine and glycine synthesis are not increased upon the removal of dietary serine/glycine. In fact, studies have shown that serine/glycine-free diet reduce tumor growth in mouse xenografts and increase survival in relevant autochthonous tumors of *Apc*-mutant intestinal cancers and *Myc*-activated lymphoma mouse models (Maddocks et al., 2017).

Asparagine and arginine are also non-essential amino acid whose biosynthesis branches off from the TCA cycle and the urea cycle, respectively. Most human cells

express asparagine synthetase (ASNS) which uses ATP and glutamine to convert aspartate to asparagine but lack asparaginase activity that catalyzes the reverse reaction. Even though most cancer cells are still capable of *de novo* asparagine synthesis, it is often still a limiting amino acid for proliferation (J. Jiang et al., 2021). Moreover, heterologous L-asparaginase treatment, which depletes circulating asparagine, is the standard of care for children with acute lymphoblastic leukemia (ALL) since lymphocytes do not express ASNS (Egler et al., 2016). However, recent research suggests that asparagine limitation from L-asparaginase treatment results in ATF4-dependent activation of ASNS to compensate, which could lead to therapeutic resistance (Krall et al., 2021). Additionally, ETC complex I inhibition can synergize with asparagine limitation to further reduce tumor growth in xenografts and mouse models of cancer (Krall et al., 2021).

Many cancers also are not able to synthesize sufficient arginine for the demands of cell proliferation and are thus reliant on exogenous sources. Asparagine and arginine are both membrane-permeable amino acids, which allows cells to uptake them from the environment. Both asparagine and arginine are synthesized downstream of yet another non-essential amino acid: aspartate. However, synthesis of both these amino acids are costly, requiring intracellular aspartate and ATP. In fact, aspartate limitation resulting from arginine synthesis slows nucleotide synthesis and therefore cell proliferation and tumor growth (Rabinovich et al., 2015) Therefore, genes in the aspartate to arginine synthesis pathway including arginosuccinate synthase 1 (ASS1) are tumor suppressive and often silenced in cancers, but cancer cells in culture are capable of reactivating ASS1 when environmental arginine becomes limiting (Lee 2018, (Apiz Saab et al., 2023).

Interestingly, in pancreatic ductal adenocarcinoma (PDAC) cells, arginine biosynthesis is activated as a metabolic adaptation to survive in the tumor microenvironment (TME) (Apiz Saab et al., 2023). Together, these results suggest that metabolic demands for various amino acids are largely context dependent across cancer subtypes and fluctuate depending on the environmental conditions of the cells (Muir et al., 2017).

1.6 Respiration Supports Aspartate Synthesis in Proliferating Cells

Aspartate exists at the nexus of proliferative cell metabolism and is of particular interest to the Sullivan Lab. Aspartate is synthesized through the TCA cycle intermediate oxaloacetate (OAA) which can be directly transaminated by glutamic-oxaloacetic transaminase (GOT). This terminal aspartate synthesis reaction can occur in the cytoplasm or the mitochondria by GOT1 or GOT2, respectively. Aspartate can also be salvaged from the cellular environment; however, its molecular properties make it impermeable to the plasma membrane. Specialized cells such as glial cells express aspartate/glutamate transporters including SLC1A3, but most cancer cells lack these transporters, rendering cancer cells dependent on *de novo* aspartate biosynthesis. interestingly, guinea pigs possess asparaginase activity which allows cells to convert environmental cell-permeable asparagine to aspartate. When guinea pig asparaginase (gpASNase1) was expressed in human cancer cells, asparagine-derived aspartate pools and proliferation rates were restored when *de novo* aspartate synthesis was blocked (L. B. Sullivan et al., 2018). Importantly, gpASNase1 expressing tumor xenografts grew much faster than their WT counterparts and were resistant to ETC complex I inhibition, which

normally suppressed tumor growth (L. B. Sullivan et al., 2018). Aspartate is upstream of several metabolic fates including protein synthesis, purine and pyrimidine nucleotide synthesis, and asparagine and arginine synthesis as previously mentioned. Altogether, this information corroborates the notion that aspartate is a salient and endogenous limiting amino acid for cell proliferation and tumor growth (Garcia-Bermudez et al., 2018; Gui et al., 2016; L. B. Sullivan et al., 2018).

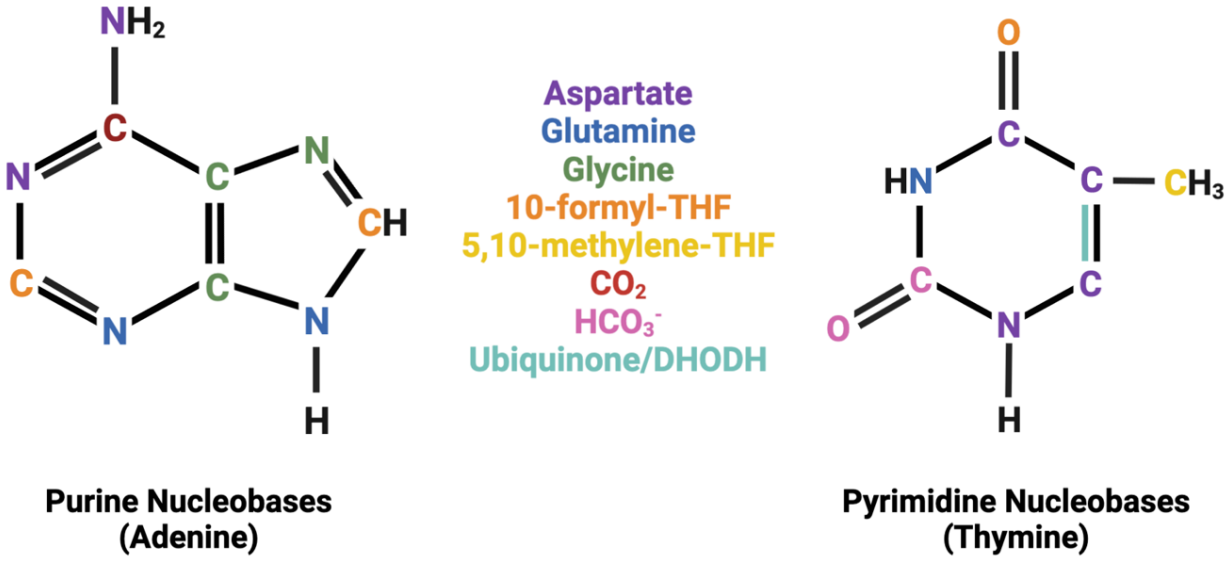

Figure 1.3. Aspartate donates carbons and nitrogen to purine and pyrimidines. Aspartate incorporation into the purine and pyrimidine nucleobases adenine and thymidine. Adapted from Ahn and Metallo, 2015.

In cancer cells, even though ATP demands were quickly met by the Warburg Effect, impairments to cellular respiration still had severe impacts on cancer cells and tumor growth. Indeed, cancer cells lacking mtDNA (and therefore functional ETC) cannot proliferate unless the culture media is supplemented with pyruvate and uridine (King & Attardi, 1989). However, the mechanisms by which exogenous pyruvate and uridine enabled proliferation were unknown. Dihydroorotate dehydrogenase (DHODH) is linked to complex III and is involved in the uridine biosynthesis pathway, which directly leads to

pyrimidines and therefore nucleotides. Therefore, uridine supplementation could maintain genome replication in respiration-deficient cells, but the role of pyruvate was still a mystery. As pyruvate is the product of glycolysis, it seems strange that cells undergoing aerobic glycolysis would require exogenous pyruvate even when respiration is impaired. In fact, pyruvate is an electron acceptor that regenerates NAD+ in the lactate dehydrogenase (LDH) reaction. Since pyruvate also has other metabolic fates, Sullivan and colleagues replaced pyruvate with a similar molecule, alpha-ketobutyrate (AKB), another electron acceptor capable of regenerating NAD+. Respiration-deficient cells have no complex I function, meaning that the NAD+/NADH ratio decreases, which in turn curbs TCA cycling. Exogenous electron acceptors like pyruvate and AKB supply the cell with more NAD+, restoring the NAD+/NADH ratio, and enabling TCA activity.

Aspartate, a product of the TCA cycle, was also depleted in respiration-deficient cells and robustly restored when pyruvate or AKB was supplemented in the media (L. B. Sullivan et al., 2015). Thus, aspartate depletion likely impairs core metabolic processes necessary for cell proliferation. Indeed, providing cells with exogenous sources of aspartate circumvents the proliferative defects of impairments to complexes I, III, and IV. Importantly, aspartate rescue does not correct the NAD+/NADH imbalance caused by mitochondrial inhibitors, indicating that ETC impairments block cell proliferation primarily by suppressing aspartate synthesis (Birsoy et al., 2015; Sullivan et al., 2015). Nonetheless, it remains unclear how alterations to other components of mitochondrial metabolism affect redox homeostasis and aspartate production, as well as how cells with mitochondrial dysfunction may adapt to the disruption of canonical aspartate production pathways.

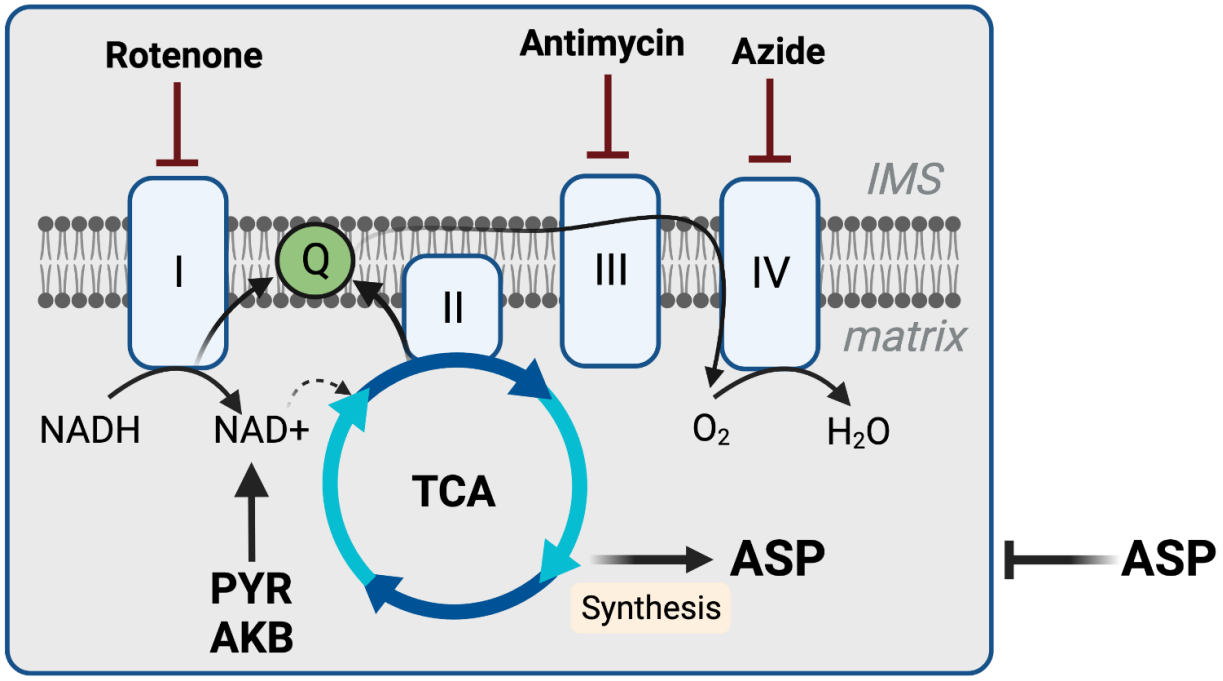

Figure 1.4. An essential function of the ETC is to enable aspartate synthesis. Nutrients in cell culture media and human serum including glucose and glutamine are metabolized through the electron transport chain (ETC). Molecular oxygen is the terminal electron acceptor in a functional ETC which is critical for aspartate production. If ETC complexes I, III, or IV are compromised, exogenous electron acceptors including pyruvate (PYR) and alpha-ketobutyrate (AKB) can fulfill the role of the ETC, enabling aspartate synthesis via its canonical route of the TCA cycle, therefore supporting proliferation.

1.7 Metabolism of Respiration-Deficient Cancers

If Otto Warburg had lived into the 21st century, he would have been thrilled to find that there are indeed cancers that display a complete loss of respiration. These cancers are exceptions to the norm, and are largely driven by mutations in complex I, or mutations in oxygen sensing machinery (e.g. VHL) that result in downregulation of complex I. Interestingly, the phenomenon of complex I loss is observed most often in kidney neoplasias, including fumarate hydratase (FH) mutant type 2 papillary renal cell carcinomas (pRCC), renal oncocytomas driven by mitochondrial DNA mutations, and VHL-mutant clear cell renal cell carcinomas (ccRCC), which are characterized by

suppression of oxidative mitochondrial metabolism (Courtney et al., 2018; Crooks et al., 2021; Mayr et al., 2008; Simonnet et al., 2003; Tomlinson et al., 2002). The fact the kidney cancers appear to be the dominant organ in which respiration-deficient cancer rise probes an interesting tissue-specificity question. However, about 60% of Hürthle cell thyroid carcinomas (HTC) are also driven by mtDNA mutations in complex I, highlighting that this feature is not completely unique to the kidney (Kumari et al., 2020).

How complex I loss drives tumor formation remains elusive in the field. If complex I is dysfunctional, then mitochondrial NADH turnover is also impaired, leading to a lower NAD+/NADH ratio. The oxidative TCA cycle, which is powered by NAD+, also shuts down, which would impair the canonical aspartate synthesis route. Indeed, in cultured cancer cells, complex I inhibition results in aspartate depletion and completely impairs cell proliferation. However, cancer cells arising from complex I loss and cancer cells cultured in hypoxic conditions still proliferate despite the lack of glucose-derived TCA metabolites (Metallo et al., 2011; Wise et al., 2011).

An increase in mitochondrial NADH caused by complex I impairment can drive reductive carboxylation of glutamine-derived AKG (RCQ), or a backwards NADPH-powered TCA cycle through IDH1 and IDH2 in order to replenish TCA metabolites and synthesize aspartate (Birsoy et al., 2015; Mullen et al., 2012). Interestingly, IDH3 does not contribute to RCQ, likely because its affinity for NAD(H) maintains its preference for the catabolic direction (Mullen et al., 2012). RCQ requires glutaminolysis and subsequent steps to transaminate glutamate to AKG. Previously discussed was GDH, which utilizes NAD+ as a cofactor to convert glutamate to AKG, releasing free ammonia (NH4+) in the process. However, high NADH from complex I impairments would make this reaction

unfavorable in the mitochondrial compartment. One option is that cytosolic AKG is synthesized from GDH1, and NADPH powers IDH1 in the reverse direction, and ACO1 synthesizes citrate. Then, this glutamine-derived citrate is cleaved by ATP citrate lyase (ACLY) to generate acetyl Co-A and OAA in the cytoplasm. Conversely, citrate has been shown to contribute to de novo lipid synthesis under hypoxia (Metallo et al., 2011). Studies have shown that RCQ is a source of alternatively synthesized aspartate via cytosolic GOT, but not GOT2 in cells with defects in oxidative mitochondrial metabolism (Metallo et al., 2011; Mullen et al., 2012, 2014; Wise et al., 2011).

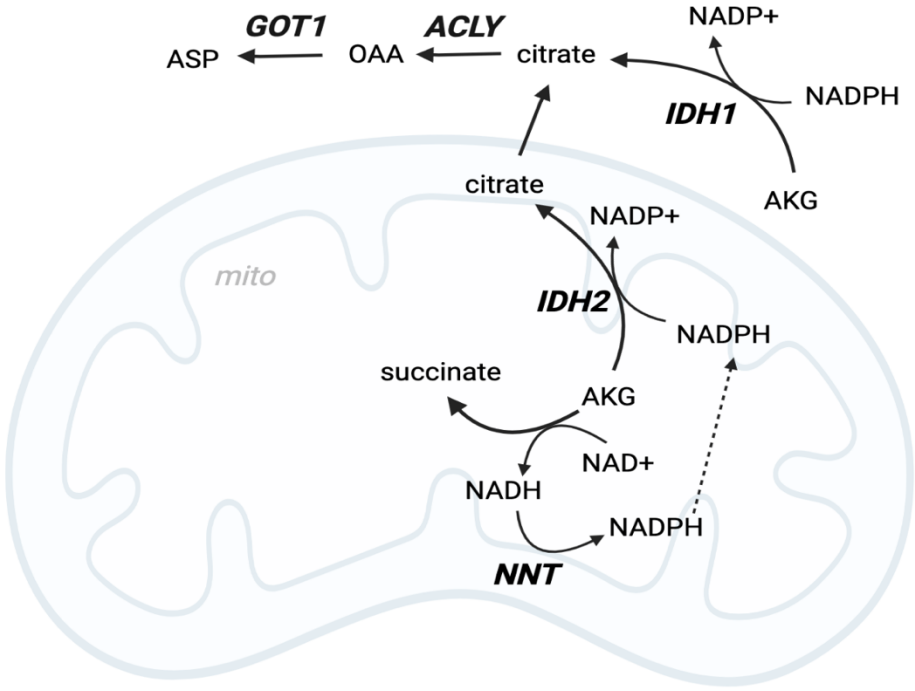

Figure 1.5. Mechanisms of Reductive Carboxylation of Glutamine. Figure of reductive carboxylation (RCQ) pathways when complex I is impaired, and one proposed mechanism of transhydrogenase activity to power mitochondrial RCQ. Citrate is transported to the cytosol by SLC25A1 where it is cleaved by ACLY to OAA and acetyl co-A and aspartate is synthesized by GOT1.

Since citrate synthase is thermodynamically unlikely to go in reverse, citrate generated from mitochondrial RCQ must be exported to the cytoplasm through the transporter SLC25A1 (L. Jiang et al., 2016). Prior research has suggested that the AKG

must be oxidized to succinyl-CoA in the mitochondria, and that impairing the a-KGDH reaction depleted NADPH availability therefore suppressing RCQ (Metallo et al., 2011; Mullen et al., 2014). Therefore, this oxidative step of the TCA cycle was important for powering nicotinamide nucleotide transhydrogenase (NNT), which interconverts NADH and NADPH using the mitochondrial membrane potential for proton transfer (Ciccarese & Ciminale, 2017; Mullen et al., 2014). RCQ has also been reported to recycle cytosolic NADH to NAD+ via MDH1, which could promote aerobic glycolysis and also replenish malate and fumarate levels (Gaude et al., 2018). Several studies have indicated that expanding NADP(H) pools through complex I impairments or other mechanisms is a feature in models of metastatic disease (Gaude et al., 2018; Ilter et al., 2023). Together, these results suggest intricate metabolic interplay between compartmental redox environments that vary based on overall cell state and their corresponding metabolic requirements. However, many aspects of RCQ under various models of mitochondrial impairments and how complex I loss mediates reductive carboxylation for tumorigenesis remain poorly understood.

1.8 Succinate Dehydrogenase: A Paradoxical Tumor Suppressor

An additional link between the TCA cycle and the ETC is shared enzyme succinate dehydrogenase (SDH, aka complex II). SDH serves important functions in mitochondrial metabolism yet is also a target of biological disruption. SDH is a heterotetrameric nuclear-encoded protein complex located in the IMM that catalyzes the oxidation of succinate to fumarate and shuttles electrons to ubiquinone in the ETC. Biallelic loss-of-function

mutations to the subunits of SDH (A-D) or SDH assembly factors (SDHAF2), can lead to neoplasms in neuroendocrine tissues and the kidney (Astuti et al., 2001; Bardella et al., 2011a; Baysal et al., 2000; Burnichon et al., 2010; Hao et al., 2009; Niemann & Müller, 2000).

SDHA encodes the flavoprotein subunit responsible for the oxidation of succinate to fumarate, coupled to the reduction of FAD to $FADH_2$. *SDHAF2* is responsible for the flavination of *SDHA,* and therefore is essential for SDH-dependent respiration and electron transfer (Hao et al., 2009). The *SDHB* gene encodes the subunit containing the iron-sulfur clusters that carry the electrons to ubiquinone. Together, these two subunits encode the catalytic domain of SDH, which play a critical role in transferring electrons from succinate to ubiquinone. The *SDHC* and *SDHD* genes form a dimer to anchor the protein complex to the IMM but differ from the other complexes in that they are not transmembrane proteins. This dimer also contains the ubiquinone binding site, which is fully reduced to ubiquinol. Interestingly, it has been reported that mutations in *SDHB* specifically, lead to more severe disease, metastatic extra-adrenal disease, and worse outcomes, while other *SDH* mutations often result in benign or more low-grade tumors (Badenhop et al., 2004; Eijkelenkamp et al., 2020; Klein et al., 2008).

Cancer cells arising from mutations in SDH components display a complete loss of oxidative TCA cycle metabolism at the SDH step and have a substantial accumulation of the upstream metabolite succinate, which can impair enzymes involved in oxygen sensing, epigenetic regulation, and metabolism (Letouzé et al., 2013; L. B. Sullivan et al., 2016). Hypoxia, the condition in which tissues are deprived of adequate oxygen supply, is common in tumors since they rapidly outgrow their blood supply (Kluckova & Tennant,

2018). Hypoxia-inducible factor 1-α (HIF-1α) is a transcription factor that is rapidly degraded by the cell in normoxia but is stabilized when oxygen levels are low in the cellular environment. HIF-1α stabilization promotes adaptation to hypoxia by upregulating genes involved in processes such as angiogenesis, erythropoiesis, and glycolysis, thereby promoting cell survival and proliferation (Semenza, 2003). In fact, SDH impairment causes a 200-fold increase in intracellular succinate levels, which has been coined an 'oncometabolite.' (Cardaci et al., 2015; Eijkelenkamp et al., 2020; Kluckova & Tennant, 2018a). Succinate accumulation can trigger HIF-1a stabilization due to competitive interference with prolyl hydroxylase domain (PHD), an AKG-dependent dioxygenase that is required for HIF degradation (Kluckova & Tennant, 2018). This effect is known as pseudohypoxia, which also leads to inhibition of DNA and histone demethylases, sparking hypermethylator phenotypes that are commonly associated with cancer (Bardella et al., 2011a; Castro-Vega et al., 2015; Eijkelenkamp et al., 2020; Letouzé et al., 2013).

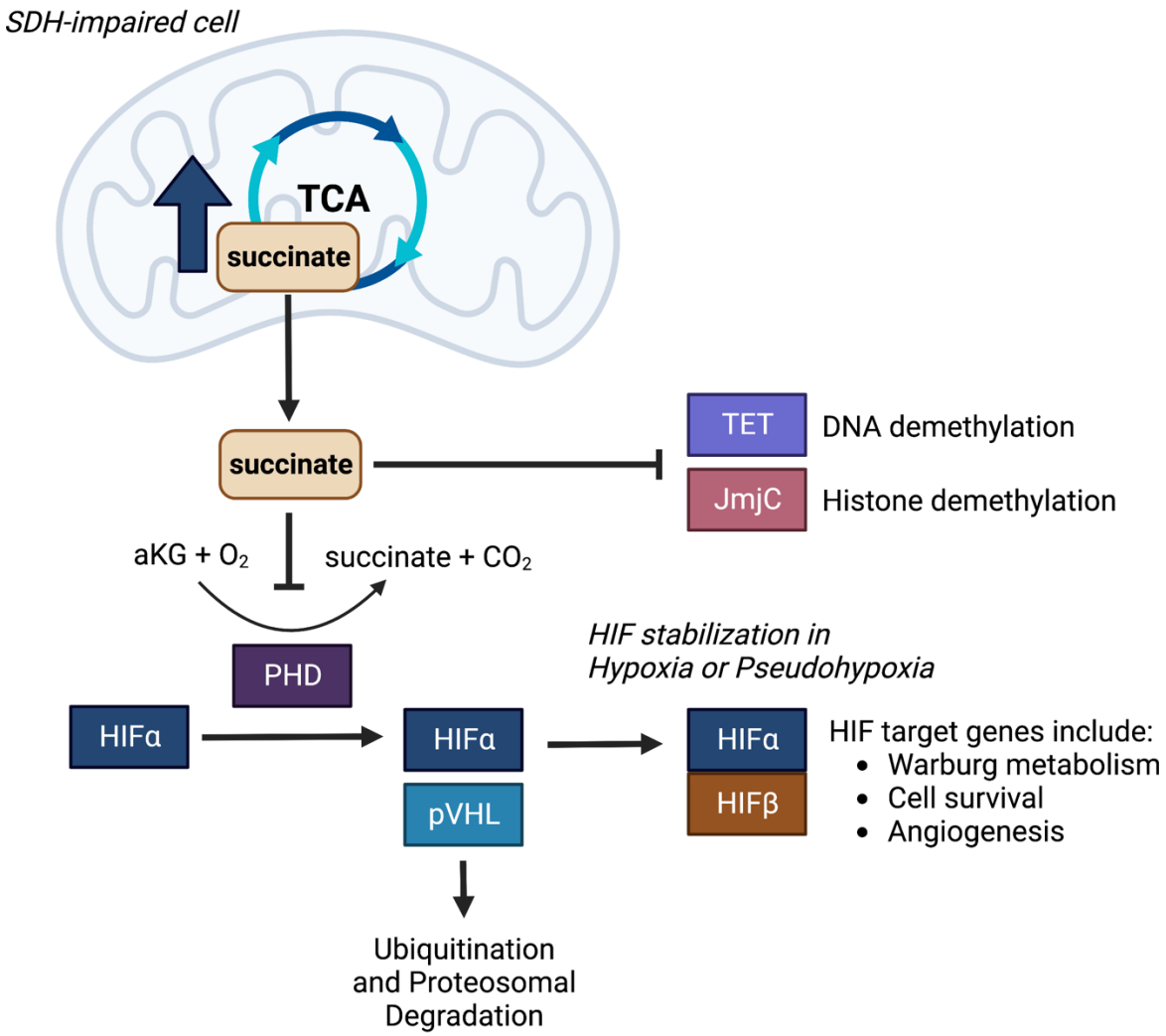

Figure 1.6. Molecular consequences of SDH loss and pseudohypoxia. When succinate dehydrogenase (SDH) is impaired, accumulated succinate levels interfere with DNA and histone demethylases. Additionally, high levels of succinate inhibit aKG-dependent dioxygenases including prolyl hydroxylase domain (PHD) which is responsible for the proteasomal degradation of HIF in normoxia. Therefore, high succinate levels induce a cellular state known as pseudohypoxia, where HIF is stabilized, inducing transcription of target genes normally intendent to adapt and survive under low oxygen conditions (hypoxia). Figure adapted from Eijkelenkamp et al. 2020.

Importantly, SDH loss also blocks the canonical route for aspartate biosynthesis (TCA cycle), making it unclear how SDH-deficient cells adapt to fulfill their anabolic demands for cell proliferation. Previous studies have shown that SDHB KO cells increase expression and activity of biotin-containing pyruvate carboxylase (PC), an anaplerotic enzyme that carboxylates pyruvate to generate OAA using ATP. PC, canonically known

for its role in gluconeogenesis, was shown to be essential for overcoming aspartate insufficiency in SDHB KO cancer cells (Cardaci et al., 2015; Lussey-Lepoutre et al., 2015). SDH ablation increases glucose-derived aspartate synthesis through PC activity and inhibition of SDH was shown to increase PC activity in neuroendocrine tumor cell models, which replenished intracellular aspartate (Cardaci et al., 2015; Lussey-Lepoutre et al., 2015). However, these studies did not determine whether aspartate was terminally synthesized in the mitochondria or cytosol, nor did they overexpress PC to assess whether it was sufficient to increase aspartate levels and proliferation of SDHB KO cells. Additionally, it is not clear how PC is activated to overcome aspartate limitation in SDH-impaired cells, or if PC activity is solely responsible for alternative aspartate synthesis in SDH-deficient tumors.

1.9 Summary

The ways in which cancer cells undergo metabolic reprogramming to aid their survival, proliferation, and metastasis are numerous, and many of these mechanisms have only recently gained appreciation, lending to the idea that there are still many yet to uncover. Since the nutrient requirements seem to vary across cancer subtype and may depend on genotype within a subset of tumor, there are many potential methods to implement precision medicine and metabolism to treat almost any type of tumor. Indeed, amino acid metabolism and glucose metabolism overlap in several aspects, which has enabled a more holistic view of cancer cell metabolism. Aspartate is tightly linked to respiration and proliferation of cancer cells. This dissertation dissects a paradoxical tumor

subset characterized by SDH mutations which cannot synthesize aspartate by canonical means. Indeed, we found that SDH-impaired cancer cells adapt to aspartate deficiency by downregulating complex I, altering the mitochondrial NAD+/NADH ratio, and enabling alternative aspartate synthesis. These advantageous alternations increase intracellular aspartate levels and increase proliferation rate. Subsequently, we found that activating complex I activity in SDHB-mutant renal cell carcinoma cells is deleterious for aspartate production, proliferation rate, and tumor growth.

Chapter 2. Materials and Methods

Materials and Methods:

Cell Culture

Cell lines were acquired from ATCC (143B, HEK293T, A549, HCT116), as a gift from Dr. W. Marston Linehan, NCI (UOK269), or as a gift from Dr. Stanley Lee, Fred Hutch (TF-1). 143B cells are deficient in thymidine kinase (TK). Cell identities were confirmed by satellite tandem repeat profiling and cells were tested to be free from mycoplasma (MycoProbe, R&D Systems). Cells were maintained in Dulbecco's Modified Eagle's Medium (DMEM) (Gibco, 50-003-PB) supplemented with 3.7 g/L sodium bicarbonate (Sigma-Aldrich, S6297), 10% fetal bovine serum (FBS) (Gibco, 26140079) and 1% penicillin-streptomycin solution (Sigma-Aldrich, P4333). TF-1 cells were also supplemented with the 2 ng/ml Human Granulocyte Macrophage-Colony Stimulating Factor (GM-CSF) (Shenandoah Biotechnology, 100-08). Cells were incubated in a humidified incubator at 37°C with 5% CO_2.

Proliferation Assays

Cells were trypsinized (Corning, 25051CI), resuspended in media, and counted (Beckman Coulter Counter Multisizer 4 or Nexcelom Auto T4 Cellometer) and seeded overnight onto 6-well dishes (Corning, 3516) with an initial seeding density of 20,000 cells/well (143B, HEK293T, HCT116, 786-O, A549) or 30,000 cells/well (UOK269, SDHB KO 143B). After overnight incubation, 3-6 wells were counted for a starting cell count at the time of treatment. Cells were washed twice in phosphate-buffered saline (PBS) and

4 mL of treatment media was added. Experiments were conducted in DMEM without pyruvate (Corning 50-013-PB) supplemented with 3.7 g/L sodium bicarbonate 10% dialyzed fetal bovine serum (FBS) (Sigma-Aldrich, F0392) and 1% penicillin-streptomycin solution, with or without 1 mM sodium pyruvate (PYR) (Sigma-Aldrich, P8574), 1 mM 2-ketobutyric acid (AKB) (Sigma-Aldrich, K401), 1-20 mM Aspartic Acid (ASP) (Sigma-Aldrich, A7219), or 1 mM Asparagine (Sigma-Aldrich, A7094). Proliferation assays contain 1 mM PYR unless otherwise noted. Proliferation assays using Human Plasma-Like Medium (HPLM) (ThermoFisher, A4899101) were supplemented with 10% dialyzed FBS, 1% penicillin-streptomycin solution, with or without 20 mM ASP. Drug treatments included rotenone (Sigma-Aldrich, R8875), metformin (Sigma-Aldrich, D150959), piericidin A (Cayman Chemical, 15379), atpenin A5 (Cayman Chemical, 11898; AdipoGen, AG-CN2-0110; Abcam, ab144194; or Enzo Life Sciences, ALX-380-313), doxycycline hydrochloride (Sigma-Aldrich, D3447), AZD7545 (Cayman Chemical, 19282), antimycin A (Sigma-Aldrich, A8674), oligomycin (Sigma-Aldrich, 495455), BMS-303141 (Cayman, 16239; MedChemExpress, HY-16107) and DMSO vehicle (D2650). Cells were incubated in a humidified incubator at 37°C with 5% CO_2 then counted after 4-6 days. Cells for the hypoxia experiments were incubated in a 37°C humidified hypoxia chamber (Coy Lab Products, 8375065) at various O_2 concentrations after drug treatment. Proliferation rate was determined by the following equation: Proliferation rate (doublings per day, 1/d) = ($\log_2$(final cell count / initial cell count))/total days.

Lentiviral Production and Infection

The following plasmids were obtained from DNASU Plasmid Repository: pLenti6.3-V5 DEST_SLC1A3, pLenti6.3-V5-DEST_SDHB, pLX304_PC, pLX304_GOT1, pLenti6.3-V5-DEST_MPC1, pLX304_MDH1, and pDONR201-NDI1. pLX304-gpASNase1 and pDONR-cyto*LbNOX* were previously described. Cyto*LbNOX* was cloned into pLX304 (Addgene, 25890) and NDI1 was cloned into pInducer20 (Addgene, 44012, gift from Stephen Elledge) using LR Clonase II (Fisher, 11791100). pLentiCMV-GOT2 was constructed by purchasing GOT2 cDNA (Integrated DNA Technologies), which was amplified by PCR and assembled with the pENTR1A vector using NEBuilder HiFI DNA Assembly Cloning Kit (New England BioLabs, E2621). pENTR1A-GOT2 was then used to transfer GOT2 to the pLenti-CMV-Hygro Destination vector (w117-1) (Addgene, 17454 a gift from Eric Campeau & Paul Kaufman) using Gateway LR Clonase II (Fisher, 11791020). Lentivirus was generated by transfection of HEK293T cells with expression construct plasmid DNA with pMDLg/pRRE (Addgene, 12251), pRSV-Rev, (Addgene, 12253) and pMD2.G (Addgene, 12259) packaging plasmids. and FuGENE transfection reagent (Fisher, PRE2693) in DMEM (Fisher, MT10017CV) without FBS or penicillin-streptomycin. The supernatant containing lentiviral particles was filtered through 0.45 μM membrane (Fisher, 9720514) and was supplemented with 8 μg/μL polybrene (Sigma, TR-1003-G) prior to infection. 143B and UOK269 cells were seeded at 50% confluency in 6 well dishes and centrifuged with lentivirus (900 xg, 90 mins, 30°C). After 24 hours media was replaced with fresh media and 48 hours after infection cells were treated with either 1 μg/mL blasticidin (Fisher, R21001), 150 μg/mL hygromycin (Sigma, H7772), or 1 mg/mL G418 (Sigma, A1720) and maintained in selection media until all uninfected control cells died.

Generation of mitoLbNOX expressing cells

LbNOX-FLAG DNA was amplified from pDONR-cyto*LbNOX* by PCR, an oligonucleotide containing the zmLOC100282174 mitochondrial translocation sequence (MTS), which causes potent mitochondrial localization, was purchased (Integrated DNA Technologies) and the pENTR1A vector (Fisher, A10462) was amplified by PCR to create a linear fragment. The three fragments were assembled using the NEBuilder HiFi DNA Assembly Cloning Kit (New England BioLabs, E2621) to generate pENTR1A-mito*LbNOX*, which was then used as a donor to transfer mitoLbNOX into pLenti-CMV-Hygro-DEST (w117-1) (Addgene, 17454 a gift from Eric Campeau & Paul Kaufman) using Gateway LR Clonase II (Fisher, 11791020). Lentivirus was generated with pLentiCMV-mito*LbNOX* as described above and 143B cells were infected and then selected in 150 µg/mL Hygromycin B (Sigma, H7772) for four days.

LbNOX-FLAG primers:

5'-GCCGCGAGACCGTATGCTCATAAGGTCACCGTG-3' (fw primer)

5'-CAAGAAAGCTGGGTCTAGTTACTTGTCATCGTCATCC-3' (rv primer)

pENTR primers:

5'-CTAGACCCAGCTTTCTTGTAC-3' (fw)

5'-CTGGCTTTTAGTAAGCGAATTC-3' (rv)

MTS sequence:

5’-
CGCTTACTAAAAGCCAGGCCACCATGGCACTGCTTCGCGCCGCCGTTTCAGAACT
CAGACGGAGAGGACGGGGTGCGCTTACTCCCCTCCCGGCGCTGTCTAGCTTGCTT
TCCTCACTTAGCCCCCGAAGTCCCGCCTCAACGCGCCCAGAGCCAAACAATCCAC
ACGCAGATCGACGCCATGTCATCGCTTTGAGGCGATGCCCCCCACTTCCTGCCTC
TGCCGTTCTGGCACCTGAACTCCTGCATGCACGAGGATTGCTCCCGAGACATTGG
TCTCATGCCTCTCCCTTGTCCACGTCCTCTTCATCCAGTAGACCAGCAGATAAGGC
GCAGTTGACCTGGGTCGATAAATGGATCCCAGAAGCCGCGAGACCGTAT-3’

Generation of Knockout Cell Lines

Protocol was adapted from Hoellerbauer et al., 2020. Three chemically synthesized 2'-O-methyl 3’phosphorothioate-modified single guide RNA (sgRNA) sequences targeting the gene of interest were purchased (Synthego) and are listed in the table below. Each sgRNA was resuspended in nuclease-free water, combined with SF buffer (Lonza, V4XC-2032), and sNLS-spCas9 (Aldevron, 9212). $2x10^5$ 143B or HEK293T cells were resuspended in the resulting solution containing ribonucleoprotein complexes (RNPs) and electroporated using a 4D-Nucleofector (Amaxa, Lonza) programs FP-133 (143B) and DS-150 (HEK293T). Nucleofected cells were then moved to a 12-well plate (Corning, 3513) and, after achieving confluence, were single-cell cloned by limiting dilution by plating 0.5 cells/well in a 96 well plate. Gene knockout was confirmed using western blots on the nucleofected pool and each single cell clone used in this study.

Gene	**sgRNA sequence (5’-3’)**
SDHB	UCGCCCUCUCCUUGAGGCG AGAAAUUUGCCAUCUAUCGA CUUUGUUAGAUGUGGCCCCA
PC	GCAGGCCCGGAACACACGGA GCUGGAGGAGAAUUACACCC ACACCGGCCGCAUUGAGGU
MPC1	UUGCCUACAAGGUACAGCCU GGGCUACUUCAUUUGUUGCG AUGUCAAAGAAUAGCAACAG

GOT1	CAGUCAUCCGUGCGAUAUGC GCACGGAUGACUGCCAUCCC CGAUCUUCUCCAUCUGGGAA
GOT2	UUUCUCAUUUCAGCUCCUGG CGGACGCUAGGCAGAACGUA UCCUUCCACUGUUCCGGACG
MDH1	CCAAUCAGAGUCCUUGUGAC CCACAAGAAUGGCCACAUCC GUGAAAAUCUUCAAAUCCCA

Table 2. sgRNA sequences for each gene knocked out in this dissertation.

Oxygen Consumption

Oxygen consumption measurements were conducted using an Agilent Seahorse Xfp Analyzer. 143B or UOK269 cell lines were trypsinized and seeded at $2.5x10^5$ cells/well of a Seahorse XFp cell culture miniplate (Agilent, 103025-1000) overnight in 80 µL media. The following day, 100 µL cell culture media was added with or without pretreatment, as indicated. Before the assay Seahorse XFp sensor cartridges (Agilent, 103022-100) were incubated with calibrant solution, following manufacturer's instructions and loaded with injection solutions yielding the following final concentrations: AA5; 5 µM, rotenone; 100 nM. AZD7545; 5 µM, antimycin A; 10 µM. Following each assay, cells of each well were counted by Coulter Counter and mitochondrial oxygen consumption rate was determined as the measured oxygen consumption rate minus the average of post-antimycin oxygen consumption rates, per 100,000 cells.

Mitochondrial Fractionation

$2x10^7$ cells were trypsinized, washed with PBS, and centrifuged (300 xg, 5 min, 4°C). Pellets were washed with ice-cold PBS and resuspended in Homogenization buffer (10 mM Tris-HCl pH 6.7, 10 mM KCl, 0.15 mM $MgCl_2$, 1 mM PMSF (Sigma, 10837091001)).

Cells were then vortexed, incubated on ice for 2 minutes, then transferred to a Dounce Homogenizer (Sigma, D9063) and homogenized with 40-60 strokes. Cells were transferred to mitochondrial suspension buffer (10 mM Tris-HCl pH 6.7, 0.15 mM $MgCl_2$, 0.25 mM sucrose, 1 mM PSMF) and centrifuged (700 xg, 10 min, 4°C). The supernatant was transferred and centrifuged again (10,500 xg, 15 min, 4°C). The resulting supernatant (cytosolic fraction) was transferred and centrifuged once more, (17,000 xg, 15 min, 4°C) while the pellet containing the mitochondrial fraction was washed in suspension buffer and centrifuged again (12,000 xg, 15 min, 4°C). Mitochondrial proteins were then harvested with RIPA buffer (see below).

Western Blotting

Protein lysates were harvested in RIPA buffer (Sigma, R0278) supplemented with protease inhibitors (Fisher, A32953). Protein concentration was determined using a Bicinchoninic Acid Assay (Fisher, 23225) using bovine serum albumin (BSA) as a protein standard. Equal amounts of protein were denatured with Bolt 4x Loading Dye (ThermoFisher, B0007) and Bolt 10x reducing agent (ThermoFisher, B0004), heated at 95°C for 5 min, and loaded onto 4-12% by SDS-polyacrylamide gels (Invitrogen, NW04127), apart from MPC1, for which we used 16% Novex Tricine gels for separation of low molecular weight proteins (Invitrogen, EC6695C). After electrophoretic separation, proteins were transferred onto a 0.22 mm nitrocellulose using iBlot2 transfer stacks (Fisher, IB23001) and transferred with the P0 system setting. Membranes were blocked with 5% milk in Tris-buffered saline with 0.1% Tween-20 (TBS-T) and incubated at 4°C overnight with the following antibodies: anti-FLAG (Sigma, F1804; 1:1,000), anti-

SLC1A3 (Genetex, GTX20262; 1:500), anti-SDHB (Atlas, HPA002868; 1:1,000), anti-PC (Proteintech, 66615-1-IG, 1:1000), anti-MPC1, (Cell Signaling, 14462S, 1:1000), anti-GOT2 (Proteintech, 14800-1-AP, 1:750), anti-GOT1 (Cell Signaling, 34423S, 1:1,000), anti-MDH1 (Proteintech, 15904-1-AP, 1:5,000), anti-NDUFA8 (Atlas, HPA041510; 1:1,000), anti-Vinculin (Sigma, SAB4200729; 1:10,000), and anti-Tubulin (Sigma, T6199; 1:10,000). The next morning, membranes were washed three times with TBS-T and the following secondary antibodies were added: 800CW Goat anti-Mouse IgG (LiCOR, 926-32210; 1:15,000), 680RD Goat anti-Rabbit IgG (LiCOR, 926-68071; 1:15,1000). Membranes were washed three more times with TBS-T and imaged on a LiCOR Odyssey Near-Infrared imaging system.

TMT-Quantitative Mitochondrial Proteomics

Sample preparation. Mitochondrial fractions of WT 143B, SDHB AB 143B, EP SDHB KO 143B, and LP SDHB KO 143B cells in quadruplicate were fractionated using the protocol described above. Mitochondrial pellets were kept at -80˚C until analysis. *Disulfide bond reduction/alkylation.* Protein solutions (100 µg) were diluted to 2 µg/µL in 100 mM ammonium bicarbonate. Protein disulfide bonds were reduced by adding tris (2-carboxyethyl) phosphine to a final concentration of 5 mM and mixing at room temperature for 15 min. The reduced proteins were alkylated by adding 2-chloroacetamide to a final concentration of 10 mM and mixing in the dark at room temperature for 30 min. Excess 2-chloroacetamide was quenched by the addition of dithiothreitol to 10 mM and mixing at room temperature for 15 min. *Methanol-chloroform precipitation and protease digestion.* Samples (100 µg) were diluted to 1 µg/µL with 100 mM ammonium bicarbonate in a 1.5

mL Eppendorf low bind tube. Protein precipitation was done as follows: 400 µL of methanol was added to each sample and vortexed for 5 seconds. 100 µL of chloroform was added to each sample and vortexed for 5 seconds. 300 µL of water was added to each sample and vortexed for 5 seconds. The samples were centrifuged for 1 min at 14,000 xg. The aqueous and organic phases were removed, leaving a protein wafer in the tube. The protein wafers were washed with 400 µL of methanol and centrifuged at 21,000 g at room temperature for 2 min. The supernatants were removed, and the pellets were allowed to air dry, but not to complete dryness. The samples were resuspended in 70 µL 100 mM HEPES (pH 8.5) and digested with rLys-C protease (100:1, protein to protease) with mixing at 37 ˚C for 4 hr. Trypsin protease (100:1, protein to protease) was added and the reaction was mixed overnight at 37 ˚C. *TMT-labeling.* TMTpro16plex labeling reagent (Pierce) (500 µg) was brought up in 30 µL acetonitrile and added to the digested peptide solution (100 µg) yielding a final organic concentration of 30% (v/v) and mixed at room temperature for 1 hr. A 2 µg aliquot from each sample was combined, dried to remove the acetonitrile, concentrated on a C18 ZipTip (Millipore) and analyzed via LC/MS as a "label check". The label check was used for two purposes. First, it ensured the TMT labeling efficiency was greater than 95%. Second, sample equalization volumes were determined after summing the total intensity from each sample TMT "channel" and calculating the volume of each sample that should be mixed to provide equal amounts from each sample in the final mixture. After labeling efficiency was determined, the reactions were quenched with hydroxylamine to a final concentration of 0.3% (v/v) for 15 min with mixing. The TMTpro16plex labeled samples were pooled at 1:1 ratio based on calculated equalization volumes and concentrated by vacuum

centrifugation to remove acetonitrile. Half of the material was desalted over an Oasis HLB 3cc cartridge (Waters) and taken to dryness. *bRP Fractionation.* Pierce's High pH Reversed-Phased Peptide Fractionation kit (part# 84868) was used to fractionate the sample (100 ug) into 8 fractions with cuts at 5, 7.5, 10.0, 12.5, 15, 17.5, 20.0, 22.5, 25.0 and 50.0% acetonitrile in 0.1% triethylamine following the manufacturer's protocol. The fractions were dried in a speedvac. *Mass Spectrometry Analysis.* The generated basic reverse phase fractions were brought up in 2% acetonitrile in 0.1% formic acid (20 µL) and analyzed (2 µL) by LC/ESI MS/MS with a Thermo Scientific Easy1200 nLC (Thermo Scientific, Waltham, MA) coupled to a tribrid Orbitrap Eclipse with FAIMS pro (Thermo Scientific, Waltham, MA) mass spectrometer. In-line de-salting was accomplished using a reversed-phase trap column (100 µm × 20 mm) packed with Magic C_{18}AQ (5-µm, 200 Å resin; Michrom Bioresources, Auburn, CA) followed by peptide separations on a reversed-phase column (75 µm × 270 mm) packed with ReproSil-Pur C_{18}AQ (3-µm, 120 Å resin; Dr. Maisch, Baden-Würtemburg, Germany) directly mounted on the electrospray ion source. A 180-minute gradient from 4% to 44% B (80% acetonitrile in 0.1% formic acid/water) at a flow rate of 300 nL/minute was used for chromatographic separations. A spray voltage of 2300 V was applied to the electrospray tip in-line with a FAIMS pro source using varied compensation voltage -40, -60, -80 while the Orbitrap Eclipse instrument was operated in the data-dependent mode. MS survey scans were in the Orbitrap (Normalized AGC target value 300%, resolution 120,000, and max injection time 50 ms) with a 3 sec cycle time and MS/MS spectra acquisition were detected in the linear ion trap (Normalized AGC target value of 100% and injection time 50 ms) using CID activation with a normalized collision energy (NCE) of 32% using turbo speed scan. Selected ions

were dynamically excluded for 60 seconds after a repeat count of 1. Following MS2 acquisition, real time searching (RTS) was employed, and spectra were searched against a Human database (UP00005640 Human 120119) using COMET. Searches were performed with settings for the proteolytic enzyme trypsin. Maximum missed cleavages were set to 1 and maximum variable modifications on peptides was set to 3. Variable modifications included oxidation (+15.995 Da on M) with static modifications TMTpro (+304.207 DA on K) and carbamidomethyl (+57.021 on C). Maximum search time was 35 ms. Scoring thresholds were set to the following: Xcorr 1.4, dCn 0.1, precursor PPM 10 and charge state 2. TMT Synchronous precursor selection (SPS) MS3 was collected on the top 10 most intense ions detected in the MS2 spectrum. SPS-MS3 precursors were subjected to higher energy collision-induced dissociation (HCD) for fragmentation with an NCE of 45% and analyzed using the Orbitrap (Normalized AGC target value of 400%, resolution 60,000 and max injection time 118 ms). *Data Analysis.* Data analysis was performed using Proteome Discoverer 2.5 (Thermo Scientific, San Jose, CA). The data were searched against a Human database (UP00005640 Human 120119) that included common contaminants (cRAPome). Searches were performed with settings for the proteolytic enzyme trypsin. Maximum missed cleavages were set to 2. The precursor ion tolerance was set to 10 ppm and the fragment ion tolerance was set to 0.6 Da. Dynamic peptide modifications included oxidation (+15.995 Da on M). Dynamic modifications on the protein terminus included acetyl (+42.-11 Da on N-terminus), Met-loss (-131.040 Da on M) and Met-loss+Acetyl (-89.030 Da on M) and static modifications TMTpro (+304.207 Da on any N-termius), TMTpro (+304.207 DA on K) and carbamidomethyl (+57.021 on C). Sequest HT was used for database searching. All search results were run through

Percolator for scoring. Unsupervised clustering of the 16 proteomic samples was performed using the z-score based R (version 4.0.3) package GMD (Zhao & Sandelin, 2012) and visualized with the heatmap.3 function.

Polar Metabolite Extractions

Adherent cells. For standard metabolic analysis, cells were seeded overnight at $2x10^5$ cells per well of a 6-well dish. The next morning, cells were washed twice with PBS and changed to the indicated medias supplemented with 10% dialyzed FBS, 1% penicillin-streptomycin, and treatments as indicated, and returned to the tissue culture incubator. After 6 hours, polar metabolites were extracted from cells by three rapid washes with ice-cold blood bank saline, (Fisher, 23293184) then 250 µL of 80% HPLC grade methanol in HPLC grade water containing 2.5 µM D8 Valine (Cambridge Isotope Laboratories, DLM-488) or ^{13}C amino acid mix (Cambridgre Isotope Laboratories, MSK-CAA-1) was added to each well and cells were scraped with the back of a P1000 pipet tip and transferred to Eppendorf tubes. Tubes were centrifuged (17,000 xg, 15 mins, 4°C) and the supernatant containing polar metabolites was transferred to a new centrifuge tube and placed in a centrivap until lyophilized. *Suspension cells.* TF-1 cells were seeded at $2.5x10^5$ cells per well of a 6-well dish the night before treatment and extraction in standard media containing 2 ng/mL human GM-CSF. The next day, cells were washed with PBS and treated with media containing 2 ng/mL human GM-CSF, 10% dialyzed FBS, and the treatments as indicated. After 6 hours, cells were collected and washed in 1 mL of ice-cold saline containing 2% dialyzed FBS. Metabolism was quenched and metabolites were extracted with 600 µL of 80% HPLC grade methanol in HPLC grade water. Samples were

centrifuged, (17,000 xg, 15 mins, 4°C) moved to new Eppendorf tubes, lyophilized, and stored at -20˚C until analysis.

Isotope Tracing

Aspartate Uptake. SLC1A3 143B cells were plated at $2x10^5$ cells per well of a 6-well dish. The next morning, cells were washed twice with PBS and changed to DMEM without pyruvate supplemented with 10% dialyzed FBS, 1% penicillin-streptomycin, and treated with the indicated concentrations of 1,4-^{13}C2 aspartate (Cambridge Isotopes, CLM-4455) for one hour. *Glutamine Tracing.* WT and SDHB KO 143B cells were seeded at $2x10^5$ cells and UOK269 cell lines were plated at $3x10^5$ cells per well of a 6-well dish. The next morning, cells were washed twice with PBS and changed to DMEM without glucose, glutamine, pyruvate, or phenol red (Sigma, D5030) supplemented with 10% dialyzed FBS, 1% penicillin-streptomycin, 1 mM pyruvate, 25 mM ^{12}C glucose (Sigma, G7528), and 4 mM U-^{13}C glutamine (Cambridge Isotopes, CLM-1822). 143B cells were treated as indicated for 6 hours. *Glucose Tracing.* WT and SDHB KO 143B cells were seeded at $2x10^5$ cells per well of a 6-well dish. The next morning, cells were washed twice with PBS and swapped to DMEM without glucose, glutamine, pyruvate, or phenol red supplemented with 10% dialyzed FBS, 1% penicillin-streptomycin, 1 mM AKB, 25 mM U-^{13}C glucose (Cambridge Isotopes, CLM-1396), and 4 mM ^{12}C glutamine (Sigma, G5792). Polar metabolites were extracted with the above technique.

Rapid Subcellular NAD+/NADH Detection

Rapid subcellular fractionation. 143B cells were plated at $1x10^5$ cells per well of a 6-well dish the night before rapid subcellular fractionation, a protocol adapted from Lee et al., 2019. Cells were washed twice with PBS and treated with DMEM containing 10% dialyzed FBS, 1% penicillin-streptomycin, 1 mM pyruvate, and treatments as indicated. After 6 hours of treatment, cells were washed with ice cold PBS and scraped into a 1.5 mL microcentrifuge tube. After a brief centrifuge (13,500 xg, 10 sec, 4˚C), the supernatant was discarded, and the cells were resuspended in 250 µL of digitonin (Sigma, D141) dissolved at 1 mg/mL in ice cold PBS and triturated 5 times with a P1000 micropipette tip. The sample was then centrifuged (13,500xg, 10 sec, 4˚C) and the supernatant was collected for the cytosolic fraction, while the remaining pellet contained the mitochondria. The cytosolic fraction was mixed 1:1 with 250 µL of 0.2 N NaOH containing 1% dodecyl trimethylammonium bromide (DTAB) (Sigma, D5047). Metabolites for the mitochondrial fraction were extracted immediately using 500 µL of cold lysis buffer (1% DTAB in 0.2 N NaOH at 1:1 (v/v) with PBS). Whole cell lysates were obtained by the same manner as the mitochondrial fraction. *Compartmentalized NAD+/NADH Measurements.* NAD+ and NADH were then detected using the NAD/NADH-Glo™ Assay (Promega, G9072) according to the manufacturer's directions and previous reports (Gui et al., 2016; L. B. Sullivan et al., 2015). To detect NAD+, 50 µL of sample was transferred to a PCR tube and treated with 25 µL of 0.4N HCl and heated to 60˚C for 15 min where acidic conditions selectively degrade NADH. For NADH detection, 50 µL of sample was transferred to a PCR tube and heated to 75˚C for 30 min for selective basic degradation of NAD+. Following incubation, samples were equilibrated at room temperature, then quenched by neutralizing the NAD+ acid treated samples with 25 µL of 0.5M Trizma base (Sigma,

T6066) and the NADH base treated samples with 50 µL of 1:1 (v/v) 0.4N HCl:0.5M Trizma base. Once neutralized, 50 µL of each sample was then mixed with 50 µL of NAD/NADH-Glo™ Detection Reagent in an opaque white 96-well flat bottom plate. Selective degradation protocols and detection in the linear range were confirmed using chemical standards for NAD+ (Sigma, N1511) and NADH (Sigma N8129). Enzyme-linked luminescence measurements were then recorded on a Tecan Infinite M Plex microplate reader according to the manufacturer instructions.

Liquid Chromatography-Mass Spectrometry (LCMS)

Lyophilized samples were resuspended in 80% HPLC grade methanol in HPLC grade water and transferred to liquid chromatography-mass spectrometry (LCMS) vials for measurement by LCMS. Metabolite quantitation was performed using a Q Exactive HF-X Hybrid Quadrupole-Orbitrap Mass Spectrometer equipped with an Ion Max API source and H-ESI II probe, coupled to a Vanquish Flex Binary UHPLC system (Thermo Scientific). Mass calibrations were completed at a minimum of every 5 days in both the positive and negative polarity modes using LTQ Velos ESI Calibration Solution (Pierce). Polar Samples were chromatographically separated by injecting a sample volume of 1 µL into a SeQuant ZIC-pHILIC Polymeric column (2.1 x 150 mm 5 mM, EMD Millipore). The flow rate was set to 150 mL/min, autosampler temperature set to 10 °C, and column temperature set to 30 °C. Mobile Phase A consisted of 20 mM ammonium carbonate and 0.1 % (v/v) ammonium hydroxide, and Mobile Phase B consisted of 100 % acetonitrile. The sample was gradient eluted (%B) from the column as follows: 0-20 min.: linear gradient from 85 % to 20 % B; 20-24 min.: hold at 20 % B; 24-24.5 min.: linear gradient

from 20 % to 85 % B; 24.5 min.-end: hold at 85 % B until equilibrated with ten column volumes. Mobile Phase was directed into the ion source with the following parameters: sheath gas = 45, auxiliary gas = 15, sweep gas = 2, spray voltage = 2.9 kV in the negative mode or 3.5 kV in the positive mode, capillary temperature = 300 °C, RF level = 40 %, auxiliary gas heater temperature = 325 °C. Mass detection was conducted with a resolution of 240,000 in full scan mode, with an AGC target of 3,000,000 and maximum injection time of 250 msec. Metabolites were detected over a mass range of 70-1050 *m/z*. Quantitation of all metabolites was performed using Tracefinder 4.1 (Thermo Scientific) referencing an in-house metabolite standards library using ≤ 5 ppm mass error. Metabolite abundances were quantified by comparing ion counts relative to cells reflecting the most unmodified metabolic state for each experiment (WT cells, vehicle treatment, AB cells, as indicated) from cells cultured in DMEM containing an electron acceptor (PYR or AKB, as indicated). In situations where the LCMS dataset contained one or more samples had high sample loading variance, all samples in that dataset were normalized to isotopically labeled loading controls (either valine D8 or U-^{13}C aspartate from ^{13}C amino acid mix) as annotated in Supplementary File 1. Isotopically labeled standards for NAD+ and NADH are not widely available, so LCMS experiments measuring NAD+/NADH ratios do not incorporate differences in ionization efficiencies or matrix effects for each analyte. Thus, while changes in the ratio of measured ion counts for NAD+ and NADH reflect biological changes, they should not be interpreted as an absolute intracellular ratio, which is more accurately quantified by enzymatic methods. Individual ion counts for NAD+ and NADH are available in Supplementary File 1. Data from stable isotope labeling

experiments includes correction for natural isotope abundance using IsoCor software v.2.2.

Complex I Activity Assay

Complex I activity was measured using an assay kit (Abcam, ab109721) according to the manufacturer's instructions. Absorbances at 450 nm were read every 30 seconds for 40 minutes on a Tecan Infinite M Plex microplate reader.

Gene Set Enrichment Analysis

Gene Set Enrichment Analysis (GSEA) (Subramanian et al., 2005) was conducted on the proteomics dataset utilizing 149 hierarchical, mitochondrial specific pathways curated by MitoCarta3.0 (Rath et al., 2021) as the *a priori* defined gene/protein sets. Proteins were ranked by the signed (negative or positive by the direction of the fold-change), -log of the adjusted p-value, both of which were calculated during differential expression analysis between LP and WT cells and used as input for GSEA. Individual MitoCarta3.0 pathways were evaluated for enrichment of upregulated proteins (positive normalized enrichment score) and downregulated proteins (negative normalized enrichment score). GSEA analysis was implemented in R (*R Core Team 2020*) (version 4.0.3) using the Bioconductor package fgsea (Korotkevich et al., 2021). Adjusted p-values and normalized enrichment scores have been reported.

Mouse Xenografts

All mouse work was performed in accordance with FHCC-approved IACUC protocol 51069 and AAALAS guidelines and ethical regulations. iNDI1 UOK269 cells were suspended in 100 µl PBS and injected subcutaneously into both flanks of ten 6–8-week-old, NSG (NOD.*Cg-Prkdc*^{scid}*Il2rg*^{tm1Wjl}/SzJ) male mice at 5 × 10^6 cells per injection. When tumors became palpable, one cage (n=5 mice per cage) was randomly assigned DOX chow with 625 mg/kg doxycycline hyclate (Envigo, TD.01306), while the other continued with standard chow. Tumor volumes were measured by calipers in two dimensions and estimated volumes were calculated using the equation $V = (\pi/6)(L \times W^2)$.

Statistical Analysis

All graphs and statistical analyses were made in GraphPad Prism 9.0. Technical replicates, defined as parallel biological samples independently treated, collected, and analyzed during the same experiment, are shown. Experiments were verified with independent repetitions showing qualitatively similar results. Details pertaining to all statistical tests can be found in the figure legends.

Chapter 3. Mitochondrial Redox Adaptations Enable Aspartate Synthesis in SDH-deficient Cancer Cells

Note: *This chapter is adapted from the manuscript published in eLife.*

Mitochondrial Redox Adaptations Enable Alternative Aspartate Synthesis in SDH-deficient Cells

Madeleine L. Hart[1,2], Evan Quon[1], Anna-Lena B. G. Vigil[1], Ian A. Engstrom[1], Oliver J. Newsom[1], Kristian Davidsen[1], Pia Hoellerbauer[1], Samantha M. Carlisle[3], and Lucas B. Sullivan[1]

[1]Human Biology Division, Fred Hutchinson Cancer Research Center, Seattle, WA, 98109, USA.

[2]Molecular Medicine & Mechanisms of Disease Program, University of Washington, Seattle, WA, 98109, USA.

[3]Department of Chemistry and Biochemistry, New Mexico State University, Las Cruces, NM, 88003, USA.

3.1 Introduction

Here we investigate the consequences of acute and chronic SDH deficiency and observe that SDH impairment causes aspartate-dependent proliferation defects. We begin by characterizing the metabolic and functional effects of an SDH inhibitor and comparing those effects to that of a complex I inhibitor. However, unlike impairments to other ETC complexes, exogenous electron acceptors are insufficient to restore aspartate levels and cell proliferation to SDH-deficient cells. Surprisingly, we find that additional impairment to ETC CI is required to enable aspartate synthesis and cell proliferation in SDH-deficient cells. CI inhibition decreases mitochondrial NAD+/NADH, which aspartate synthesis, thereby supporting proliferation in SDH-impaired cells. We observe that disrupting or restoring SDH prompts selective pressure for progressive changes in CI

activity to directly correspond to SDH activity, identifying distinct metabolic states that enable aspartate production. Altogether, our data reveal a novel metabolic relationship where compartmentalized redox changes are required to enact alternative aspartate biosynthetic pathways that support cell proliferation during TCA cycle dysfunction.

3.2 Contributions

M.L.H. and L.B.S. conceived of the project and performed all the experiments with assistance from E.Q., A.B.G.V., O.J.N., I.A.E., K.D., A.I. and P.H; E.Q. performed subcellular NAD+/NADH measurements. S.M.C. performed GSEA on our proteomics dataset. L.B.S. supervised the project. Ayaha Itokawa generated the data for figure 3.1A-B.

3.3 Results

SDH inhibition impairs proliferation, which is partially restored by electron acceptors but robustly restored by aspartate.

To understand the metabolic contributions of SDH/complex II (hereafter, SDH) to cell proliferation, we characterized the proliferative consequences of the inhibitors atpenin A5 (AA5), a specific inhibitor of SDH. First, we conducted a dose titration of AA5 (0, 0.156, 0.30125, 0.625, 1.25, 2.5, and 5 μM) on respiration-intact 143B osteosarcoma cells. At 5 μM, AA5 is sufficient to completely inhibit cell proliferation, which matches the consequences of all other ETC inhibitors in media lacking electron acceptors (Figure

3.1A) (Birsoy et al., 2015; L. B. Sullivan et al., 2015). Interestingly, the dose-dependent decrease in proliferation correlates to increases in median cell volume (Figure 3.1B). These data may indicate that nucleotide imbalance in these cells is impeding DNA synthesis and therefore evoking a state of replication stress (Diehl et al. 2022). Next, we conducted liquid chromatography-mass spectrometry (LCMS) metabolomics on cells treated with AA5 and as expected for SDH impairment, AA5 caused robust succinate accumulation and depleted fumarate levels (Figure 3.1C, 3.1D). Due to these findings, we selected a dose of 5 μM AA5 for most experiments presented in this dissertation. Since the contributions of SDH to the ETC are functionally independent from complex I, whose electrons account for the majority of respiration, it is not inherently obvious that SDH-deficient cells would be unable to maintain robust respiration activity. In support of this, we found that treatment with AA5 only partially impairs respiration after several hours of treatment, whereas the classic complex I inhibitor, rotenone, severely abrogates respiration within minutes (Figure 3.1E).

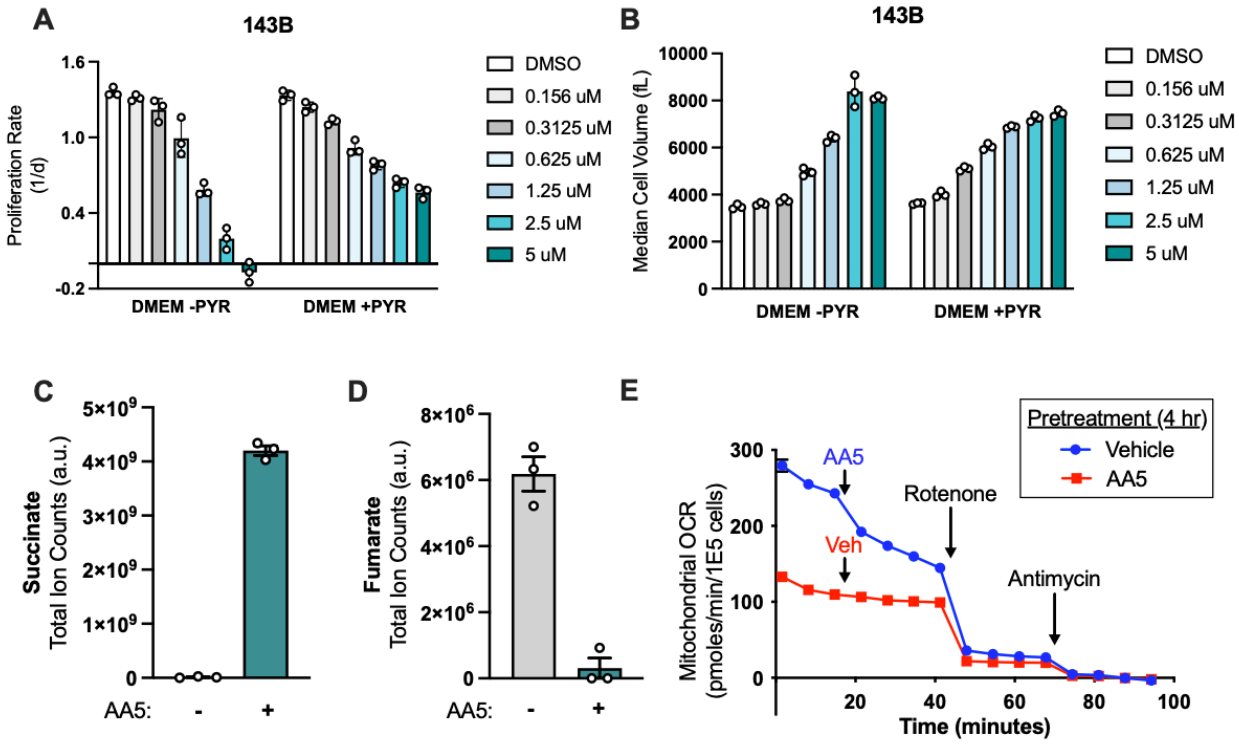

Figure 3.1. AA5 is a specific SDH inhibitor. A) Proliferation rates of respiration-intact 143B osteosarcoma cells treated with a dose titration of Atpenin A5 (AA5) (vehicle, 0.156, 0.3125, 0.625, 1.25, 2.5, and 5 μM) in pyruvate free DMEM or DMEM with 1 mM pyruvate. **B)** Median cell volume of 143B osteosarcoma cells treated with a dose titration of Atpenin A5 (AA5) (vehicle, 0.156, 0.3125, 0.625, 1.25, 2.5, and 5 μM) in pyruvate free DMEM or DMEM with 1 mM pyruvate. **C)** Succinate levels measured by LCMS metabolomics from 143B cells treated with vehicle (DMSO) or 5 μM AA5 for 6 hours (n=3). **D)** Fumarate levels measured by LCMS metabolomics from 143B cells treated with vehicle (DMSO) or 5 μM AA5 for 6 hours (n=3). **E)** Mitochondrial oxygen consumption rates in WT 143B cells pre-treated with vehicle (DMSO) or 5 μM AA5 for 4 hours, then injected with vehicle (DMSO) or 5 μM AA5 as indicated, followed by treatment of all conditions with 100 nM rotenone and 10 μM antimycin (n=3) in DMEM with 1 mM pyruvate.

Next, we compared proliferation rates of 143B cells treated with either AA5 or rotenone. Prior studies have shown that inhibitors of complex I, III, and IV all result in a complete abrogation of cell proliferation, also validating our choice to selection of the 5 μM dose of AA5 (Figure 3.1A) Both inhibitors effectively blocked cell proliferation when cultured in media without electron acceptors (DMEM without pyruvate), consistent with an essential role of mitochondrial metabolism in support of cell proliferation (Figure 3.2A). Previous work from us and others identified that supplementation with the exogenous

electron acceptors pyruvate (PYR) or alpha-ketobutyrate (AKB) can restore proliferation to cells with CI impairments by regenerating NAD+ to support aspartate biosynthesis (Birsoy et al., 2015; Sullivan et al., 2015). While we confirm that PYR and AKB can robustly restore proliferation upon rotenone treatment, proliferation of AA5 treated cells was only modestly improved by electron acceptor supplementation (Figure 3.2A). In contrast, aspartate supplementation equivalently, albeit incompletely, restored cell proliferation to both rotenone and AA5 treated cells (Figure 3.2A).

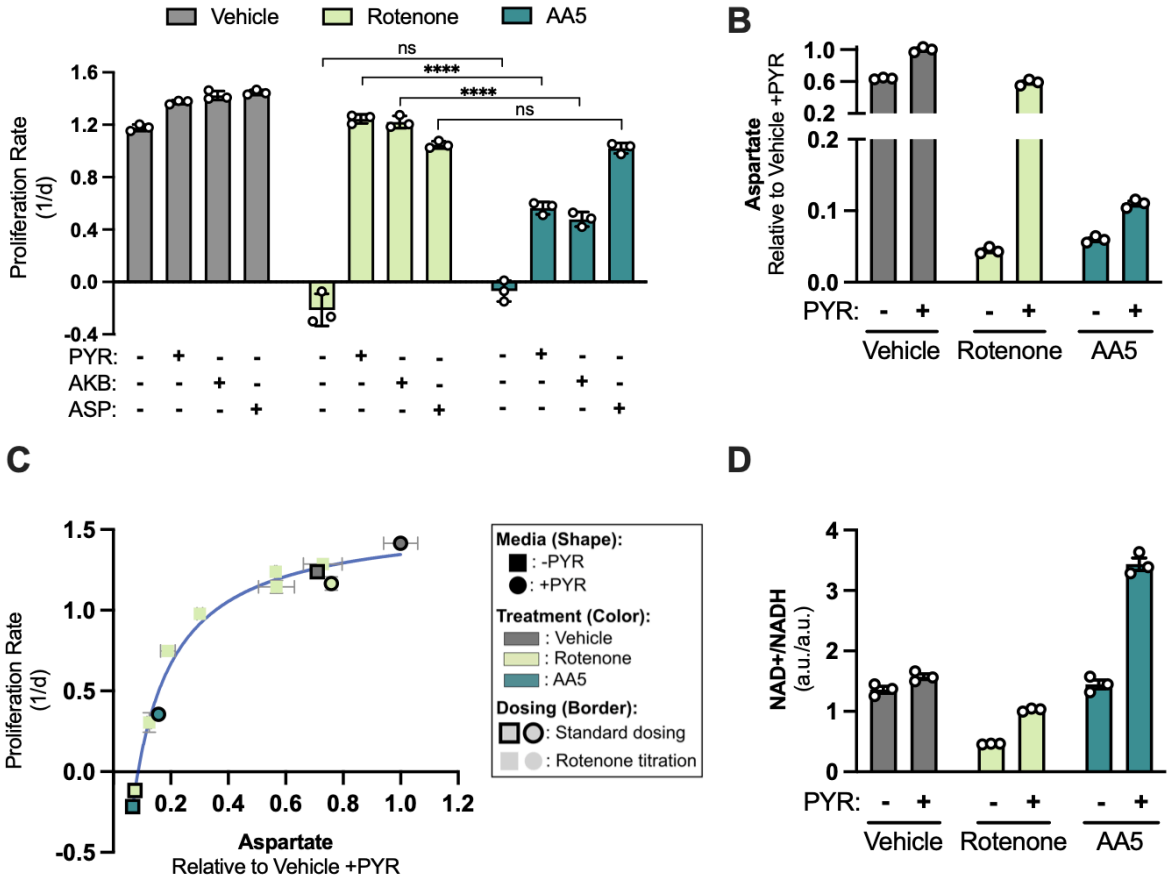

Figure 3.2. SDH inhibition blocks proliferation, which is incompletely rescued by electron acceptors but robustly restored by aspartate. A) Proliferation rates of 143B cells treated with vehicle (DMSO), 50 nM rotenone, or 5 μM atpenin A5 (AA5) cultured in pyruvate free DMEM with no addition, 1 mM pyruvate (PYR), 1 mM alpha-ketobutyrate (AKB), or 20 mM aspartate (ASP). **B)** Aspartate levels measured by liquid chromatography-mass spectrometry (LCMS) metabolomics in 143B cells, comparing normalized aspartate ion counts (a.u.; arbitrary units) from cells treated with vehicle (DMSO), 50 nM rotenone, or 5 μM AA5 in pyruvate free DMEM with no addition or 1 mM PYR for 6 hours (n=3). **C)** Proliferation rate (y-axis) versus

normalized aspartate levels (x-axis) of 143B cells after 6 hours of the indicated treatments (n=3). Data points without borders correspond to a dose titration of rotenone (25 12.5, 6.25, 3.125, 1.565 and 0 nM) in pyruvate free DMEM. Data points with a black border correspond to cells treated with standard dosing of 50 nM rotenone and 5 μM AA5 in DMEM, with and without pyruvate as indicated. See Supplementary Figure 1K-L for additional information. **D)** NAD+/NADH measured by LCMS metabolomics of 143B cells treated with vehicle (DMSO), 50 nM rotenone, or 5 μM AA5 in pyruvate free DMEM with no addition or 1 mM PYR for 6 hours (n=3). Data are plotted as means ± standard deviation (SD) and compared with an unpaired two-tailed student's t-test. $p<0.05$*, $p<0.01$**, $p<0.001$***, $p<0.0001$****

We next evaluated the metabolic differences between impairments to CI or SDH, consistent with aspartate being the mediator of proliferation defects from either inhibitor, aspartate levels were depleted by both drugs, fully restored by pyruvate in rotenone treated cells, and only partially increased in cells treated with AA5 (Figure 3.2B). Thus, although either inhibitor is associated with proliferation defects corresponding with aspartate levels, CI impairments have distinct metabolic phenotypes from SDH inhibition.

Next, we conducted liquid chromatography-mass spectrometry (LCMS) metabolomics on cells treated with either inhibitor, with or without pyruvate supplementation. While intracellular aspartate levels correlate with proliferation rate in our datasets of mitochondrial impaired cells, the quantitative relationship between the two is non-linear making it unclear how to predict the degree to which changes in aspartate levels will constitute a functionally meaningful change for proliferation rate (Figure 3.2A, 3.2B). To contextualize these findings, we generated a dose response curve measuring the effects of a range of rotenone concentrations on proliferation rate and intracellular aspartate levels, comparing them to SDH inhibition by AA5, with or without PYR treatment. Notably, combining these datasets revealed that the correlation between proliferation rate and aspartate levels was consistent across inhibitors and environmental conditions, manifesting as a hyperbolic relationship (Figure 3.2C). These data are

consistent with a model where the phenotypic consequences for changes in aspartate levels depend on the degree to which aspartate limits proliferative cell metabolism. Basal conditions are not aspartate-limited and so decreases in aspartate will only a have a small effect on cell proliferation; however, as aspartate becomes metabolically limited (around 0.4, compared to vehicle treated cells in media containing PYR), changes in aspartate have more severe consequences on cell proliferation, until aspartate levels are insufficient to support proliferation (around 0.05). These data therefore provide critical context to understand how changes in aspartate levels correspond to proliferation upon mitochondrial inhibition.

We next investigated how each inhibitor affects intracellular NAD+/NADH, a critical mediator of the effects of CI inhibition on aspartate levels and cell proliferation. Unlike with rotenone treatment, AA5 treatment was not associated with suppression of NAD+/NADH, breaking the direct correlation between NAD+/NADH, aspartate levels, and proliferation rate seen with rotenone and other CI inhibitors (Figure 3.2D) (Gui et al., 2016). Pyruvate supplementation increased NAD+/NADH in all cases; restoring NAD+/NADH in rotenone treated cells to near vehicle treated levels and increasing NAD+/NADH beyond vehicle treated cells upon AA5 treatment (Figure 3.2D). These data are consistent with a model where CI impairments suppress aspartate production by lowering NAD+/NADH and thereby slowing the oxidative TCA cycle, whereas SDH inhibition directly blocks the oxidative TCA cycle, impairing aspartate synthesis and NADH production (Figure 3.3A). Indeed, we measured M+4 aspartate in cells cultured in U-^{13}C glutamine, reflective of aspartate produced via canonical oxidative TCA cycle

activity and found that pyruvate treatment restores metabolic progression through the TCA cycle in rotenone treated cells but not in cells treated with AA5 (Figure 3.3B).

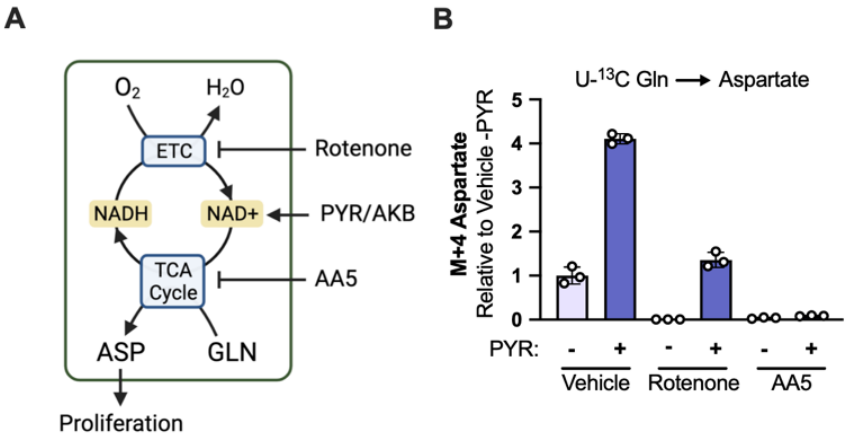

Figure 3.3. SDH inhibition blocks canonical aspartate synthesis, which is not restored by electron acceptors. A) Schematic showing that rotenone inhibits the ETC, blocking NADH oxidation causing an indirect TCA cycle impairment that can be overcome by exogenous electron acceptors (PYR/AKB), while AA5 directly blocks the TCA cycle and aspartate synthesis. **B)** M+4 aspartate levels measured by LCMS metabolomics from 143B cells cultured with pyruvate/glutamine free DMEM with 4 mM U-^{13}C glutamine and treated with vehicle (DMSO), 50 nM rotenone, or 5 μM AA5 in the absence and presence of 1 mM pyruvate for 6 hours (n=3).

Aspartate is poorly permeable to most cells even at supraphysiological concentrations, so we generated 143B cells expressing the glial-specific aspartate transporter SLC1A3, which we confirm supports aspartate uptake at micromolar extracellular concentrations (Figures 3.4A-C). Notably, improved aspartate uptake with SLC1A3 expression allowed aspartate to fully restore proliferation upon AA5 treatment, regardless of PYR co-treatment (Figure 3.4D). Similarly, orthogonal aspartate acquisition by intracellular expression of the guinea pig asparaginase (gpASNase1) combined with asparagine treatment was also able to restore proliferation to AA5 treated cells (Figure 3.4E-G) (L. B. Sullivan et al., 2018). These data indicate that aspartate is a primary metabolic limitation of SDH-impaired cells, consistent with previous findings (Cardaci et

al., 2015; Lussey-Lepoutre et al., 2015). However, these data also indicate that the metabolic determinants of aspartate limitation upon SDH inhibition are distinct from those of CI loss.

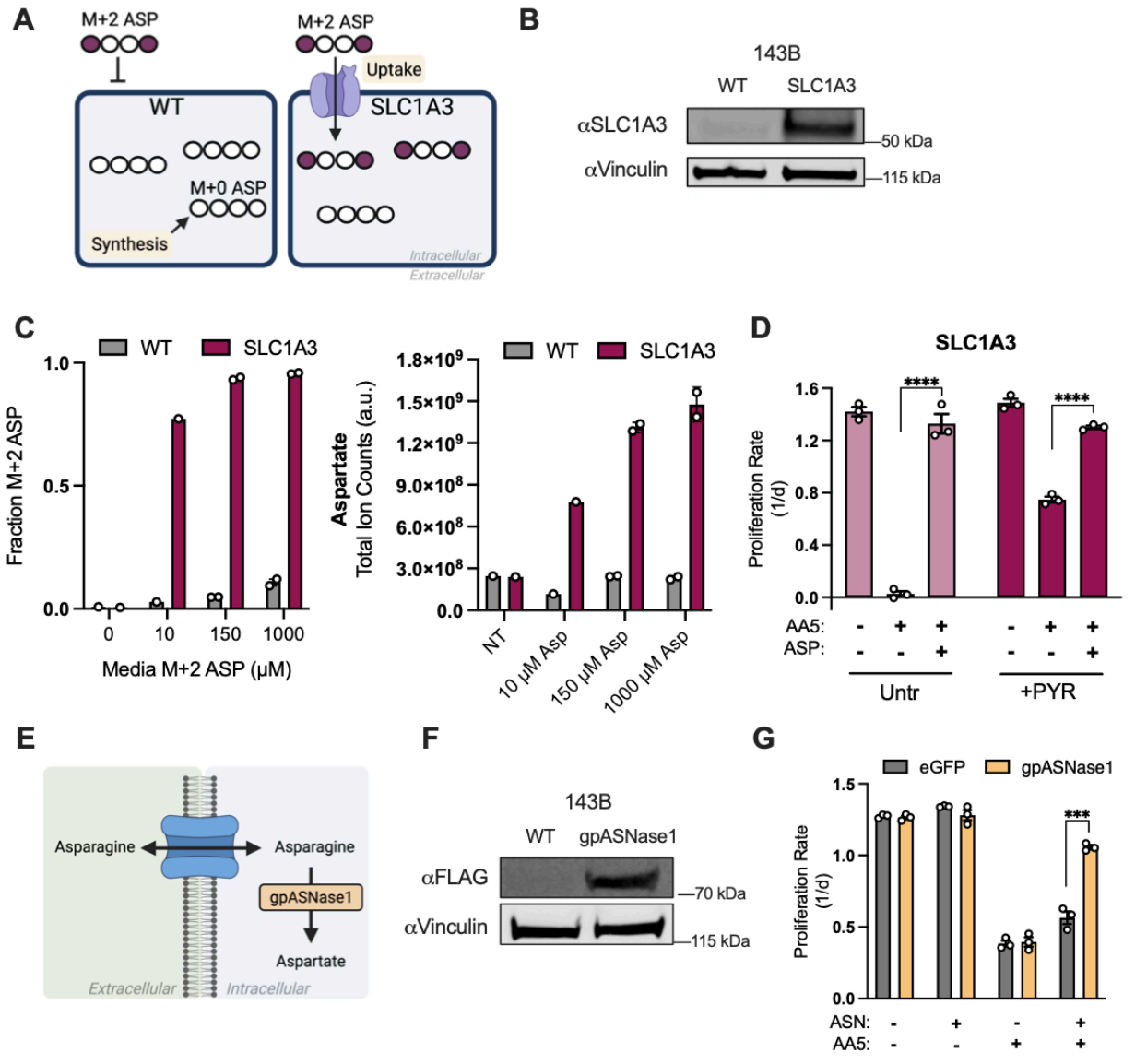

Figure 3.4. Alternative methods of aspartate acquisition and characterization of metabolic phenotypes in SDH-impaired cells. A) Schematic demonstrating how the aspartate transporter SLC1A3 allows for cells to uptake aspartate, which can be measured by the incorporation of isotopically labeled extracellular aspartate (M+2). **B)** Western blot for SLC1A3 and vinculin in 143B cells expressing SLC1A3 or wild type (WT) control 143B cells. Vinculin is used as a loading control. **C)** Fractional labeling of aspartate and total aspartate levels measured by LCMS metabolomics from 143B cells with or without SLC1A3 expression after 1 hour of exposure to the indicated concentrations of 1,4-^{13}C labeled (M+2) aspartate (n=1 or n=2). **D)** Proliferation rates of SLC1A3 expressing 143B cells treated with vehicle (DMSO), 5 μM AA5 or

5 μM AA5 and 1 mM aspartate in pyruvate-free DMEM with no addition or 1 mM pyruvate (n=3). **E)** Schematic depicting how expression of gpASNase1 permits environmental asparagine (ASN) to be used to support intracellular aspartate levels. **F)** Western blot for FLAG and tubulin from WT 143B cells and 143B cells expressing FLAG-tagged gpASNase1. Tubulin is used as a loading control. **G)** Proliferation rates of 143B cells expressing eGFP or gpASNase1 cultured in DMEM with 1 mM pyruvate and supplemented with vehicle (H_2O) or 1 mM asparagine (ASN) and treated with vehicle (DMSO) or 5 μM AA5 (n=3). Data are plotted as means ± standard deviation (SD) and compared with an unpaired two-tailed student's t-test. p<0.05*, p<0.01**, p<0.001***, p<0.0001****

We also evaluated the metabolic effects of alterations to SDH activity in UOK269 cells, a patient derived renal cell carcinoma cell line that arose from a heterozygous point mutation (R46Q) in SDHB and deletion of the other allele (Saxena et al., 2016). Re-expression of wild type SDHB in UOK269 cells had the expected metabolic effects by alleviating the accumulation of succinate and increasing aspartate levels (Figures 3.5A-C). Similar to 143B cells, an intact TCA cycle ameliorated the dependence of UOK269 cells on pyruvate or aspartate for cell proliferation (Figure 3.5D). However, in contrast to AA5 treated 143B cells, pyruvate and aspartate treatment were equally effective at restoring cell proliferation in UOK269 cells (Figure 3.5D). These data suggest that long-term SDH loss may be associated with metabolic adaptations that allow cells to fully take advantage of exogenous electron acceptors to restore aspartate and cell proliferation.

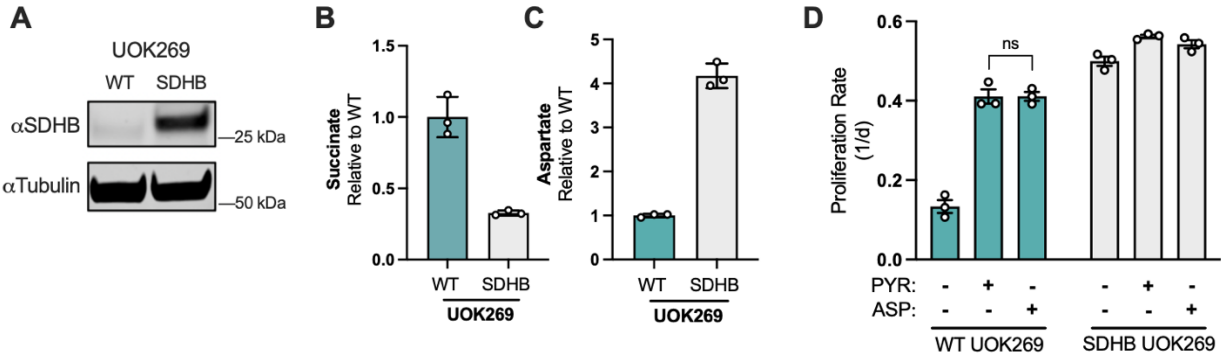

Figure 3.5. Proliferation of SDHB-mutant UOK269 cells is restored equally with either pyruvate or aspartate supplementation. A) Western blot for SDHB and α-tubulin (tubulin) in WT UOK269 cells or UOK269 cells with restoration of SDHB (SDHB UOK269) as indicated. Tubulin is used as a loading control. **B)** Relative succinate levels measured by LCMS metabolomics from WT and SDHB UOK269 cells in DMEM

with 1 mM pyruvate for 6 hours (n=3). **C)** Relative aspartate levels measured by LCMS metabolomics from WT and SDHB UOK269 cells in DMEM with 1 mM pyruvate for 6 hours (n=3). **D)** Proliferation of WT UOK269 and SDHB UOK269 cells cultured in pyruvate free DMEM supplemented with vehicle (H_2O), 1 mM PYR, or 20 mM ASP (n=3). Data are plotted as means ± standard deviation (SD) and compared with an unpaired two-tailed student's t-test. p<0.05*, p<0.01**, p<0.001***, p<0.0001****

CI inhibition promotes aspartate synthesis and cell proliferation in SDH-deficient cancer cells

We next questioned what metabolic adaptations may occur in SDH-deficient cells to promote cell proliferation. Intriguingly, several cell lines generated with genetic defects in SDH components have diminished respiration rates (Cardaci et al., 2015; Lorendeau et al., 2017; Saxena et al., 2016). One potential explanation for the respiration loss in SDH-mutant cells is the observation that they manifest with decreased CI expression and activity (Cardaci et al., 2015; Lorendeau et al., 2017, Saxena et al., 2016). Indeed, it was reported that dual inhibition of SDH and CI is required to mimic the metabolic phenotype of SDH-mutant cancer cells (Lorendeau et al., 2017). Nonetheless, while these data suggest that CI loss may serve a metabolic role in SDH-deficient cells, no functional benefit for CI loss in this context has yet been described.

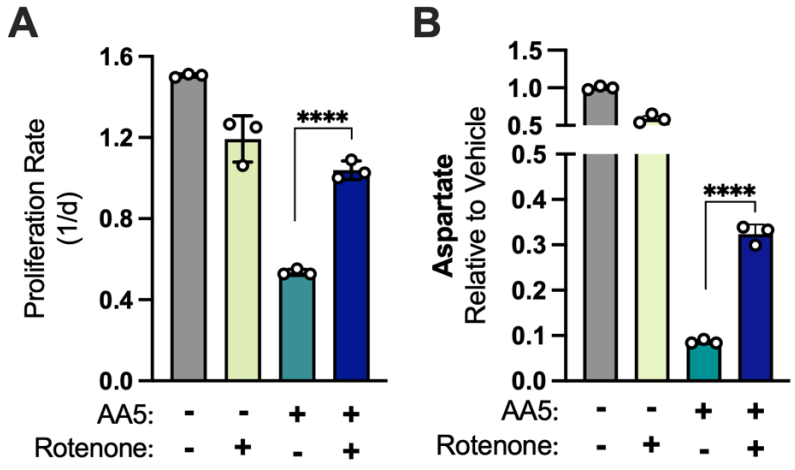

Figure 3.6. CI inhibition is sufficient to induce aspartate synthesis and cell proliferation in SDH-deficient cancer cells. A) Proliferation rates of 143B cells cultured in DMEM with 1 mM PYR treated with

vehicle (DMSO), 50 nM rotenone, 5 μM AA5, or 5 μM AA5 and 50 nM rotenone (n=3). **B)** Aspartate levels of 143B cells cultured in DMEM with 1 mM PYR treated with vehicle (DMSO), 50 nM rotenone, 5 μM AA5, or 5 μM AA5 and 50 nM rotenone for 6 hours (n=3). Data are plotted as means ± standard deviation (SD) and compared with an unpaired two-tailed student's t-test. $p<0.05$*, $p<0.01$**, $p<0.001$***, $p<0.0001$****

We tested if, in the presence of electron acceptors, rotenone could alter the proliferation of cells treated with AA5 and, surprisingly, found it caused a robust restoration of cell proliferation (Figure 3.6A). Since aspartate levels define the proliferation rate of SDH-impaired cells, we then measured aspartate levels and found that CI co-inhibition partially restored aspartate to SDH-impaired cells to a level consistent with their improved proliferation rate (Figure 3.2C, Figure 3.6B). CI co-inhibition also restored proliferation and increased aspartate levels across a panel of diverse human cell lines treated with AA5, including both transformed (A549, HCT116) and non-transformed (293T, TF-1) cells, indicating that this metabolic relationship was generalizable (Figure 3.7A, 3.7B). To test these effects genetically, we used CRISPR/Cas9 to generate gene knockouts (KO) of SDHB, the most frequently mutated subunit in SDH-null human cancers (Amar et al., 2007; Badenhop et al., 2004; Klein et al., 2008; Linehan & Ricketts, 2013).

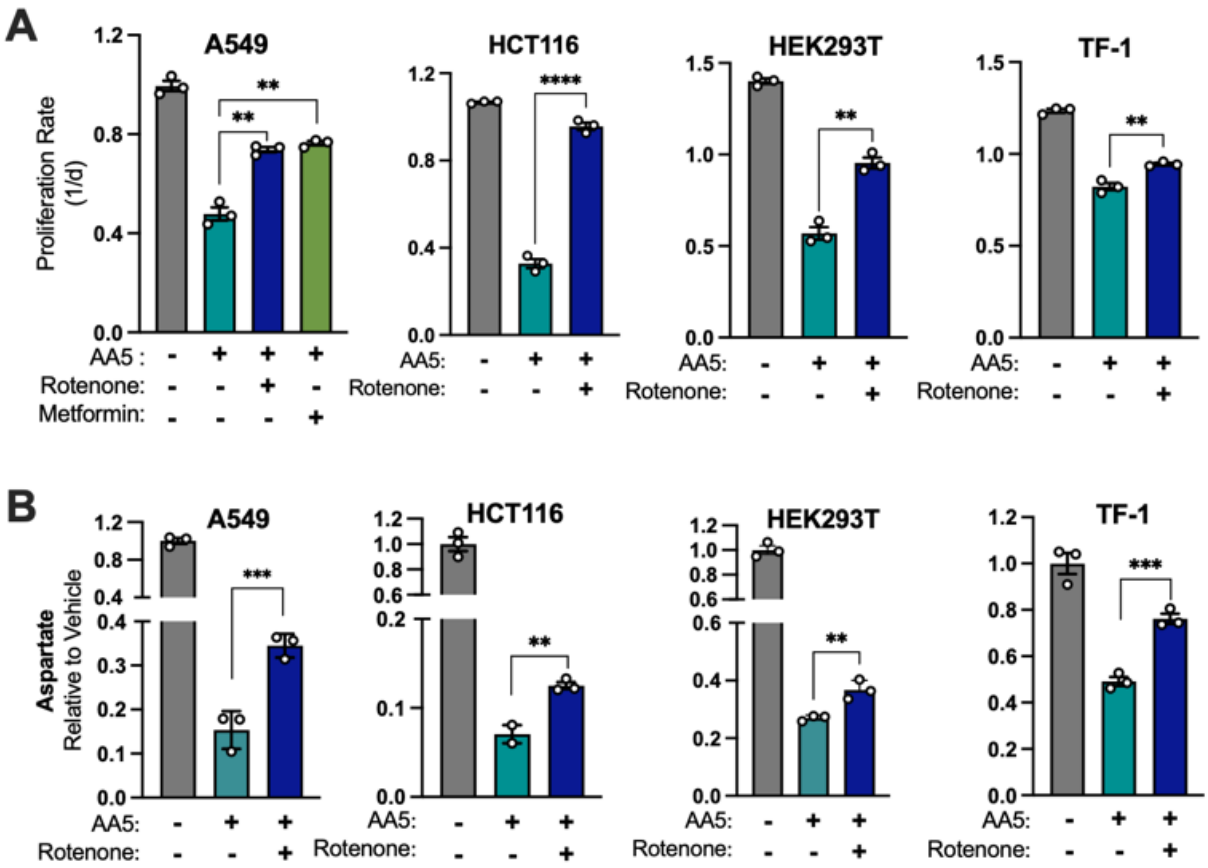

Figure 3.7. CI inhibition is sufficient to increase aspartate synthesis and proliferation in several cell lines. A) Proliferation rates of A549, HCT116, HEK293T, and TF-1 cells cultured in DMEM with 1 mM pyruvate and treated with vehicle (DMSO), AA5, or AA5 and rotenone. A549 cells were treated with 2.5 μM AA5, 80 nM rotenone, and 500 μM metformin and HCT116, HEK293T, and TF-1 cells were treated with 5 μM AA5 and 50 nM rotenone (n=3). **B)** Relative aspartate levels measured by LCMS metabolomics of A549, HCT116, HEK293T, and TF-1 cells cultured in DMEM with 1 mM pyruvate and treated with vehicle (DMSO), AA5, or AA5 and rotenone for 6 hours as done above in A (n=3). Data are plotted as means ± standard deviation (SD) and compared with an unpaired two-tailed student's t-test. $p<0.05$*, $p<0.01$**, $p<0.001$***, $p<0.0001$****

While we were able to achieve efficient disruption of SDHB, with ~96% loss in 143B cells, we were initially unable to generate single cell SDHB KO clones in standard media (Figure 3.8A, 3.8B). Based on our previous observations, we repeated colony selection with or without rotenone and found that CI inhibition was sufficient for successful generation of clones from Cas9/sgSDHB nucleofected 143B cells (Figure 3.8B). We isolated one SDHB KO clone and found their proliferation was slowed relative to their

parental cells but was improved by treatment with the CI inhibitors rotenone or metformin, or by supplementation with aspartate (Figures 3.8C, 3.8D). We then measured aspartate levels in WT and the same SDHB KO clone with or without rotenone treatment and found that rotenone decreases aspartate levels in WT cells but increases aspartate in SDHB KO cells, consistent with proliferation restoration (Figure 3.8E). We also restored SDHB expression and found that it rescued proliferation to parental rates and reinstated wild type relationships with rotenone and AA5 treatment (Figures 3.8F, 3.8G). Our data demonstrate that CI inhibition is sufficient to induce aspartate levels and cell proliferation in diverse cell lines and media conditions upon SDH disruption (Figure 3.8H).

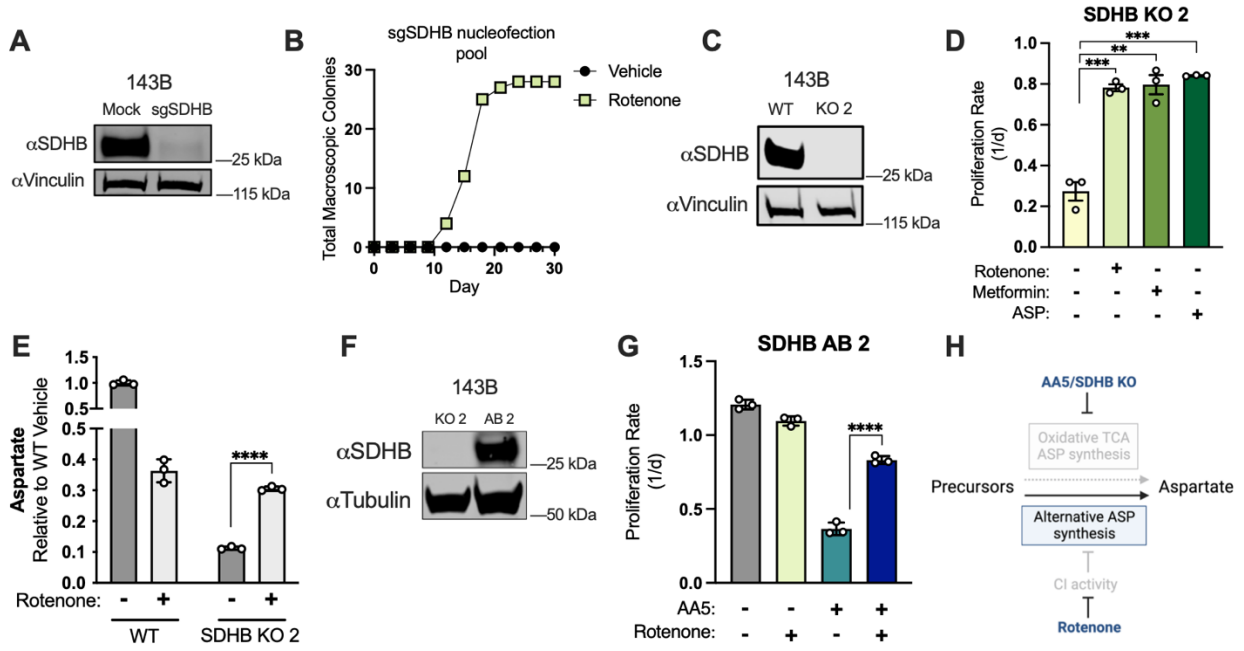

Figure 3.8. CI inhibition is sufficient to induce aspartate synthesis and cell proliferation in SDHB KO cancer cells. A) Western blot for SDHB and vinculin from 143B cells 3 days after nucleofection with plasmid GFP (Mock) or sgRNAs and sNLS-SpCas9 for SDHB as indicated. Vinculin is used as a loading control. **B)** Number of single cell clones that formed colonies from sgSDHB pool in 143B cells treated with vehicle (DMSO) or 30 nM rotenone during a 30-day period. **C)** Western blot for SDHB and vinculin from WT 143B cells and SDHB KO 143B clone 2. Vinculin is used as a loading control. **D)** Proliferation rates of SDHB KO 143B cells (clone 2) cultured in DMEM with 1 mM PYR and treated with vehicle (DMSO), 50 nM rotenone, 1 mM metformin, or 20 mM ASP (n=3). **E)** Aspartate levels measured by LCMS metabolomics of WT 143B cells and SDHB KO 2 cells cultured in DMEM with 1 mM PYR and treated with vehicle (DMSO) or 50 nM rotenone for 6 hours (n=3). **F)** Western blot for SDHB and tubulin from SDHB KO clone 2 (KO 2) and the

cells with SDHB cDNA added back (AB 2). Tubulin was used as a loading control. **G)** Proliferation rates of SDHB AB 2 cells treated with vehicle (DMSO), 50 nM rotenone, 5 μM AA5, or 5 μM AA5 and 50 nM rotenone (n=3). **H)** Schematic showing that CI inhibition promotes alternative aspartate synthesis pathways upon SDH disruption). Data are plotted as means ± standard deviation (SD) and compared with an unpaired two-tailed student's t-test. $p<0.05$*, $p<0.01$**, $p<0.001$***, $p<0.0001$****

To validate that our results weren't an artifact of nucleofection and single cell cloning, we confirmed that four more KO clones were devoid of SDHB expression and they followed the same proliferation trend as Figure 3.8D when treated with rotenone, metformin or aspartate (Figures 3.9A, 3.9B). We also found that AA5 treatment of an SDHB KO clone had no significant effects on proliferation, aspartate levels or the NAD+/NADH ratio, indicating on-target effects of AA5 (Figure 3.9C-E). Finally, to test if this metabolic relationship was an artifact of our cell culture media choice, which contains high levels of pyruvate, we also tested the effects of SDH inhibition in 143B cells cultured in Human Plasma-Like Media (HPLM), which closely matches the nutrient composition of human plasma (Cantor et al., 2017). We found that AA5 still impaired cell proliferation and that rotenone or aspartate co-treatment restored cell proliferation in HPLM (Figure 3.9F).

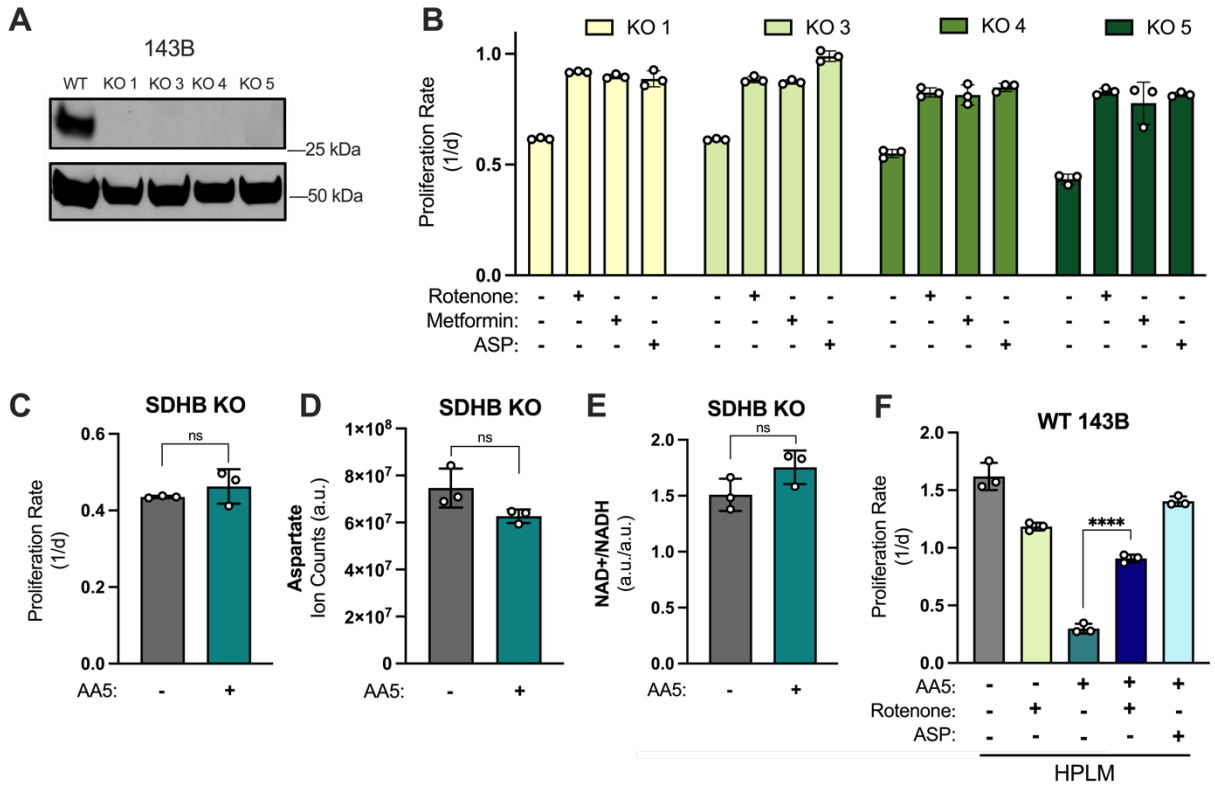

Figure 3.9. Characterization of interactions between CI inhibition and SDH status. A) Western blot for SDHB and tubulin from WT 143B cells and four SDHB KO 143B clones. Tubulin is used as a loading control. **B)** Proliferation rates of corresponding SDHB KO clones from (D) treated with vehicle (DMSO), 50 nM rotenone, 1 mM metformin, or 20 mM ASP in DMEM with 1 mM pyruvate (n=3). **C)** Proliferation rates of SDHB KO 143B cells (clone 5) treated with either vehicle (DMSO) or 5 μM AA5 in DMEM with 1 mM pyruvate (n=3). **D)** Aspartate levels measured by LCMS metabolomics from SDHB KO 143B cells (clone 5) treated with either vehicle (DMSO) or 5 μM AA5 in DMEM with 1 mM pyruvate for 6 hours (n=3). **E)** NAD+/NADH measured by LCMS metabolomics of SDHB KO 143B cells (clone 5) treated with either vehicle (DMSO) or 5 μM AA5 in DMEM with 1 mM pyruvate for 6 hours (n=3). **F)** Proliferation rates of WT 143B cells cultured in HPLM and treated with vehicle (DMSO), 50 nM rotenone, 5 μM AA5, 5 μM AA5 and 50 nM rotenone, or 5 μM AA5 and 20 mM ASP (n=3). HPLM contains 50 μM pyruvate. Data are plotted as means ± standard deviation (SD) which are and compared with an unpaired two-tailed student's t-test. $p<0.05$*, $p<0.01$**, $p<0.001$***, $p<0.0001$****

Mitochondrial redox alterations are required for CI inhibition to rescue SDH-deficient cells

We next investigated the metabolic mechanism for how CI impairment could be providing a benefit to SDH-deficient cells. CI activity contributes to several metabolic

processes, including NADH oxidation, mitochondrial membrane potential generation, and the reduction of ubiquinone (Figure 3.10A). To ascertain which of these processes is deleterious to SDH-deficient cells, we co-treated cells with AA5 and conditions that target other aspects of the ETC and oxidative phosphorylation. While rotenone directly inhibits CI, the complex III inhibitor Antimycin A similarly impairs NADH oxidation and mitochondrial membrane potential generation but differs from CI inhibition by preventing ubiquinol oxidation (Figure 3.10A). Oligomycin blocks the IMM complex ATP synthase, inhibiting mitochondrial membrane potential utilization, inducing hyperpolarization of the IMM, and thereby causing collateral inhibition of ETC activity. Oligomycin treatment therefore similarly impairs NADH oxidation but differs from CI inhibitors by increasing the mitochondrial membrane potential and slowing electron flux through all three proton pumping complexes (Figure 3.10A). Lastly, hypoxia limits the terminal electron acceptor activity of complex IV, slowing upstream ETC function (Figure 3.10A). Importantly, we found that treatment with antimycin or oligomycin can substitute for CI inhibitors, albeit less effectively, to restore the proliferation and aspartate levels of AA5 treated cells (Figure 3.10B, 3.10C). Gratifyingly, since complex III inhibition collaterally impairs both complex I and II, antimycin treatment alone had near identical effects on aspartate levels and proliferation as AA5 and rotenone cotreatment (Figure 3.10B, 3.10C). Finally, culturing cells in severe hypoxia (1%) was sufficient to improve the proliferation of SDH-impaired cells, albeit to a smaller degree than CI inhibition, while physiological O_2 tensions (3-11%) had little effect on the proliferation of AA5 treated cells (Figure S3.10D). Collectively, these results suggest that the shared effect of each treatment on mitochondrial NAD+/NADH, rather than other downstream effects on ETC function, is

likely a primary mechanism by which ETC inhibition supports aspartate production and proliferation in SDH-deficient cells.

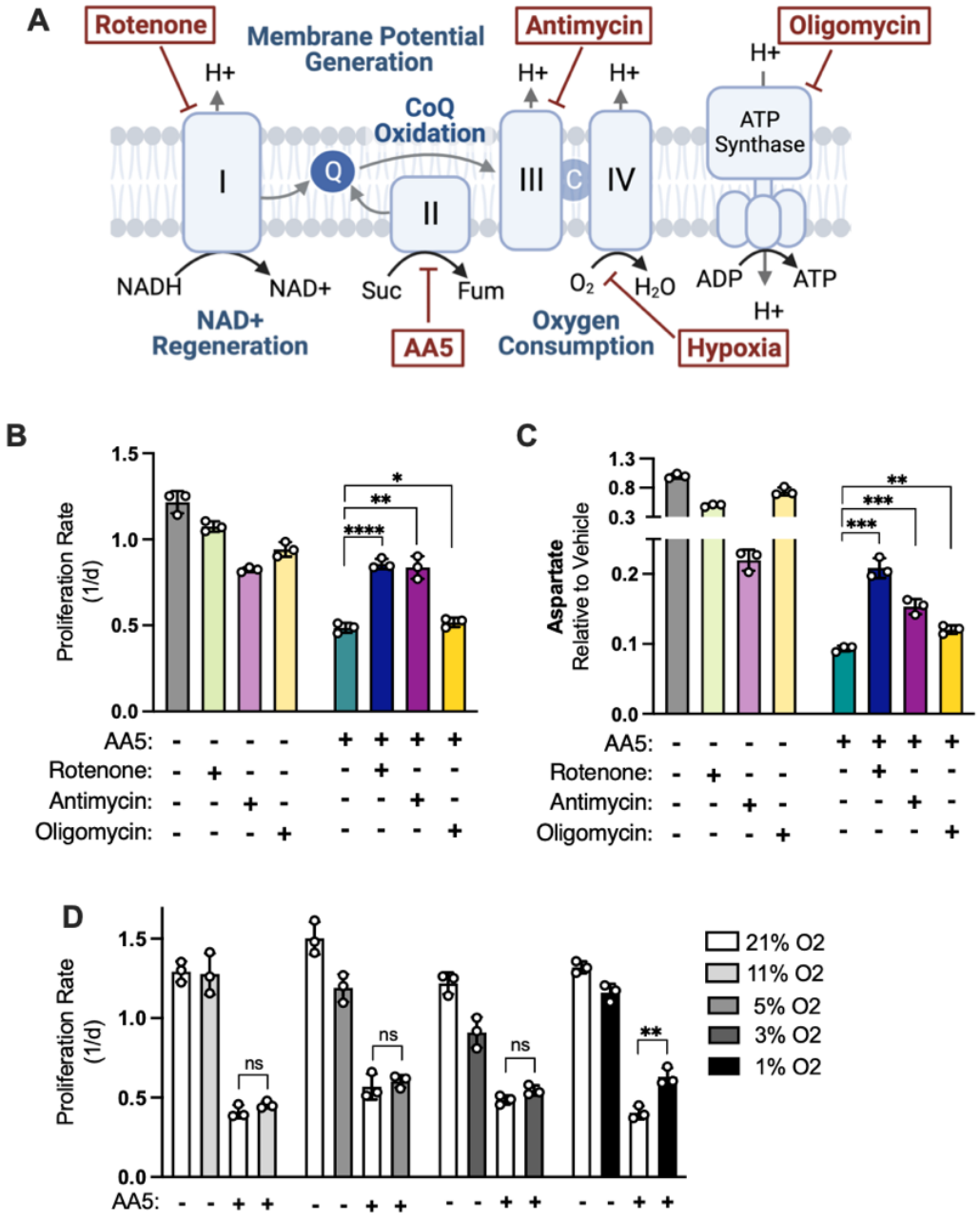

Figure 3.10. Effects of ETC inhibition in SDH-deficient cells. A) Schematic showing the metabolic roles of the electron transport chain and ATP synthase and depicting the sites of action for rotenone, AA5, antimycin A, hypoxia, and oligomycin. **B)** Proliferation rates of WT 143B cells cultured in DMEM with 1 mM pyruvate and treated with vehicle (DMSO), 50 nM rotenone, 5 μM AA5, 800 nM Antimycin A, 1 μM oligomycin, and 5 μM AA5 and 50 nM rotenone, 5 μM AA5 and 800 nM Antimycin A, or 5 μM AA5 and 1 μM oligomycin (n=3). **C)** Relative aspartate levels measured by LCMS metabolomics of WT 143B cells

cultured in DMEM with 1 mM pyruvate and treated with vehicle (DMSO), 50 nM rotenone, 5 μM AA5, 800 nM Antimycin A, 1 μM oligomycin, and 5 μM AA5 and 50 nM rotenone, 5 μM AA5 and 800 nM Antimycin A, or 5 μM AA5 and 1 μM oligomycin for 6 hours (n=3). **D)** Proliferation rates of WT 143B cells cultured in DMEM with 1 mM pyruvate and treated with either with vehicle (DMSO) or 5 μM AA5. Experiments were done in 11, 5, 3, and 1% O_2, with paired control conditions at 21% O_2 shown for each experiment (n=3). Data are plotted as means ± standard deviation (SD) and compared with an unpaired two-tailed student's t-test. $p<0.05$*, $p<0.01$**, $p<0.001$***, $p<0.0001$****

To investigate how CI inhibition changes the redox state of SDH-impaired cells, we measured the effects of co-inhibition on NAD+/NADH by LCMS. While AA5 treatment alone increased NAD+/NADH in the presence of pyruvate, as in Figure 1D, the effects of rotenone co-treatment were epistatic to AA5 treatment and reduced cellular NAD+/NADH to that of cells treated with rotenone alone (Figure 3.11A). The increase in NAD+/NADH in cells upon SDH impairment alone is thus likely a consequence of decreased NADH production in the TCA cycle coinciding with persisting NADH oxidation by active mitochondrial CI. We next adapted a selective membrane permeabilization protocol to rapidly isolate and extract metabolites from the cytosol and mitochondria and used an enzymatic assay that enables low sample inputs to measure NAD+/NADH in each compartment (Figure 3.11B) (Lee et al., 2019; L. B. Sullivan et al., 2015). As expected, in vehicle treated conditions, mitochondrial NAD+/NADH was lower than cytosolic NAD+/NADH (Figure 3.11C) (Williamson et al., 1967). In addition, the effects on NAD+/NADH from rotenone and/or AA5 treatment were predominantly observed at their site of action in the mitochondria (Figure 3.11C). Notably, the absence of changes to cytosolic NAD+/NADH upon mitochondrial inhibitor treatments is expected in this context due to exogenous pyruvate pinning cytosolic NAD+/NADH through lactate dehydrogenase activity.

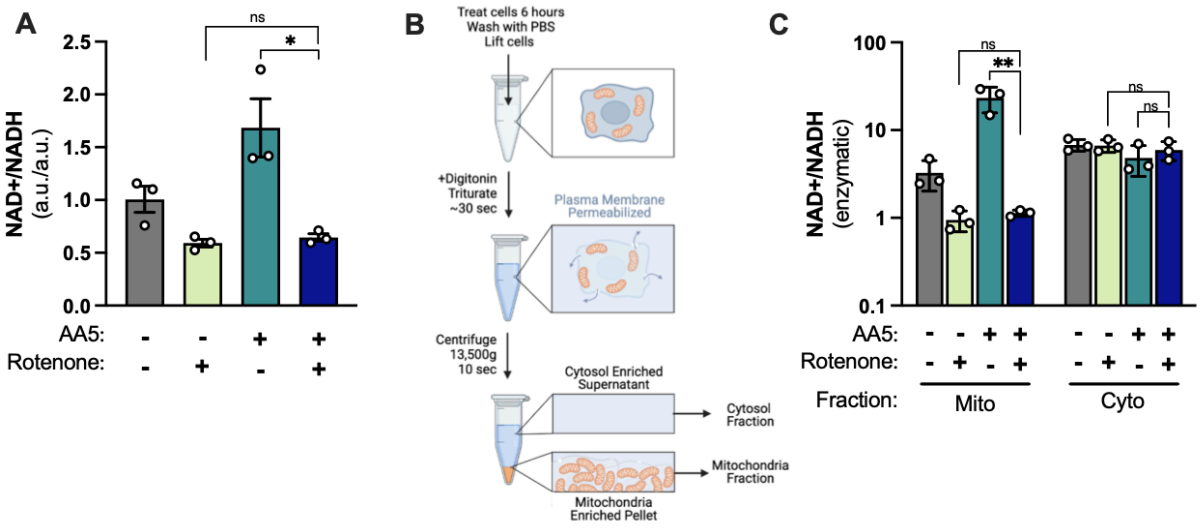

Figure 3.11. CI inhibition decreases mitochondrial NAD+/NADH. A) Whole cell NAD+/NADH measured by LCMS metabolomics of 143B cells cultured in DMEM with 1 mM PYR and treated with vehicle (DMSO), 50 nM rotenone, 5 μM AA5, or 5 μM AA5 and 50 nM rotenone for 6 hours (n=3). **B)** Diagram showing how mitochondrial fractions were obtained for the compartmentalized NAD+/NADH ratio measurements in Figure 3B. Protocol adapted from Lee et al. 2019. **C)** Cytosolic and mitochondrial NAD+/NADH measured by enzymatic assay of 143B cells cultured in DMEM with 1 mM PYR and treated with vehicle (DMSO), 50 nM rotenone 5 μM AA5, or 5 μM AA5 and 50 nM rotenone for 6 hours (n=3). Data are plotted as means ± standard deviation (SD) with the exception of A which is plotted as means ± standard error of the mean (SEM) and compared with an unpaired two-tailed student's t-test. $p<0.05$*, $p<0.01$**, $p<0.001$***, $p<0.0001$****

We next asked if mitochondrial NAD+/NADH alterations are required for the proliferation benefits of CI inhibition in SDH-impaired cells. To do so, we expressed cytosolic or mitochondrial-targeted FLAG-tagged *Lactobacillus brevis* NADH oxidase (cyto*LbNOX*/mito*LbNOX*) in 143B cells, an enzyme that directly utilizes molecular oxygen to oxidize NADH to NAD+ without requiring ETC function or other carbon substrates (Figure 3.12A) (Titov et al., 2016). Subcellular fractionation and immunoblotting verified successful subcellular targeting, as each construct was enriched in its expected compartment (Figure 3.12B). Notably, since these cells are cultured in the presence of the cytosolic electron acceptor pyruvate, we thus expected cyto*LbNOX* to be redundant and ineffective to change cell metabolism, whereas mitoLbNOX would be positioned to

disrupt the mitochondrial redox changes from rotenone treatment. Indeed, whereas cells expressing cyto*LbNOX* behaved similarly to parental cells expressing eGFP, mito*LbNOX* expression impeded the restorative effect of rotenone treatment on SDH-impaired cell proliferation (Figure 3.12C). Moreover, the increase in aspartate levels upon rotenone co-treatment was similarly diminished by mito*LbNOX* expression, but not by cyto*LbNOX* expression (Figure 3.12D). These data indicate that decreased mitochondrial NAD+/NADH is required for the benefits of CI inhibition when SDH is impaired (Figure 3.12E).

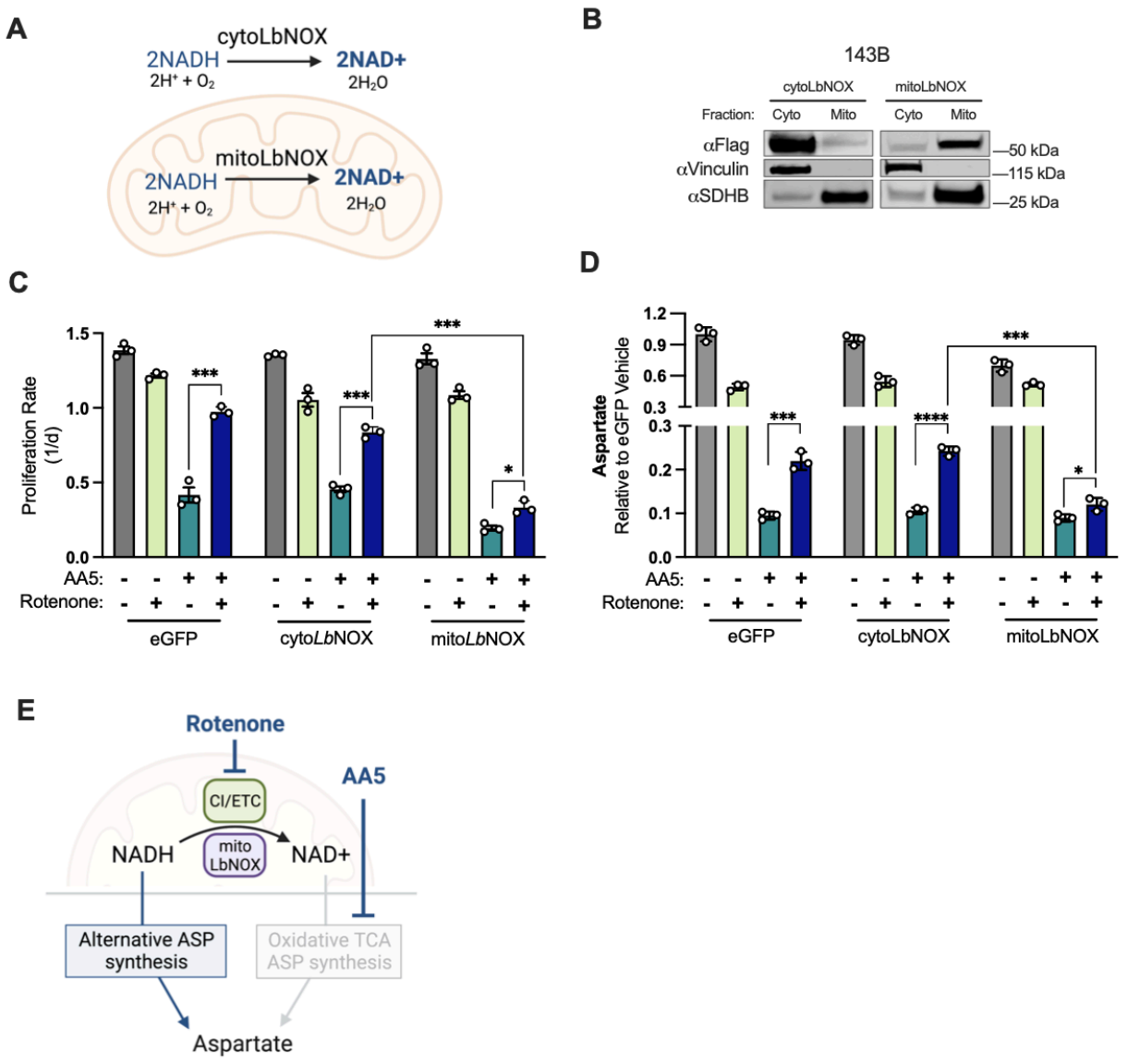

Figure 3.12. CI inhibition decreases mitochondrial NAD+/NADH, which is required for aspartate synthesis and proliferation in SDH-impaired cells. A) Schematic depicting the functions of FLAG-tagged cyto*LbNOX* and mito*LbNOX* is each compartment as indicated. **B)** Western blot for FLAG, Vinculin, and SDHB from 143B cells expressing FLAG-tagged cyto*LbNOX* or mito*LbNOX*, in cytosolic or mitochondrial fractions isolated by differential centrifugation. Vinculin is a loading control for cytosol and SDHB is a loading control for mitochondria. **C)** Proliferation rates of eGFP, cyto*LbNOX,* and mito*LbNOX* expressing 143B cells cultured in DMEM with 1 mM PYR treated with vehicle (DMSO), 50 nM rotenone, 5 μM AA5, or 5 μM AA5 and 50 nM rotenone (n=3). **D)** Aspartate levels measured by LCMS metabolomics of eGFP, cyto*LbNOX,* and mito*LbNOX* expressing 143B cells cultured in DMEM with 1 mM PYR and treated with vehicle (DMSO), 50 nM rotenone, 5 μM AA5, or 5 μM AA5 and 50 nM rotenone for 6 hours (n=3). **E)** Schematic showing how compartment-specific mitochondrial redox alterations promote alternative aspartate synthesis pathways in SDH-impaired cells. Data are plotted as means ± standard deviation (SD) and compared with an unpaired two-tailed student's t-test. $p<0.05$*, $p<0.01$**, $p<0.001$***, $p<0.0001$****

We next asked if decreased mitochondrial NAD+/NADH was sufficient to improve SDH-deficient cell function without CI inhibition. Another determinant of mitochondrial NAD+/NADH is the pyruvate dehydrogenase (PDH) reaction, which converts NAD+ to NADH (Figure S3.13A). The drug AZD7545 can disinhibit PDH to increase its activity by blocking regulation by pyruvate dehydrogenase kinases (PDKs) (Morrell et al., 2003). In the context of electron acceptor limitation, AZD7545 can further drive down NAD+/NADH and impair cell function (Luengo et al., 2021); however, our data indicate that lowering mitochondrial NAD+/NADH is beneficial in SDH-deficient cells, so we hypothesized that AZD7545 may instead provide a benefit in this context. To ensure that the AZD7545 mechanism of action functions independently of CI inhibition, we confirmed that AZD7545 treatment does not impair mitochondrial oxygen consumption in AA5 treated cells (Figure S3.13B). Additionally, AA5 treated cells co-treated with AZD7545 maintained and marginally increased ^{13}C glucose-derived cis-aconitate levels, whereas rotenone co-treatment depleted them, highlighting the distinct mechanisms by which these inhibitors drive mitochondrial metabolic changes (Figure S3.13C). Importantly, treatment with AZD7545 also slightly improved cell proliferation and increased aspartate levels in AA5 treated cells (Figure S3.13D, S3.13E). Notably, these effects are likely limited by the fact that they are occurring in the presence of intact CI activity, which would likely buffer major changes in mitochondrial NAD+/NADH. Nonetheless, these data provide additional support that compartment-specific mitochondrial redox alterations are both sufficient and required to reprogram aspartate synthesis in SDH-impaired cells (Figure 3.12E).

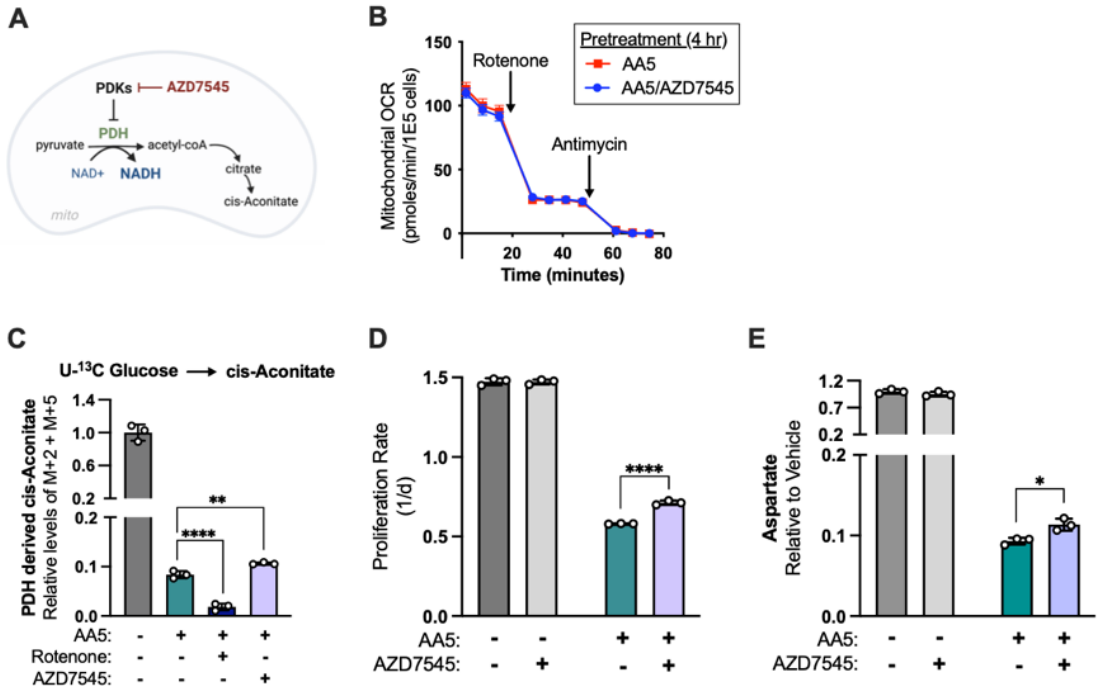

Figure 3.13. Effects of PDK inhibition in SDH-deficient cells. A) Schematic showing the mechanism of action of AZD7545 to activate pyruvate dehydrogenase (PDH) by inhibition of the negative regulators of PDH, pyruvate dehydrogenase kinases (PDKs). **B)** Mitochondrial oxygen consumption rates of WT 143B cells in DMEM with 1 mM pyruvate and pre-treated for 4 hours with 5 μM AA5 or 5 μM AA5 and 5 μM AZD7545 with indicated injections of 100 nM rotenone and 10 μM antimycin (n=3). **C)** Combined M+2 and M+5 cis-aconitate levels relative to vehicle treated cells measured by LCMS metabolomics from WT 143B cells cultured in glucose/pyruvate-free DMEM with ^{12}C 1 mM AKB and 25 mM U-^{13}C glucose and treated with vehicle (DMSO), 5 μM AA5, 5 μM AA5 and 50 nM rotenone, or 5 μM AA5 and 5 μM AZD7545 for 6 hours (n=3). **D)** Proliferation rates of WT 143B cells cultured in DMEM with 1 mM pyruvate and treated with vehicle (DMSO), 5 μM AA5, 5 μM AZD7545, or 5 μM AA5 and 5 μM AZD7545 (n=3). **E)** Aspartate levels measured by LCMS metabolomics of WT 143B cells cultured in DMEM with 1 mM pyruvate and treated with vehicle (DMSO), 5 μM AA5, 5 μM AZD, or 5 μM AA5 and 5 μM AZD for 6 hours (n=3). Data are plotted as means ± standard deviation (SD) except in B which are means ± standard error of the mean (SEM) and compared with an unpaired two-tailed student's t-test. p<0.05*, p<0.01**, p<0.001***, p<0.0001****

SDHB-null cells adapt through progressive complex I loss

While conducting these studies, we also generated a monoclonal SDHB KO HEK293T cell line, which, as expected, had a proliferation defect that was ameliorated by CI inhibition (Figure 3.14A, 3.14B). Interestingly, after several months of passaging, we observed that the basal proliferation rate of SDHB KO HEK293T cells progressively increased, and that the proliferation benefit of CI inhibition was lost (Figure 3.14B).

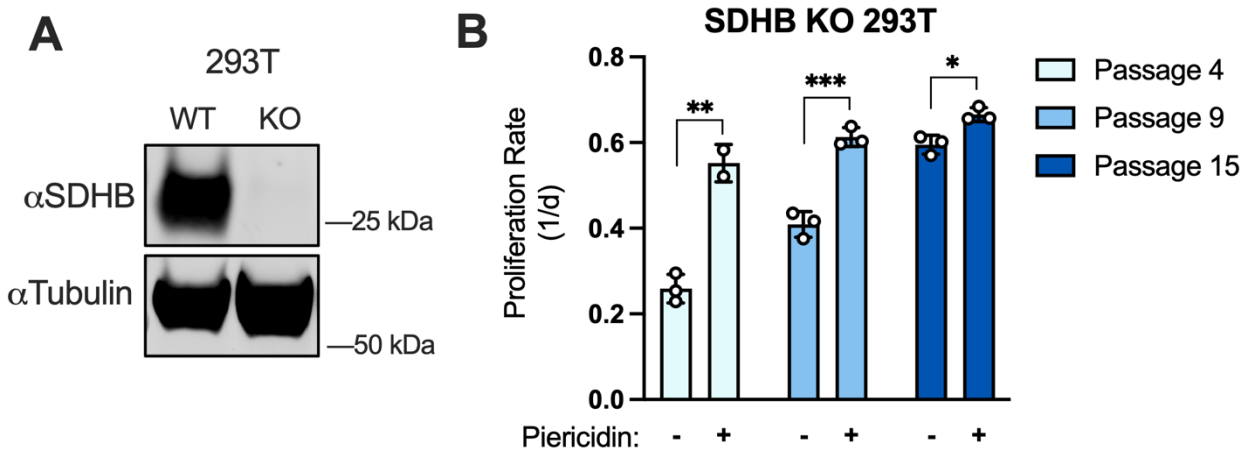

Figure 3.14. SDHB KO cells adapt over time. A) Western blot for SDHB and tubulin from WT and SDHB KO HEK293T cells. Tubulin is used as a loading control. **B)** Proliferation rates of SDHB KO HEK293T cells cultured in DMEM with 1 mM pyruvate from the indicated passage number after derivation of KO clone. For each passage, cells were treated vehicle (DMSO) or 1 μM of the CI inhibitor piericidin A. Data are plotted as means ± standard deviation (SD) and compared with an unpaired two-tailed student's t-test. $p<0.05$*, $p<0.01$**, $p<0.001$***, $p<0.0001$****

To understand this phenomenon, we created three categories of cell lines derived from one 143B SDHB KO clone: Early Passage (EP) SDHB KO, <5 passages; Late Passage (LP) SDHB KO, >15 passages; or Addback (AB), where SDHB was re-expressed immediately after SDHB KO clone generation (Figure 3.15A). We measured proliferation rates of parental cells (WT), AB, EP SDHB KO and LP SDHB KO cells and found that SDHB KO decreased their proliferation rate, but that culturing SDHB KO cells to LP allowed them to adapt to an improved proliferation rate (Figure 3.15B). Culturing

EP SDHB KO cells in the presence of rotenone or aspartate was able to improve cell proliferation, consistent with the effects of acute SDH inhibition with AA5; however, those benefits were largely lost in LP SDHB KO cells (Figure 3.15B). Consistent with their proliferation rates, aspartate levels were lowest in EP SDHB KO cells and were increased by either rotenone treatment or by culturing to LP (Figure 3.15C). Also similar to the acute effects of AA5 treatment, EP SDHB KO cells had an increased NAD+/NADH ratio that was diminished upon rotenone treatment; however, the NAD+/NADH ratio was already lowered in LP SDHB KO cells and unaffected by rotenone, suggesting redox adaptations occurred during passaging (Figure 3.15D).

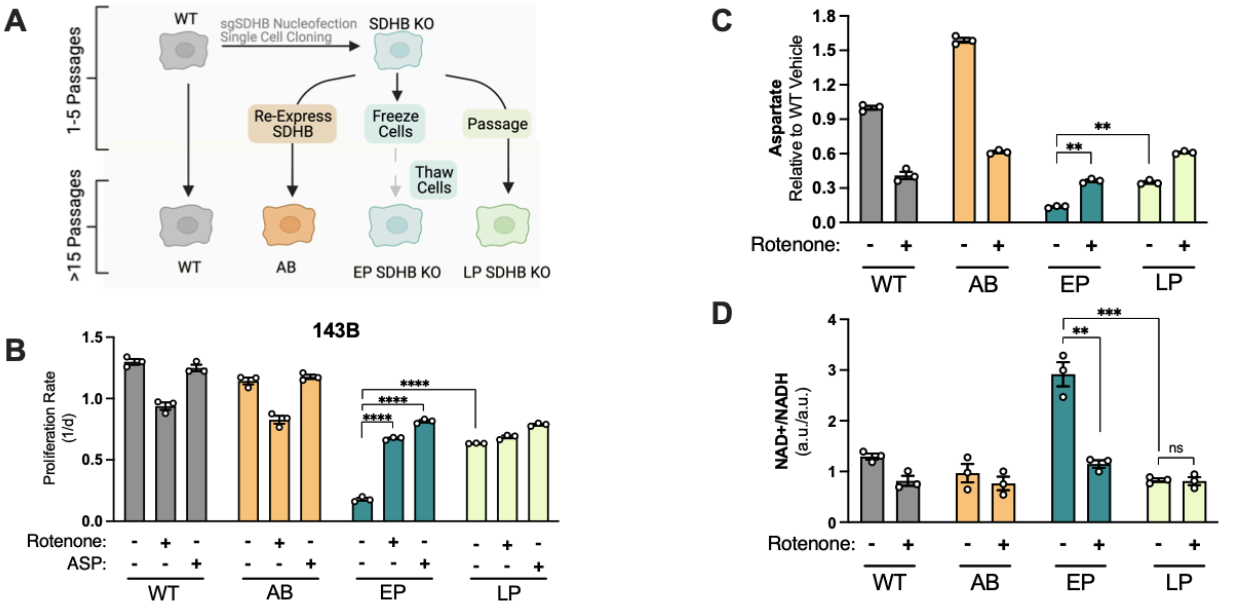

Figure 3.15. Adaptive CI activity loss supports aspartate synthesis and proliferation in SDHB-null cells. A) Schematic showing how SDHB KO 143B clones were used to generate SDHB addback cells (AB), early passage SDHB KO cells (EP), or late passage (LP) SDHB KO cells. **B)** Proliferation rates of wild-type (WT), SDHB addback (AB), early passage (EP) and late passage (LP) SDHB KO 143B cells cultured in DMEM with 1 mM PYR, treated with vehicle (DMSO), 50 nM rotenone, or 20 mM ASP (n=3). **C)** Relative aspartate levels measured by LCMS metabolomics of wild-type (WT), SDHB addback (AB), early passage (EP) and late passage (LP) SDHB KO 143B cells cultured in DMEM with 1 mM PYR and treated with vehicle (DMSO) or 50 nM rotenone for six hours (n=3). **D)** Whole cell NAD+/NADH measured by LCMS metabolomics of wild-type (WT), SDHB addback (AB), early passage (EP) and late passage (LP) SDHB KO 143B cells cultured in DMEM with 1 mM PYR and treated with vehicle (DMSO) or 50 nM rotenone for six hours (n=3).

To determine if these adaptive phenotypes were due to the selective proliferation advantages they provide or simply inherent to passaged SDH-null cells, we separately passaged EP SDHB KO cells in rotenone for 15 passages (Figure 3.16A). We found that cells cultured with continuous rotenone treatment remained phenotypically similar to EP cells when CI inhibitors were removed, suggesting the selective pressure is stalled by exogenous CI inhibition (Figure 3.16B).

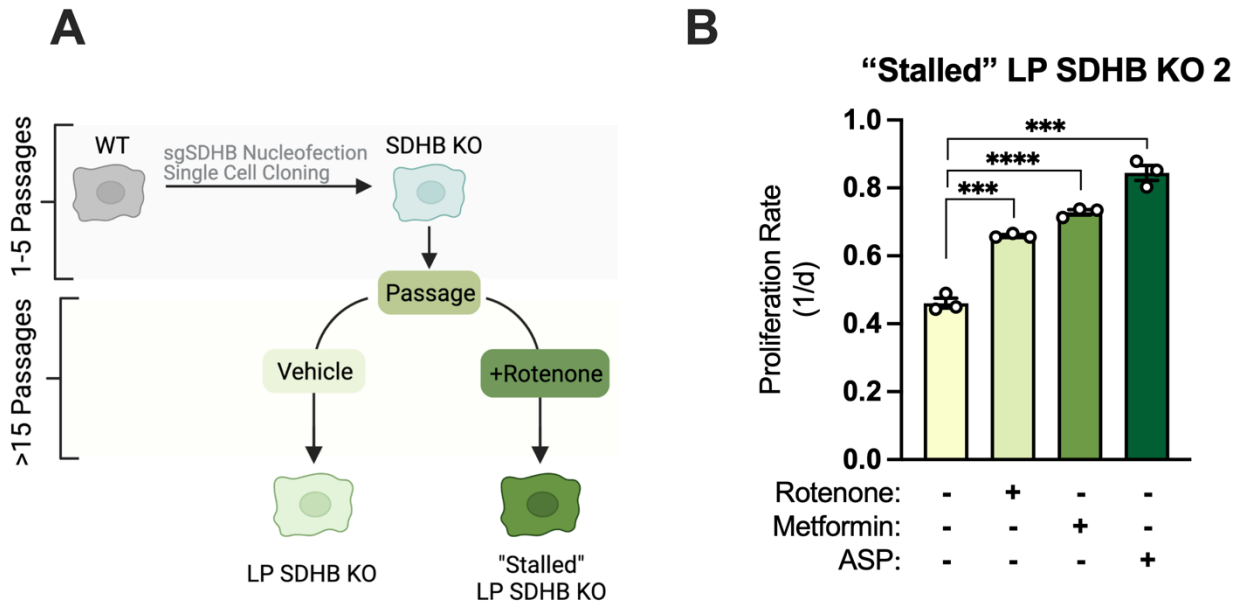

Figure 3.16. Progressive CI loss is stalled in SDHB-null cells by maintaining them in CI inhibitors. **A)** Schematic illustrating how SDHB KO 143B cells were maintained in culture with or without continuous rotenone to achieve late passage (LP) status or "Stalled" LP status. **B)** Proliferation rates of "Stalled" LP SDHB KO 143B cells treated with vehicle (DMSO), 50 nM rotenone, 1 mM metformin, or 20 mM ASP in DMEM with 1 mM pyruvate. Data are plotted as means ± standard deviation (SD) and compared with an unpaired two-tailed student's t-test. $p<0.05$*, $p<0.01$**, $p<0.001$***, $p<0.0001$****

To learn more about the mitochondrial alterations occurring during the passaging of SDHB KO cells, we conducted tandem mass tag (TMT) quantitative proteomics on isolated mitochondria from WT cells, AB cells, EP SDHB KO cells, and LP SDHB KO cells (Figure 3.15A). Comparing WT and LP samples, we conducted MitoPathways 3.0

pathway enrichment analysis (Pagliarini et al., 2008; Rath et al., 2021) of mitochondrial protein abundance changes and found that, following complex II proteins, CI proteins were the most statistically significantly different (Figure 3.17A). Indeed, the abundance of most CI subunits were decreased in LP SDHB KO cells compared to WT cells (Figure 3.17B). In addition, CI subunit levels progressively decreased from WT/AB to EP SDHB KO to LP SDHB KO and resulted in decreased CI activity, suggesting that SDHB KO cells adapt over time by selecting against CI activity (Figure 3.17C, 3.17D). We confirmed these findings by western blot, where LP SDHB KO 143B cells were associated with an ~80% reduction in the CI subunit NDUFA8 compared to WT cells (Figure 3.17E). Together, these data suggest that SDH-deficient cells suppress CI activity to generate an ideal mitochondrial redox state that enables aspartate synthesis (Figure 3.17F).

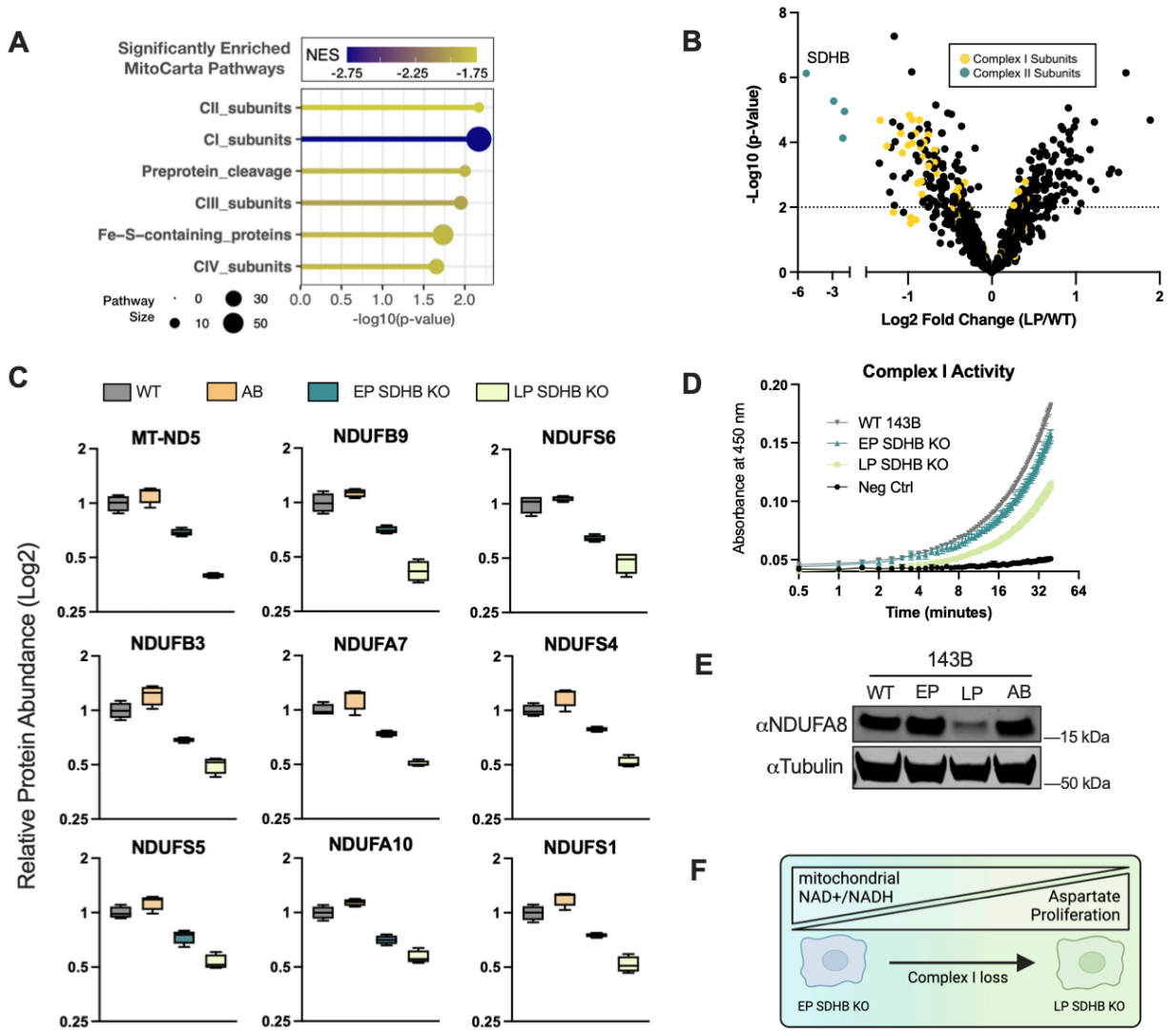

Figure 3.17. SDH-null cells demonstrate progressive loss of complex I. A) Gene set enrichment analysis (GSEA) of mitochondrial protein expression in LP SDHB KO 143B cells compared to WT 143B cells using MitoCarta 3.0 pathways. **B)** Volcano plot of compiled LP SDHB KO 143B cells compared to WT 143B cells showing all mitochondrial proteins (black), complex II subunits (blue), and complex I subunits (yellow) (n=4). **C)** Box plots of a subset of CI subunits showing relative expression in WT 143B, SDHB AB 143B, EP SDHB KO 143B, and LP SDHB KO 143B cells (n=4). **D)** Complex I activity assay of WT 143B, EP SDHB KO, and LP SDHB KO cells (n=2). **E)** Western blot for NDUFA8 and tubulin from WT 143B, EP SDHB KO, LP SDHB KO, and SDHB AB cells. Tubulin is used as a loading control. **F)** Schematic detailing how CI activity is suppressed to generate an ideal mitochondrial redox state in SDH-deficient cells to enable aspartate synthesis. Data are plotted as means ± standard deviation (SD) and compared with an unpaired two-tailed student's t-test. p<0.05*, p<0.01**, p<0.001***, p<0.0001****

3.4 Conclusion and Discussion

Our results highlight the interconnectedness of cellular metabolism by demonstrating how intercompartmental metabolic variables can collaborate to promote metabolic adaptations and support cell function. The observations that CI inhibition primarily decreases mitochondrial NAD+/NADH and that only mito*LbNOX* blocks the benefits of CI inhibition in SDH-impaired cells localize the site of redox effect to the mitochondria. Additionally, we note that SDH/CI impaired cells also require a supply of cytosolic electron acceptors to proliferate, indicating that this metabolic state depends on intercompartmental metabolic differences including a reduced mitochondrial compartment and an oxidized cytosolic environment. These results therefore reveal that compartmentally localized redox state changes can functionally alter cell phenotypes, highlighting the need for tools to measure subcellular metabolic states to gain a comprehensive understanding of cell metabolism.

Interestingly, the phenomenon of CI loss has also been observed in several other kidney neoplasias, including FH-mutant type 2 papillary renal cell carcinomas (pRCC), renal oncocytomas driven by mitochondrial DNA mutations, and VHL-mutant clear cell renal cell carcinomas (ccRCC), which are characterized by suppression of oxidative mitochondrial metabolism (Courtney et al., 2018; Crooks et al., 2021; Mayr et al., 2008; Simonnet et al., 2003; Tomlinson et al., 2002). Decreases in CI expression and/or heteroplasmic mutations in mitochondrial DNA CI genes have also been reported across diverse cancers, suggesting that activation of reductive mitochondrial anabolism may be a metabolic feature of those cancers and correspond to similar metabolic vulnerabilities (Gorelick et al., 2021; Kumari et al., 2020; Reznik et al., 2017). On the contrary, CI

inhibitors have also been identified as a therapeutic avenue for cancer treatment, which can decrease tumor growth by affecting redox homeostasis and suppressing intratumoral aspartate (Baccelli et al., 2019; Gui et al., 2016; Martínez-Reyes et al., 2020; Molina et al., 2018; L. B. Sullivan et al., 2018; Wheaton et al., 2014). Notably, the responses to these mitochondrial inhibitors have been variable across clinical trials and cancer models suggesting that heterogeneity in mitochondrial metabolism may govern the responses to CI inhibitors, and potentially to future inhibitors of reductive mitochondrial anabolism (Janku et al., 2021; Momcilovic et al., 2019; Yap et al., 2019, 2023). Thus, understanding mitochondrial phenotypes will be critical for leveraging cancer cell metabolic changes to improve cancer therapy.

Chapter 4. Alternative Aspartate Synthesis Pathways are Activated in Adapted SDH-deficient Cancer Cells

Note: *This chapter is adapted from the manuscript published in eLife.*

4.1 Introduction

In the previous chapter, I demonstrated that SDH impairments block canonical aspartate synthesis, which are only mildly restored by exogenous electron acceptors. Interestingly, additional complex I impairment is sufficient to significantly increase intracellular aspartate levels and substantially restore proliferation to SDH-deficient cells. I then showed that the alterations in mitochondrial redox homeostasis were driving this increase in aspartate levels and proliferation rate. Finally, I revealed that SDHB-null cells proliferate better over time, and through mitochondrial proteomics, enzymatic assays, and western blots, show that these cells gradually adapt to lose complex I. Chapter 3 highlights an interesting phenomenon that enables tumorigenesis of SDHB-null cells. In this next chapter, I will show how mitochondrial redox adaptations drive non-canonical aspartate synthesis through two alternative metabolic pathways.

This chapter begins by using uniformly labelled ^{13}C isotopes of glucose and glutamine to determine carbon contributions from each nutrient into newly synthesized aspartate. First, we validate that pyruvate carboxylase (PC) is essential for aspartate synthesis and proliferation of SDH-impaired cells, although complex I inhibition still partially restores aspartate levels and proliferation. Next, we find that mitochondrial pyruvate import is also required for SDH-deficient cells and is not restored with rotenone, evoking at least two metabolic requirements for pyruvate: PC and AKG generation for

RCQ. Lastly, we demonstrate that GOT1, but not GOT2 is crucial for SDH/complex I impaired cells, indicating a reversal of the malate-aspartate shuttle to enable intercompartmental aspartate synthesis stimulated from a shift in the mitochondrial redox environment.

4.2 Contributions

Experiments in this chapter are adapted from Hart et al. 2023, *eLife*. Experiments were conducted by M.L.H. with assistance from I.A.E. and A-L.B.G.V. LC-MS experiments were facilitated by Brian Milless and the Fred Hutch Proteomics and Metabolomics Shared Resource.

4.3 Results

Mitochondrial redox alterations promote alternative aspartate synthesis pathways in SDH-impaired cells

While our results demonstrate that decreased mitochondrial NAD+/NADH is a critical driver of aspartate synthesis in SDH-impaired cells, it remains unclear how these redox changes induce aspartate production. One likely contributor is reductive carboxylation of glutamine-derived AKG (RCQ), whose relative contribution to aspartate production is increased in cells with defects in oxidative mitochondrial metabolism (Metallo et al., 2011; Mullen et al., 2012, 2014; Wise et al., 2011). Another is pyruvate carboxylase (PC), which can have increased expression and activity in SDH-null cancer cells (Cardaci et al., 2015; Lussey-Lepoutre et al., 2015). To ascertain the source of increased aspartate in SDH-deficient cells upon CI inhibition we conducted stable isotope labeling of WT and low passage SDHB KO cells with or without rotenone from U-^{13}C

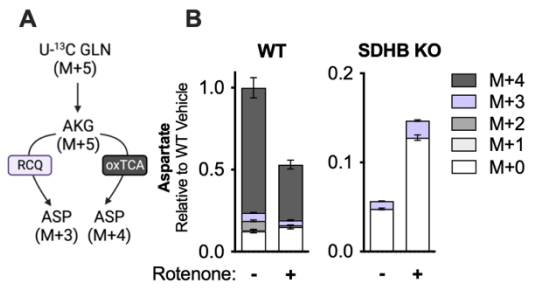

Figure 4.1. Glutamine is a minor contributor to alternative aspartate synthesis in SDHB KO cells upon CI inhibition. A) Schematic depicting metabolic pathway usage for isotopologue patterns of aspartate derived from U-^{13}C glutamine. **B)** Relative ion counts for all aspartate isotopologues derived from U-^{13}C glutamine measured by LCMS metabolomics in WT and SDHB KO 143B cells treated with either vehicle (DMSO) or 50 nM rotenone in pyruvate free DMEM with 1 mM AKB for 6 hours (n=3).

glutamine, which can delineate between aspartate generated from the oxidative TCA cycle or RCQ (Figure 4.1A). SDHB KO decreased total aspartate levels and abolished oxidative M+4 aspartate production, as expected, and RCQ-derived M+3 aspartate was slightly increased in SDHB KO cells upon rotenone treatment (Figure 4.1A, 4.1B). While RCQ can occur in both the cytoplasmic and mitochondrial compartments through IDH1 and IDH2, respectively, both RCQ routes rely on ATP-citrate lyase (ACLY) to cleave cytosolic citrate to oxaloacetate (OAA) and acetyl-CoA (Figure 4.2A). Therefore, we tested if preventing RCQ with the ACLY inhibitor BMS-303141 (BMS) would alter the proliferation rescue of CI inhibition in SDH-impaired 143B cells. Indeed, BMS had an anti-proliferative effect on AA5 and rotenone co-treated cells, which could be prevented by aspartate supplementation (Figure 4.2B). Correspondingly, aspartate levels were decreased in SDH/CI inhibited cells when treated with BMS, tracking with the small contribution of RCQ to aspartate production in this context (Figure 4.1B, 4.2C). These data indicate that RCQ is partially responsible for increased aspartate synthesis and cell proliferation upon CI inhibition in SDH-impaired cells.

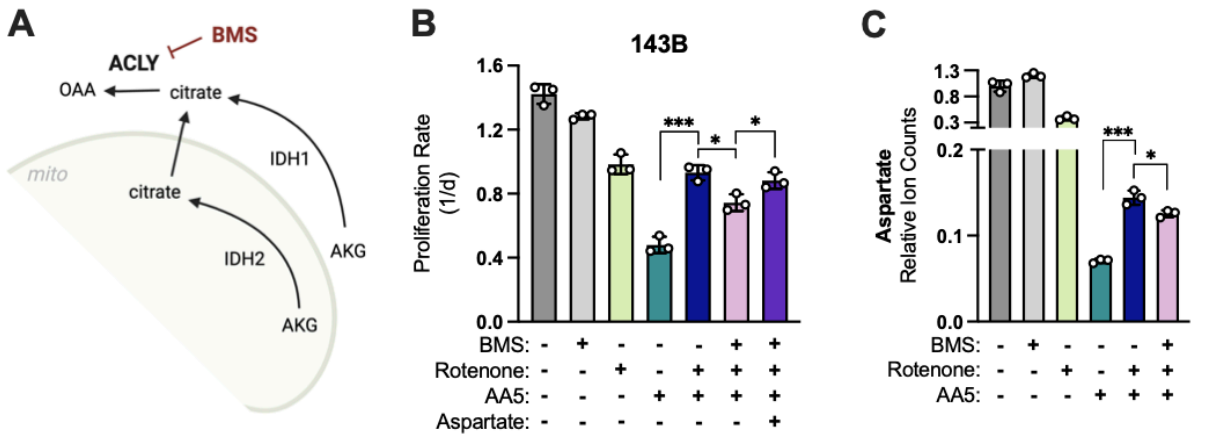

Figure 4.2. Alternative aspartate synthesis is partially driven by RCQ in SDH/CI impaired cells. A) Schematic showing how the ACLY inhibitor BMS-303141 blocks a convergent step necessary for glutamine-derived aspartate synthesis by either cytosolic or mitochondrial reductive carboxylation of glutamine derived AKG. IDH1; Isocitrate dehydrogenase 1, IDH2; Isocitrate dehydrogenase 2, ACLY; ATP-Citrate Lyase, OAA; oxaloacetate. **B)** Proliferation rates of WT 143B cells treated with either vehicle (DMSO); 25 μM BMS-303141 (BMS); 50 nM rotenone; 5 μM AA5; 5 μM AA5 and 50 nM rotenone; 5 μM AA5, 50 nM rotenone and 25 μM BMS; or 5 μM AA5, 50 nM rotenone, 25 μM BMS, and 20 mM aspartate in DMEM with 1 mM pyruvate (n=3). **C)** Relative aspartate levels measured by LCMS metabolomics of WT 143B cells treated with either vehicle (DMSO); 25 μM BMS; 50 nM rotenone; 5 μM AA5; 5 μM AA5 and 50 nM rotenone; 5 μM AA5, 50 nM rotenone and 25 μM BMS in pyruvate free DMEM with 1 mM AKB for 6 hours (n=3). Data are plotted as means ± standard deviation (SD) and compared with an unpaired two-tailed student's t-test. $p<0.05$*, $p<0.01$**, $p<0.001$***, $p<0.0001$****

Next, we measured the contributions of glucose to aspartate by culturing WT and SDHB KO cells with U-^{13}C glucose, with or without rotenone treatment. To avoid potential caveats that may confound labeling patterns from unlabeled media pyruvate, we conducted U-^{13}C glucose isotope tracing experiments in pyruvate-free DMEM with AKB, which serves a similar electron acceptor function as pyruvate but cannot fulfill its carbon fates (Figure 3.2A) (Altea-Manzano et al., 2022; L. B. Sullivan et al., 2015). We also confirmed that rotenone is still effective to restore proliferation and aspartate levels of SDH-impaired cells in pyruvate-free DMEM with AKB (Figures 4.3A, 4.3B).

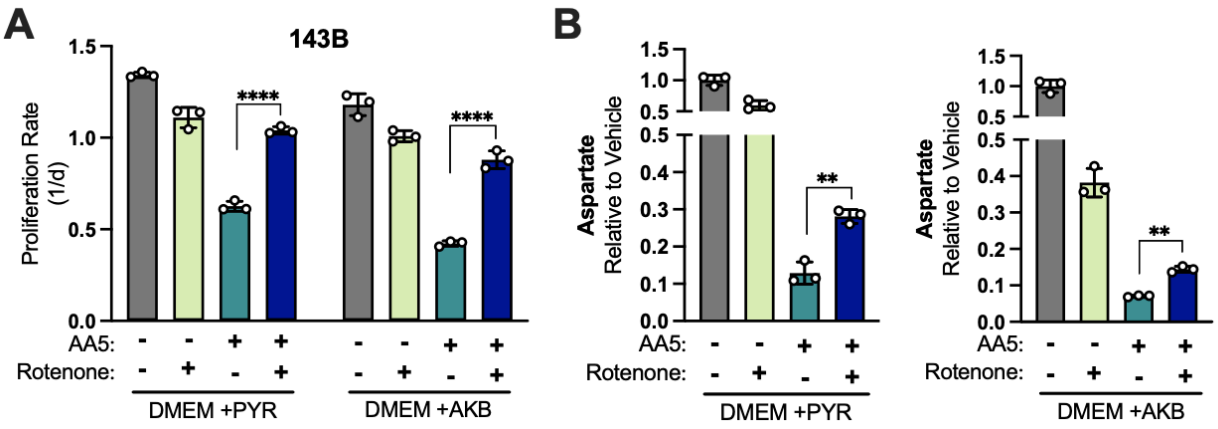

Figure 4.3. CI inhibition restores proliferation and aspartate synthesis in pyruvate-free DMEM supplemented with AKB. A) Proliferation rates of WT 143B cells treated with vehicle (DMSO), 50 nM rotenone, 5 μM AA5 or 5 μM AA5 and 50 nM rotenone in either DMEM with 1 mM pyruvate or pyruvate-free DMEM with 1 mM AKB (n=3). **B)** Relative aspartate levels measured by LCMS metabolomics of WT 143B cells treated with vehicle (DMSO), 50 nM rotenone, 5 μM AA5 or 5 μM AA5 and 50 nM rotenone in either DMEM with 1 mM pyruvate or pyruvate-free DMEM with 1 mM AKB for 6 hours (n=3). Data are plotted as means ± standard deviation (SD) and compared with an unpaired two-tailed student's t-test. p<0.05*, p<0.01**, p<0.001***, p<0.0001****

While glucose-derived carbon was a minor contributor to aspartate in WT cells, the majority of aspartate in vehicle-treated SDHB KO cells was labeled M+3 from glucose, as was most of the aspartate induced by rotenone treatment (Figures 4.4A, 4.4B). We next investigated the functional contributions of PC to SDH-impaired cells, with or without CI co-inhibition. First, we generated monoclonal PC KO 143B cells, and to control for variation from single cell cloning, we re-expressed PC cDNA in a KO clone to generate PC "addback" (AB) cells to serve as a metabolically wild type control. Consistent with previously published results, we find that

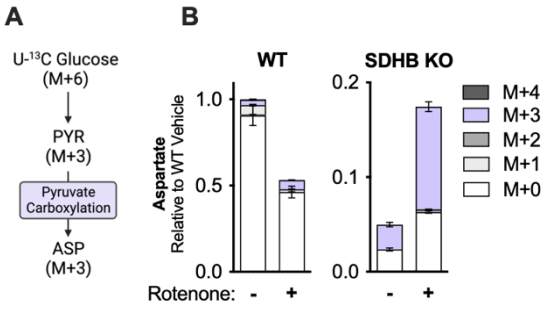

Figure 4.4. Glucose is a major contributor to alternative aspartate synthesis in SDHB KO cells upon CI inhibition. A) Schematic depicting metabolic pathway usage for isotopologue patterns of aspartate derived from U-^{13}C glucose. **B)** Relative ion counts for aspartate isotopologues derived from U-^{13}C glucose measured by LCMS metabolomics in WT and SDHB KO 143B cells treated with either vehicle (DMSO) or 50 nM rotenone in pyruvate free DMEM with 1 mM AKB for 6 hours (n=3).

PC KO cells are sensitive to SDH impairment (Figure 4.5A, 4.5B) (Cardaci et al. 2015, Lussey-Lepoutre et al. 2015). Interestingly, rotenone treatment still provided a proliferative benefit to AA5 treated PC KO cells, although the resultant proliferation rate was still decreased compared to PC AB cells (Figure 4.5A). We hypothesized that this residual proliferation benefit was driven by existing or compensatory RCQ activity, so we added BMS to SDH/CI inhibited PC KO cells, which was sufficient to completely block cell proliferation and was ameliorated by aspartate treatment (Figure 4.5A). Consistent with the proliferation defects, BMS treatment also blocked the increase in aspartate levels upon rotenone treatment in SDH-impaired PC KO cells (Figures 4.5C). Collectively, these data demonstrate that both alternative aspartate synthesis pathways, RCQ and PC, contribute to aspartate levels and cell proliferation during SDH-deficiency and are activated by CI impairment (Figure 4.5D).

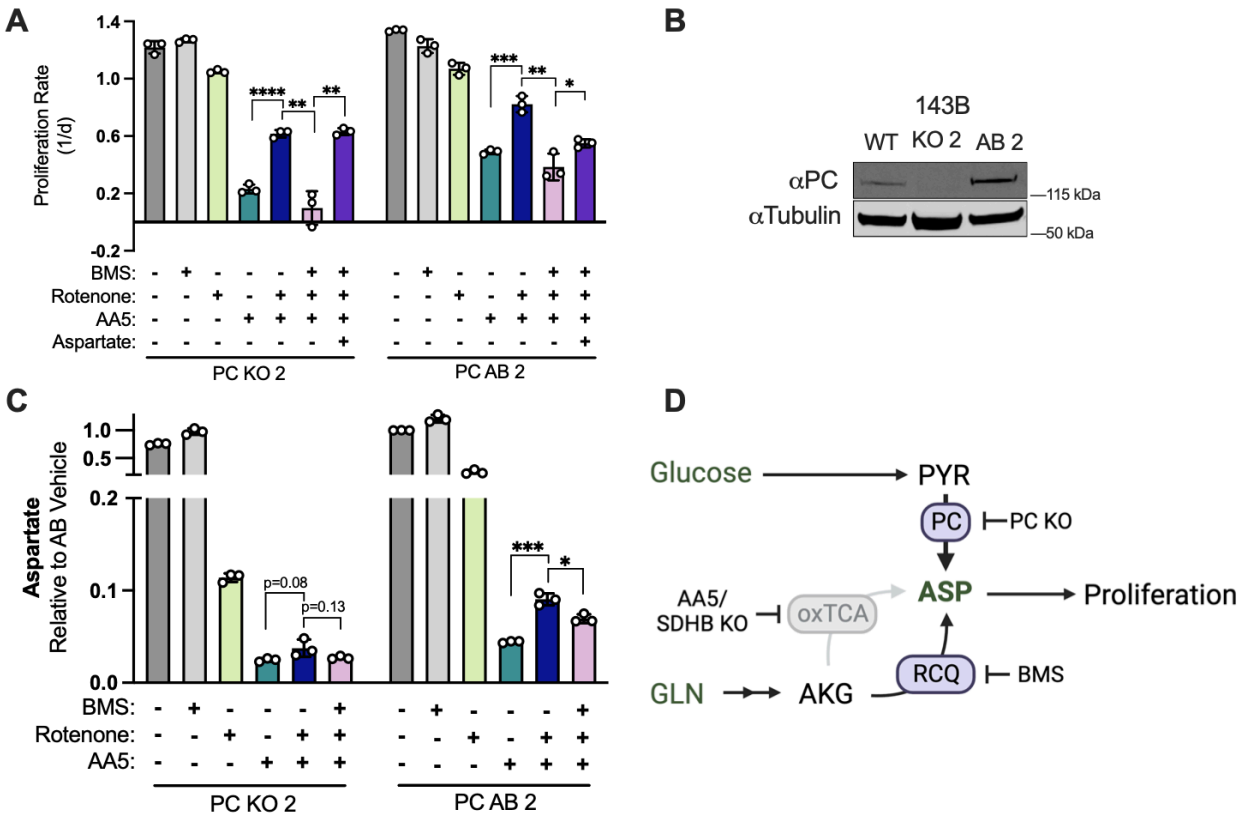

Figure 4.5. PC and RCQ contribute to aspartate levels and cell proliferation during SDH impairment and are activated by CI inhibition. A) Western blot for PC in WT 143B cells, PC KO clone 2, and PC KO clone 2 with PC cDNA added back. Tubulin is used as a loading control. **B)** Proliferation rates of PC KO and PC AB 143B cells treated with vehicle (DMSO); 25 μM BMS; 50 nM rotenone; 5 μM AA5; 5 μM AA5 and 50 nM rotenone; 5 μM AA5, 50 nM rotenone and 25 μM BMS; or 5 μM AA5, 50 nM rotenone, 25 μM BMS, and 20 mM aspartate in DMEM with 1 mM PYR (n=3). **C)** Relative aspartate levels measured by LCMS metabolomics of PC KO and PC AB 143B cells treated with vehicle (DMSO); 25 μM BMS; 50 nM rotenone; 5 μM AA5; 5 μM AA5 and 50 nM rotenone; 5 μM AA5, 50 nM rotenone and 25 μM BMS; or 5 μM AA5, 50 nM rotenone, 25 μM BMS in pyruvate free DMEM with 1 mM AKB for 6 hours (n=3). **D)** Schematic showing two alternative aspartate synthesis pathways induced by CI inhibition in SDH-impaired cells. Data are plotted as means ± standard deviation (SD) and compared with an unpaired two-tailed student's t-test. p<0.05*, p<0.01**, p<0.001***, p<0.0001****

Mitochondrial pyruvate entry is essential for alternative aspartate synthesis pathways

Both PC and RCQ have reactions that can occur in the cytosol or mitochondria, obfuscating the mechanism by which mitochondrial redox changes from CI inhibition might drive alternative aspartate synthesis pathways in SDH-impaired cells. To gain

insight into these compartmentalized factors, we tested the dependence on mitochondrial pyruvate availability by generating knockout and addback clones for MPC1, a required subunit of the mitochondrial pyruvate carrier (Figure 4.6A). Proliferation of MPC1 KO cells was moderately decreased in vehicle-treated conditions, but completely ablated by SDH impairment and no longer improved by CI co-inhibition, while MPC1 AB control cells mirrored WT cells (Figure 4.6B). Consistent with MPC activity supporting the alternative aspartate synthesis pathways induced by CI inhibition in SDH-impaired cells, we found that aspartate levels were decreased by AA5 treatment in MPC1 KO cells and were not restored during rotenone cotreatment (Figure 4.6C). To confirm that the proliferation defects in SDH-impaired MPC1 KO cells were mediated by aspartate depletion, we supplemented MPC1 KO cells with aspartate, and observed robust proliferation rescues during both SDH inhibition and SDH/CI co-inhibition (Figure 4.6D). Thus, mitochondrial pyruvate import is a critical component of alternative aspartate synthesis pathways in SDH-impaired cells (Figure 4.6E).

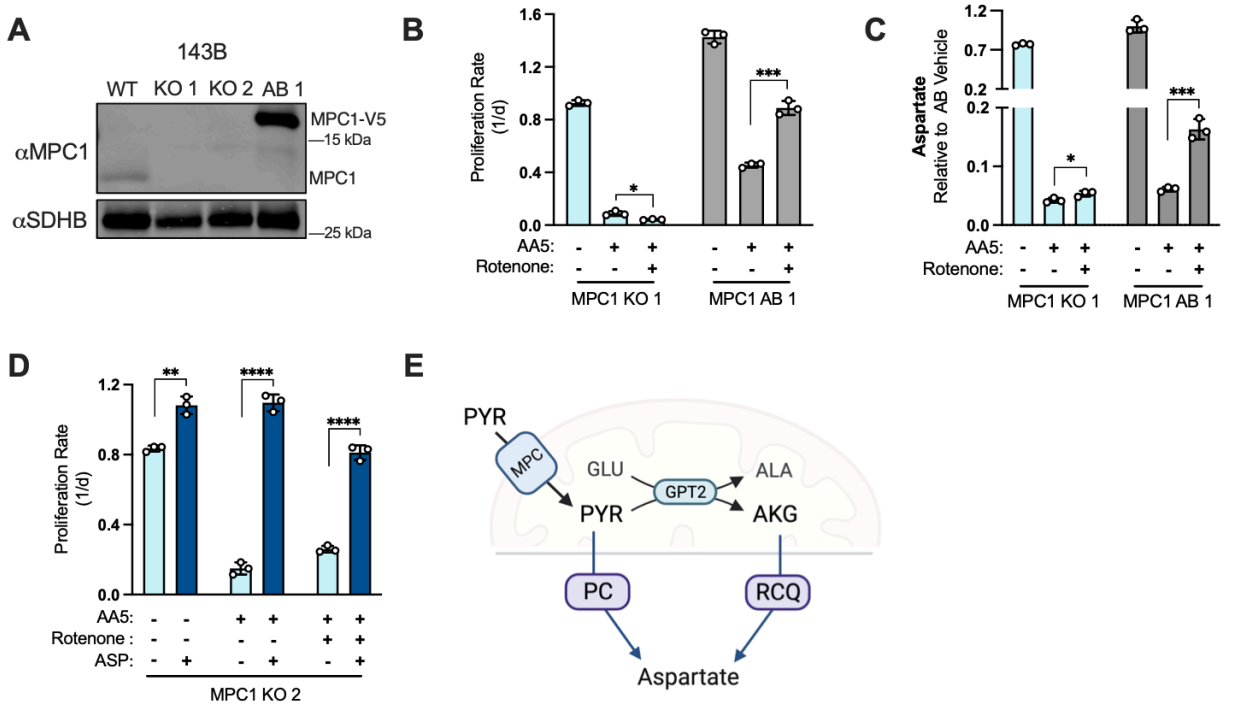

Figure 4.6. Mitochondrial pyruvate import supports alternative aspartate synthesis in SDH-impaired cells. A) Western blot for MPC1 and SDHB in WT 143B cells, two MPC1 KO 143B clones, and MPC1 KO 143B clone 1 with MPC1-V5 cDNA added back (AB). SDHB is used as a loading control. **B)** Proliferation rates of MPC1 KO 143B cells (clone 1) compared to MPC1 AB 143B cells treated with vehicle (DMSO), 5 μM AA5, or 5 μM AA5 and 50 nM rotenone in DMEM with 1mM PYR (n=3). **C)** Relative aspartate levels measured by LCMS metabolomics of MPC1 KO 143B cells (clone 1) compared to MPC1 AB 143B cells treated with vehicle (DMSO), 5 μM AA5, or 5 μM AA5 and 50 nM rotenone in pyruvate free DMEM with 1 mM AKB for 6 hours (n=3). **D)** Proliferation rates of MPC1 KO 143B cells (clone 2) treated with vehicle (DMSO), 5 μM AA5, 5 μM AA5 and 50 nM rotenone, with and without 20 mM aspartate in DMEM with 1 mM PYR (n=3). **E)** Schematic depicting the metabolic fates of mitochondrial pyruvate in SDH/CI impaired cells: PC activity to synthesize oxaloacetate and GPT2 activity to generate AKG and alanine as a byproduct. Data are plotted as means ± standard deviation (SD) and compared with an unpaired two-tailed student's t-test. $p<0.05$*, $p<0.01$**, $p<0.001$***, $p<0.0001$****

Our data suggest that MPC1 KO phenocopies the proliferative and aspartate production consequences of impairing PC and RCQ in SDH-deficient cells, raising the question of how mitochondrial pyruvate entry supports these processes. While it is evident that mitochondrial pyruvate supports PC at least in part by serving as an enzymatic substrate, the requirement of mitochondrial pyruvate for RCQ is less clear. RCQ proceeds by converting glutamine derived glutamate to AKG, which is reductively

carboxylated by IDH1 or IDH2, steps toward generating cytosolic citrate that is cleaved to OAA for aspartate synthesis (Figure 4.2A). We noted that MPC1 KO was associated with a depletion in AKG, suggesting that mitochondrial pyruvate entry may support RCQ by driving AKG generation (Figure 4.7A). Glutamate conversion to AKG can conventionally occur via three mitochondrial enzymes: GDH, which consumes glutamate and NAD+ to generate AKG, NADH, and ammonia; GOT2, which converts glutamate and OAA to aspartate and AKG; and GPT2, which converts glutamate and pyruvate to AKG and alanine. The requirement for MPC1 to maintain AKG levels suggests that pyruvate-dependent GPT2 activity is a dominant route for AKG production in these cells, consistent with recent studies (Figure 4.7B) (Rossiter et al., 2021; Wei et al., 2022; Weinberg et al., 2010). Indeed, MPC1 KO was also associated with a decrease in alanine levels, corroborating studies that identify GPT2 as a dominant source of alanine production (Figure 4.7C) (Rossiter et al., 2021). While AA5 treatment did not alter AKG levels in MPC1 KO cells, the addition of rotenone co-treatment was associated with further depletion of AKG, but not alanine, suggesting that rotenone blocked the secondary path of AKG generation through redox changes that impair the NAD+ consuming GDH reaction (Figures 4.7A, 4.7C). Together, these data support the hypothesis that a reduced mitochondrial environment promotes alternative aspartate synthesis in SDH-deficient cells through activating RCQ and PC activity, both of which require mitochondrial pyruvate import (Figure 4.6E).

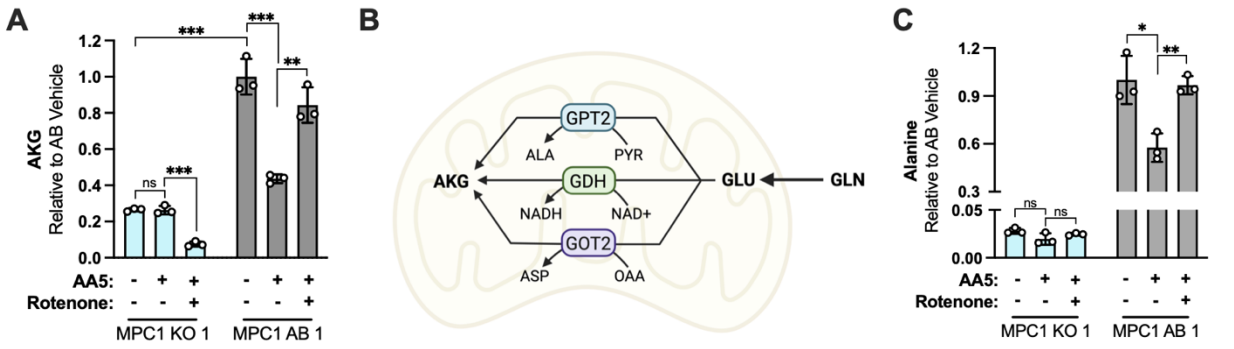

Figure 4.7. Mitochondrial AKG production is dependent on GPT2. A) Model depicting three enzymes capable of mitochondrial AKG production from glutamate (GLU) and necessary cofactors. GPT2; glutamic-pyruvic transaminase 2, GDH; glutamate dehydrogenase, GOT2; glutamic-oxaloacetic transaminase 2, ALA; alanine. **B)** Relative AKG levels measured by LCMS metabolomics of MPC1 KO 143B cells (clone 1) compared to MPC1 AB 143B cells treated with vehicle (DMSO), 5 μM AA5, or 5 μM AA5 and 50 nM rotenone in pyruvate free DMEM with 1 mM AKB for 6 hours (n=3). **C)** Relative alanine levels measured by LCMS metabolomics of MPC1 KO 143B cells (clone 1) compared to MPC1 AB 143B cells treated with vehicle (DMSO), 5 μM AA5, or 5 μM AA5 and 50 nM rotenone in pyruvate-free DMEM with 1 mM AKB for 6 hours (n=3). Data are plotted as means ± standard deviation (SD) and compared with an unpaired two-tailed student's t-test. $p<0.05$*, $p<0.01$**, $p<0.001$***, $p<0.0001$****

Alternative aspartate synthesis upon CI inhibition in SDH-impaired cells is dependent on GOT1

Since alternative aspartate synthesis pathways occur across intracellular compartments, it is unclear whether aspartate transamination occurs in SDH-impaired cells via the cytosolic glutamic-oxaloacetic transaminase (GOT) isoform GOT1 or its mitochondrial counterpart GOT2. On one hand, the mitochondrial enzymes MPC and PC are required for aspartate synthesis in this context, indicating that aspartate production by GOT2 is a plausible path. Indeed, GOT2-mediated aspartate production is observed in wild type cells using the oxidative TCA cycle for aspartate synthesis and in hypoxic pancreatic cancer cells (Garcia-Bermudez et al., 2022). However, RCQ derived OAA is produced in the cytosol, suggesting GOT1 may also drive aspartate synthesis, as has been described in cells with other mitochondrial disruptions (Birsoy et al., 2015).

Therefore, we next asked whether CI inhibition drives aspartate production in SDH-impaired cells by GOT2 or GOT1. We first generated monoclonal 143B cells with GOT2 KO and re-expressed GOT2 to generate a paired GOT2 AB cell line (Figure 4.8A). Consistent with published phenotypes, GOT2 KO cells were unable to proliferate in pyruvate free media (Figure 4.8B) (Garcia-Bermudez et al., 2022; Kerk et al., 2022).

In our standard media containing pyruvate, we found that GOT2 KO cells have increased sensitivity to SDH inhibition alone but maintained the benefits of CI co-inhibition on proliferation rate and aspartate production, similar to GOT2 AB and WT cells (Figures 4.8C, 4.8D). The enhanced depletion of aspartate upon AA5 treatment in GOT2 KO cells was also functionally related to its stronger proliferation impairment phenotype, as aspartate supplementation was able to phenocopy the proliferation benefits of rotenone co-treatment (Figure 4.8E). These data indicate that residual aspartate production in SDH-impaired cells is primarily driven by GOT2, but GOT2 is dispensable for the induction of aspartate production in SDH-impaired cells upon CI inhibition.

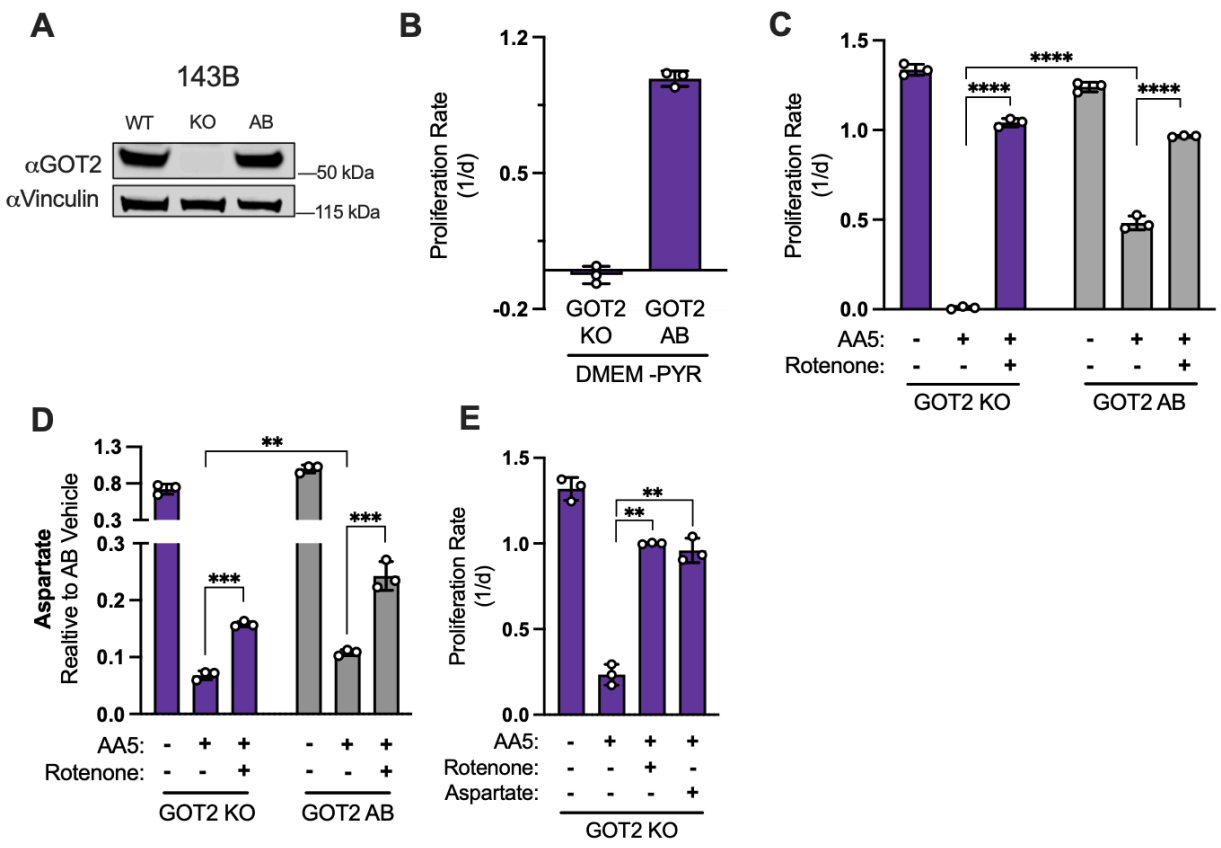

Figure 4.8. Alternative aspartate synthesis in SDH/CI impaired cells is not dependent on GOT2. A) Western blot for GOT2 and Vinculin from WT 143B cells, GOT2 KO 143B cells, and the same GOT2 KO clone expressing GOT2 cDNA (AB). Vinculin is the loading control. **B)** Proliferation rates of GOT2 KO and GOT2 AB 143B cells in pyruvate-free DMEM (n=3). **C)** Proliferation rates of GOT2 KO 143B cells compared to GOT2 AB 143B cells treated with vehicle (DMSO), 5 μM AA5, or 5 μM AA5 and 50 nM rotenone in DMEM with 1 mM pyruvate (n=3). **D)** Relative aspartate levels measured by LCMS metabolomics of GOT2 KO 143B cells compared to GOT2 AB 143B cells treated with vehicle (DMSO), 5 μM AA5, or 5 μM AA5 and 50 nM rotenone in pyruvate-free DMEM with 1 mM AKB for 6 hours (n=3). **E)** Proliferation rates of GOT2 KO 143B cells treated with vehicle (DMSO), 5 μM AA5, 5 μM AA5 and 50 nM rotenone, or 5 μM AA5 and 20 mM aspartate in DMEM with 1 mM pyruvate (n=3).

We next established monoclonal 143B cells with GOT1 KO and re-expressed GOT1 to generate a paired GOT1 AB cell line (Figure 4.9A). GOT1 KO cells had a mild proliferation defect compared to GOT1 AB or WT cells, but unlike GOT2 KO cells they were not obviously sensitized to AA5 treatment (Figure 4.9B). Importantly, SDH-impaired GOT1 KO cells differed from GOT1 AB and WT cells in that CI inhibition no longer

provided a proliferative benefit (Figure 4.9B). Correspondingly, aspartate levels were suppressed by SDH impairment in both GOT1 KO and GOT1 AB cell lines, but CI co-inhibition only increased aspartate levels in GOT1 replete cells (Figure 4.9C). Next, we found that the inability of CI inhibition to restore the proliferation of SDH-impaired GOT1 KO cells was due to its lack of aspartate restoration, as aspartate rescues proliferation of SDH/CI impaired GOT1 KO cells (Figure 4.9D). Notably, CI inhibition still increased malate levels in SDH-impaired GOT1 KO cells, suggesting that the mitochondrial redox changes from CI inhibition still drive the biochemical pathways required for alternative aspartate synthesis in these cells (i.e. PC and RCQ), but that GOT1 is required for terminal aspartate generation, indicating a reversal of the malate-aspartate shuttle (Figure 4.9E, 4.9F).

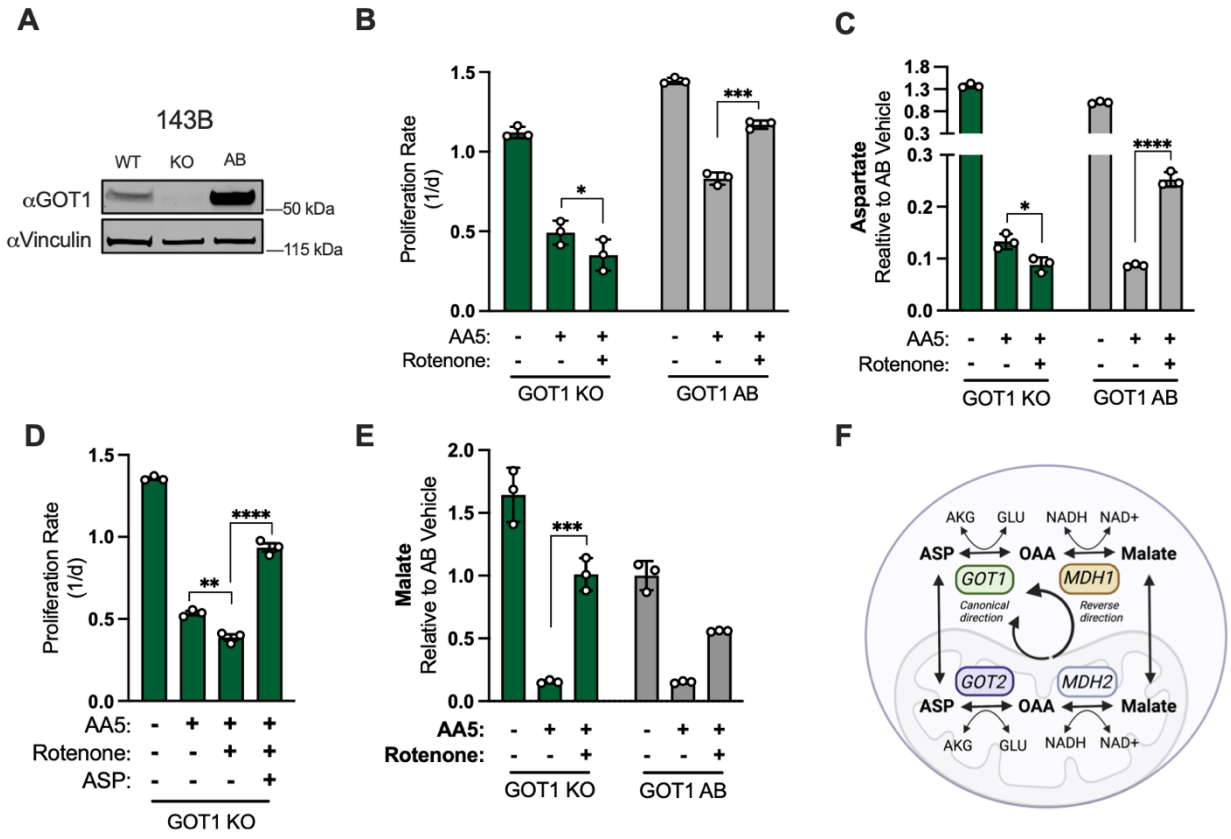

Figure 4.9. GOT1 is required for increased aspartate synthesis in SDH impaired cells upon complex I co-inhibition. A) Western blot for GOT1 and Vinculin from WT 143B cells, GOT1 KO 143B cells, and the same GOT1 KO clone expressing GOT1 cDNA (AB). Vinculin is the loading control. **B)** Proliferation rates of GOT1 KO 143B cells compared to GOT1 AB 143B cells treated with vehicle (DMSO), 5 μM AA5, or 5 μM AA5 and 50 nM rotenone in DMEM with 1 mM pyruvate (n=3). **C)** Relative aspartate levels measured by LCMS metabolomics of GOT1 KO 143B cells compared to GOT1 AB 143B cells treated with vehicle (DMSO), 5 μM AA5, or 5 μM AA5 and 50 nM rotenone in pyruvate free DMEM with 1 mM AKB for 6 hours (n=3). **D)** Proliferation rates of GOT1 KO 143B cells treated with vehicle (DMSO), 5 μM AA5, 5 μM AA5 and 50 nM rotenone, or 5 μM AA5, 50 nM rotenone and 20 mM aspartate in DMEM with 1 mM pyruvate (n=3). **E)** Relative malate levels by LCMS metabolomics of GOT1 KO 143B cells compared to GOT1 AB 143B cells, treated with vehicle (DMSO), 5 μM AA5, or 5 μM AA5 and 50 nM rotenone in pyruvate-free DMEM with 1 mM AKB for 6 hours (n=3). Malate levels are relative to the GOT1 AB vehicle condition. **F)** Model depicting the malate-aspartate shuttle in its canonical and reverse directions. Data are plotted as means ± standard deviation (SD) and compared with an unpaired two-tailed student's t-test. p<0.05*, p<0.01**, p<0.001***, p<0.0001****

Since these data also suggest that cytosolic malate dehydrogenase (MDH1) may play a role in alternative aspartate synthesis upstream of GOT1, so we also generated monoclonal MDH1 KO and paired MDH1 AB cells (Figure 4.9F, 4.10A). Similar to GOT1

KO cells, we found that neither proliferation rate nor aspartate levels were restored by CI inhibition in SDH-impaired MDH1 KO cells (Figures 4.10B, 4.10C). Interestingly, baseline aspartate levels were elevated in both GOT1 KO and MDH1 KO cells, consistent with their conventional aspartate-consuming role in the malate-aspartate shuttle (Figures 4.9C, 4.10C, 4.9F). However, the observation that GOT1 KO or MDH1 KO prevents CI inhibition from restoring aspartate levels in SDH-impaired cells confirms a reversal of the malate-aspartate shuttle to synthesize aspartate in SDH/CI impaired cells (Figure 4.9F).

Lastly, we found that the effects of each metabolic gene disruption on cell proliferation during SDH or SDH/CI inhibition were consistent across additional KO clones (Figure 4.10D). Collectively, these results indicate that in SDH-impaired cells, CI inhibition increases mitochondrial NADH to drive alternative aspartate synthesis pathways via PC and RCQ, both of which yield cytosolic oxaloacetate that is converted to aspartate by GOT1 (Figure 4.10E). Notably, in the case of PC-derived aspartate, the divergent NAD+/NADH ratios in each compartment would support reversal of mitochondrial malate dehydrogenase (MDH2) to reduce OAA to malate, which can be exported to the cytosol and oxidized to OAA by MDH1 prior to transamination to aspartate by GOT1 (Figure 4.9F, 4.10E).

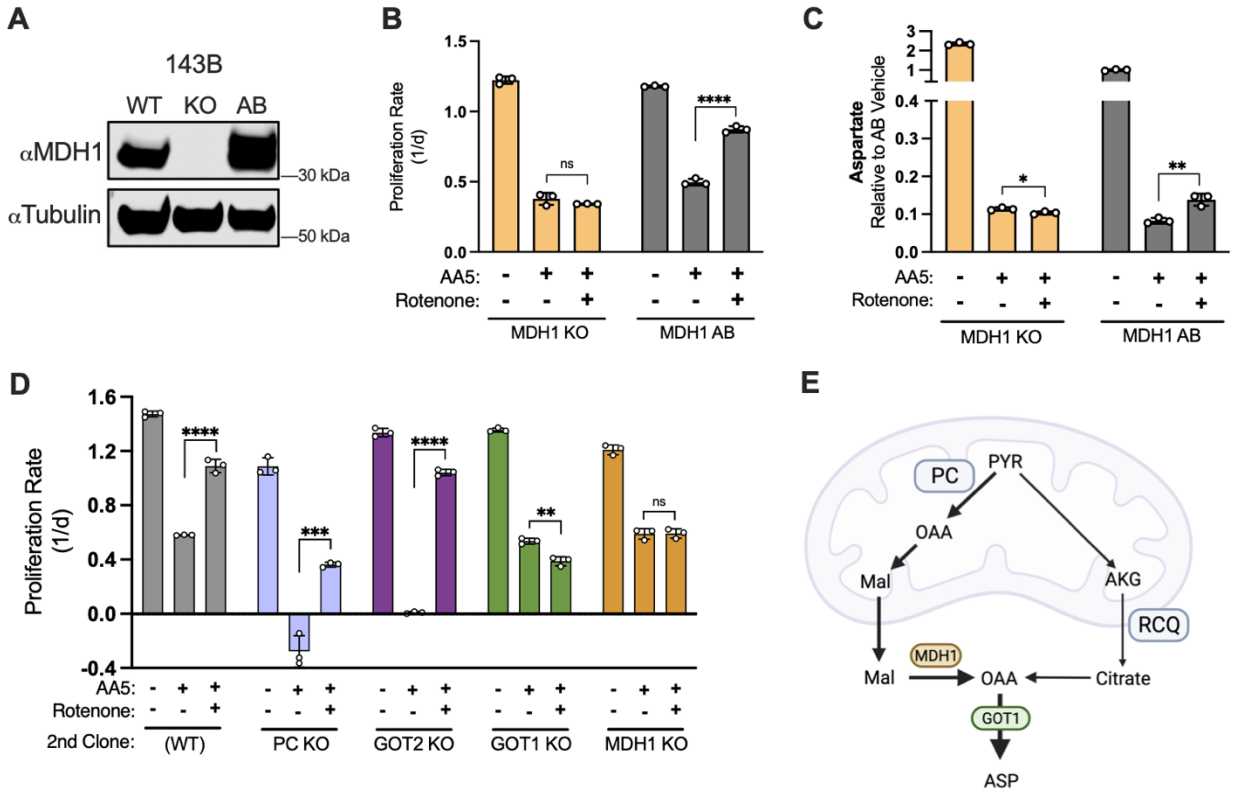

Figure 4.10. Contributions of components of the malate-aspartate shuttle to alternative aspartate synthesis in SDH-deficient cells. A) Western blot of MDH1 and tubulin in WT 143B cells, MDH1 KO 143B cells, and the same MDH1 KO clone with MDH1 cDNA added back (AB). Tubulin is the loading control. **B)** Proliferation rates of MDH1 KO 143B cells compared to MDH1 AB 143B cells treated with vehicle (DMSO), 5 μM AA5, or 5 μM AA5 and 50 nM rotenone in DMEM with 1 mM pyruvate (n=3). **C)** Relative aspartate levels measured by LCMS metabolomics of MDH1 KO 143B cells compared to MDH1 AB 143B cells treated with vehicle (DMSO), 5 μM AA5, or 5 μM AA5 and 50 nM rotenone in pyruvate-free DMEM with 1 mM AKB for 6 hours (n=3). **D)** Proliferation rates of WT 143B cells and second single cell clones for PC, GOT2, GOT1, and MDH1 KO 143B cells in DMEM with 1 mM pyruvate and treated with vehicle (DMSO), 5 μM AA5, or 5 μM AA5 and 50 nM rotenone. **E)** Schematic showing how aspartate is synthesized via GOT1 from RCQ and PC in SDH-deficient cells when complex I is also impaired. Data are plotted as means ± standard deviation (SD) and compared with an unpaired two-tailed student's t-test. $p<0.05$*, $p<0.01$**, $p<0.001$***, $p<0.0001$****

4.4 Conclusion and Discussion

Mitochondria are established contributors to catabolic cell metabolism through their canonical oxidative TCA cycle and ETC activities. In proliferating cells, the anabolic

contributions of these processes in NAD+/NADH homeostasis and TCA cycle-derived aspartate production have recently gained appreciation, defining important amphibolic roles for oxidative mitochondrial metabolism (Birsoy et al., 2015; Sullivan et al., 2015; Titov et al., 2016).

However, the fact that loss of function mutations in genes encoding the TCA cycle enzymes SDH and Fumarate Hydratase (FH) can promote tumorigenesis in some contexts challenges the notion that mitochondrial oxidative anabolism is strictly essential for aspartate production. Here, we investigate the metabolic roles of SDH and find that, in cells that employ oxidative TCA cycle function, SDH activity is primarily required for cell proliferation by supporting aspartate production. Interestingly, we found that cells can tolerate SDH loss if they also have concomitant CI impairment, which supports cell proliferation by decreasing mitochondrial NAD+/NADH to facilitate alternative aspartate synthesis.

The linked nature of SDH and CI was also revealed by reciprocal experiments where either SDHB was knocked out in wild type cells or restored in cancer cells arising from SDHB mutations. In both cases, functional SDH selects for cells with high CI activity and impaired SDH selects for cells with low CI activity, suggesting two modalities for mitochondrial anabolic metabolism: 1) CI regenerates NAD+ to drive oxidative anabolism via the TCA cycle, or 2) CI loss prevents NADH consumption, supporting NADH-driven reductive anabolism in the mitochondria of cells without canonical TCA cycle function. Overall, these findings support a growing understanding that mitochondrial function has critical roles in supporting cell function beyond its classical role in oxidative ATP synthesis, which can be revealed by divergent phenotypic effects of impairments to

discrete components of mitochondrial metabolism (Arnold et al., 2022; Martínez-Reyes et al., 2020; Mullen et al., 2012; To et al., 2019).

Metabolic changes are linked with tumorigenesis, which is epitomized by cancers deriving from mutations in TCA cycle genes. We found that cancer cells devoid of SDH activity enact further metabolic changes by suppressing CI, which is critical for optimal tumor growth and drives alternative aspartate synthesis pathways through MPC, PC, RCQ, and GOT1, suggesting that these pathways could be potential targets for SDH-mutant cancers. Interestingly, we find that CI inhibition promotes aspartate synthesis in SDH-deficient cells by driving PC and RCQ activities, however neither path directly consumes mitochondrial NADH for its function, making understanding of the mechanistic connection between mitochondrial NAD+/NADH and the activation of those pathways an important goal for future study.

Chapter 5. Complex I Activity Exacerbates Proliferation and Tumor Growth in SDH-mutant Renal Cell Carcinoma Cells

Note: *This chapter is adapted from the manuscript published in eLife.*

5.1 Introduction

Due to the rarity of SDH-null tumors, physiologically relevant cell lines and mouse models are very limited. A potential caveat of generalizing these effects to SDH-mutant cancers is that SDH wild type parental cell lines may not recapitulate the intrinsic metabolic features of naturally arising SDH-mutant cancer cells. In Chapter 3, I introduced UOK269 cells, an SDHB-null renal cell carcinoma line characterized by the pathogenic $SDHB^{R46Q}$ mutation. This mutation alters an L(I)YR motif, leading to poor Fe-S cluster delivery to SDHB, causing ablation of SDH activity. This tumor demonstrated hallmark characteristics of oncocytic SDH-deficient cancers including elevated aerobic glycolysis, high succinate levels, activated HIF1α, a global DNA CpG Island methylator phenotype, and reliance on glutaminolysis for TCA anaplerosis (Saxena et al., 2015). We obtained WT UOK269 cells, added back SDHB cDNA to them and found that WT UOK269 cells can fully capitalize on exogenous electron acceptors like pyruvate to restore their proliferation rates to the same level as when they're supplied with supraphysiological levels of aspartate. This led to the discovery that SDHB-null cells progressively lose complex I activity. In this chapter, we find that complex I activity and expression is gradually regained in SDHB UOK269 cells and that reactivating complex I activity in WT UOK269 cells exacerbates aspartate production, cell proliferation and tumor growth.

5.2 Contributions

Experiments in this chapter were conducted by M.LH. and L.B.S., with assistance from A-L.B.G.V. LC-MS experiments were facilitated by Brian Milless and the Fred Hutch Proteomics and Metabolomics Shared Resource.

5.3 Results

Complex I activity is deleterious to SDH-mutant cancer cell proliferation and tumor growth

We began by measuring CI activity of the SDH-null UOK269 cells and found that, similar to LP SDHB KO 143B cells, UOK269 cells had substantially decreased CI activity compared to WT 143B cells (Figure 5.1A). We next investigated the metabolic state of late passage (LP) SDHB restored UOK269 cells. We first conducted stable isotope labeling metabolomics from U-^{13}C glucose and U-^{13}C glutamine to measure carbon contributions to aspartate in WT and LP SDHB UOK269 cells. Consistent with the metabolic phenotypes observed in 143B cells, aspartate was predominantly labeled M+3 from U-^{13}C glucose and U-^{13}C glutamine in WT UOK269 cells. SDHB restoration was associated with a loss of glucose-derived aspartate and a restoration of oxidative TCA cycle derived M+4 aspartate from glutamine (Figures 5.1B, 5.1C).

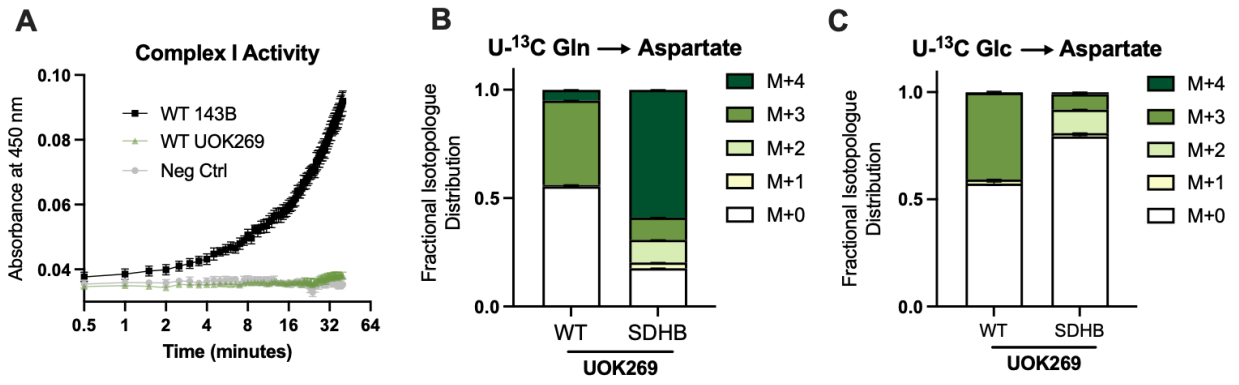

Figure 5.1. Characterization of WT and SDHB UOK269 cells. A) Complex I activity assay of extracts from WT 143Bs and WT UOK269 cells (n=3). **B)** Fractional isotopologue distribution of aspartate measured by LCMS metabolomics of WT or SDHB UOK269 cells cultured in glutamine free DMEM with 1 mM pyruvate supplemented with 4 mM U-^{13}C glutamine (Gln) for 6 hours (n=3). **C)** Fractional isotopologue distribution of aspartate measured by LCMS metabolomics of WT or SDHB UOK269 cells cultured in glucose/pyruvate-free DMEM with 25 mM U-^{13}C glucose (Glc) and 1 mM AKB for 6 hours (n=3). Data are plotted as means ± standard deviation (SD) and compared with an unpaired two-tailed student's t-test. $p<0.05$*, $p<0.01$**, $p<0.001$***, $p<0.0001$****

Consistent with their low CI activity, WT UOK269 cells had minimal NDUFA8 protein expression compared to 143B cells, but interestingly LP SDHB UOK269 cells had restored their NDUFA8 expression (Figure 5.2A). Correspondingly, LP SDHB UOK269 cells also had substantially increased mitochondrial oxygen consumption and CI activity compared to their SDH-deficient WT counterparts (Figure 5.2B, 5.2C). These results therefore indicate that the adaptations in CI status are reversible to achieve concordant activity with that of SDH.

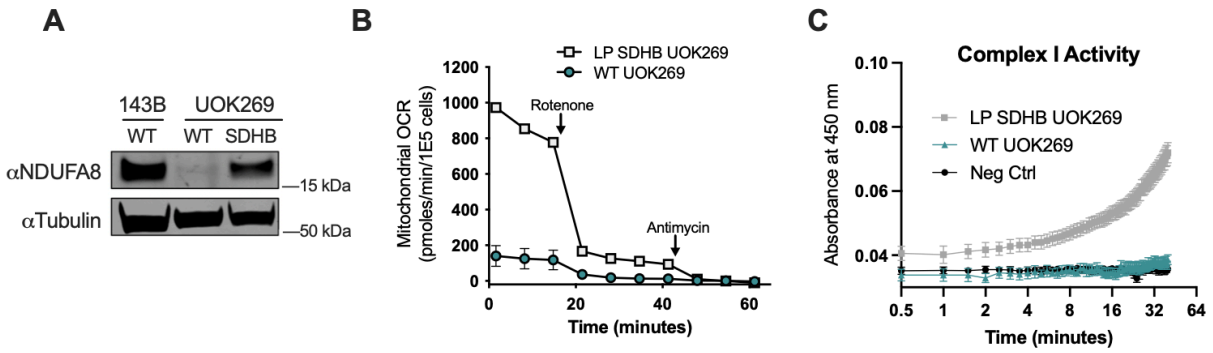

Figure 5.2. Complex I activity returns in adapted SDHB AB UOK269 cells. A) Western blot for NDUFA8 and tubulin from WT 143B, WT UOK269, and late-passage (LP) SDHB UOK269 cells. Tubulin is used as a loading control. **B)** Mitochondrial oxygen consumption rate of WT UOK269 cells compared to LP SDHB UOK269 cells with indicated injections of 100 nM rotenone and 10 μM antimycin (n=3). **C)** Complex I activity assay of WT UOK269 and LP SDHB UOK269 cells (n=3).

We next hypothesized that CI loss was critical for UOK269 cells by enabling aspartate production and cell proliferation, and that restoring CI activity would therefore be deleterious. Mammalian CI activity is dependent on the expression of >50 genes encoding core subunits and assembly factors, so increasing CI activity by traditional gene overexpression is not feasible. Instead, we expressed a doxycycline (DOX) inducible construct of the *Saccharomyces Cerevisiae* NDI1, a rotenone-insensitive CI analog that can restore NADH oxidation and ETC activity in mammalian cells when CI is impaired (Figure 5.3A) (Seo et al., 1998; Wheaton et al., 2014). Since DOX can act as a mitochondrial inhibitor at some doses, we also confirmed that DOX had no effect on proliferation rates or aspartate levels in the absence of the iNDI1 construct (Figure 5.3B, 5.3C). DOX treatment of WT UOK269 cells expressing the inducible (iNDI1) construct resulted in a substantial induction of mitochondrial oxygen consumption that was resistant to rotenone treatment, verifying NDI1 expression and confirming that decreased CI activity is a bottleneck for ETC function in UOK269 cells (Figure 5.3D). NDI1 expression

decreased the proliferation of WT UOK269 cells but had no effect on the proliferation of their SDHB-restored counterparts (Figure 5.3E). Metabolomics measurements also found that NDI1 expression lowered aspartate levels in WT UOK269 cells, but not in the SDHB-restored UOK269 cells (Figure 5.3F). Finally, we tested whether the deleterious effects of CI activity restoration on UOK269 cell proliferation were maintained in a physiological metabolic context by generating mouse xenograft tumors. Notably, DOX-mediated NDI expression also impaired the growth of tumors arising from iNDI1 UOK269 cells (Figure 5.3G). Together, these findings highlight that cells adapt to SDH loss by selecting for concordant CI loss, which is required to maximize aspartate production, cell proliferation rate, and tumorigenesis in SDH-null cancer cells (Figure 5.3H).

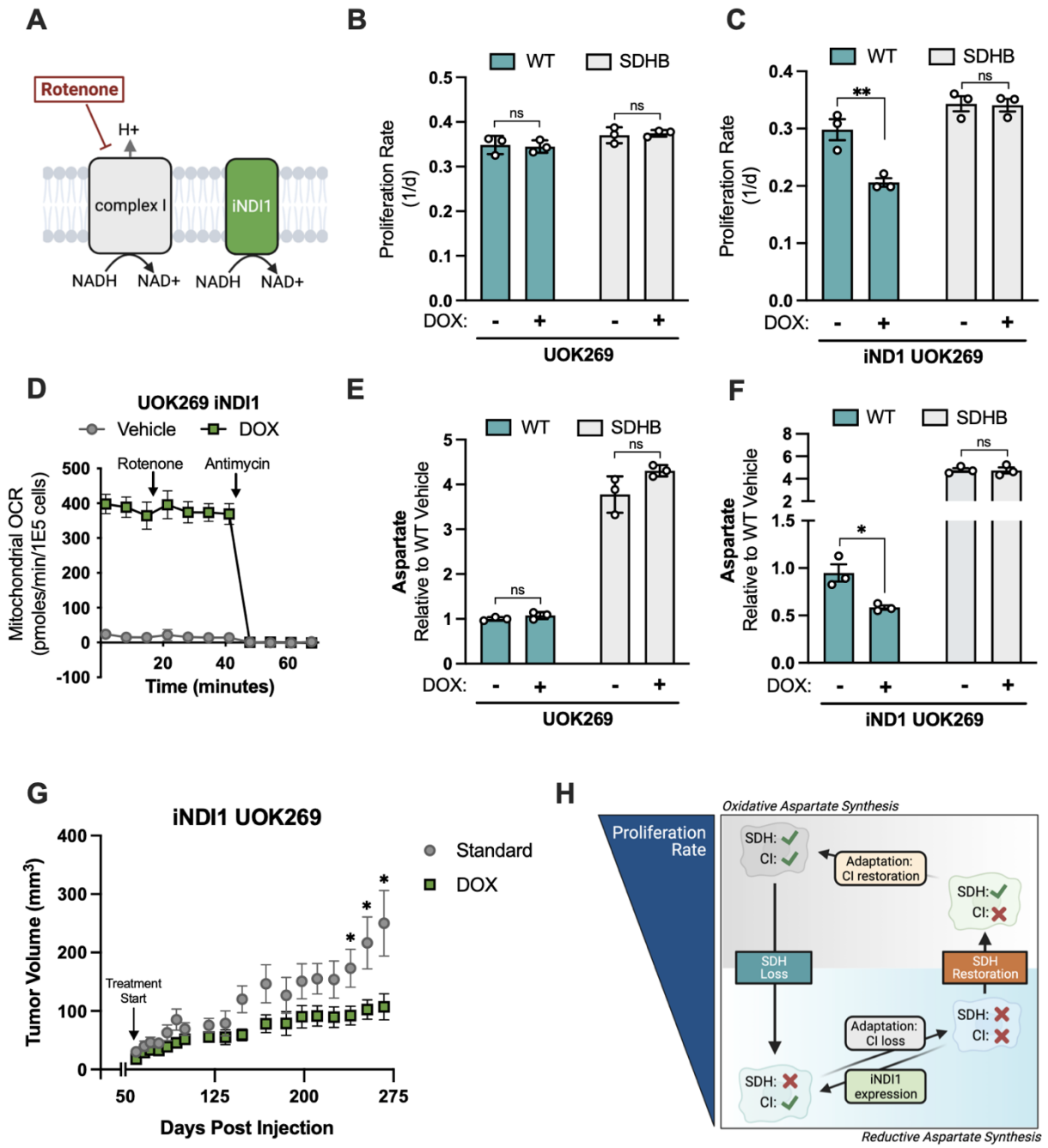

Figure 5.3. Complex I activity is deleterious in SDHB-mutant renal cell carcinoma cells. A) Diagram showing the Saccharomyces Cerevisiae single subunit complex 1 homolog, NDI1. **B)** Proliferation rate of WT UOK269 cells and SDHB AB UOK269 cells treated with vehicle (H_2O) or 1 µg/µL doxycycline in DMEM with 1 mM pyruvate (n=3). **C)** Proliferation rates of WT and SDHB UOK269 cells with expression of pInducer20-NDI1 (iNDI1) cultured in DMEM with 1 mM PYR and treated with vehicle (H_2O) or 1 µg/mL doxycycline (n=3). **D)** Mitochondrial oxygen consumption rates of pInducer20-NDI1 expressing UOK269 cells (UOK269 iNDI1) that were pre-treated with vehicle (H_2O) or 1 µg/mL doxycycline for 40 hours as indicated, followed by injections of 100 nM rotenone and 10 µM antimycin (n=3). **E)** Relative aspartate levels measured by LCMS metabolomics of WT UOK269 cells and SDHB AB UOK269 cells treated with

vehicle (H_2O) or 1 µg/µL doxycycline in DMEM with 1 mM pyruvate (n=3). **F)** Aspartate levels measured by LCMS metabolomics of WT and SDHB UOK269 cells with expression of pInducer20-NDI1 (iNDI1) cultured in DMEM with 1 mM PYR and treated with vehicle (H_2O) or 1 µg/mL doxycycline for 24 hours (n=3). **G)** Tumor volumes of iNDI1 UOK269 cells implanted into the flanks of immunocompromised SCID mice. After tumors became palpable, mice were fed either standard or doxycycline-containing chow (n=10 tumors per condition). **H)** Model demonstrating adaptations to SDH loss and SDH restoration, correlating to aspartate levels and proliferation rate. Data are plotted as means ± standard deviation (SD) except in D which are means ± standard error of the mean (SEM) and compared with an unpaired two-tailed student's t-test. $p<0.05$*, $p<0.01$**, $p<0.001$***, $p<0.0001$****

5.4 Conclusion and Discussion

In the chapter, we highlight a series of metabolic adaptations that are dependent on the status of SDH. While many metabolic regulatory enzymes frequently switch between the on and off states, SDH is constitutively and ubiquitously expressed in cells. Therefore, it makes sense that inactivating mutations in SDH and the cancers that arise from them are so rare. The functional benefit for a cancer cell to have SDH activity is the capability to synthesis aspartate which is upstream of protein, nucleotide, and amino acid synthesis. This requires a working complex I to recycle NADH to NAD+ and keep the TCA cycle (and aspartate synthesis route) flowing. Therefore, when SDH is lost, aspartate levels and proliferation rate declines because mitochondrial NADH levels decrease rapidly. Complex I is lost over time which increases mitochondrial NADH and alters the redox environment, promoting alternative aspartate synthesis via RCQ and PC. Re-establishing SDH reinstates canonical aspartate synthesis, but is dampened by the lack of NAD+ regeneration from complex I. Finally, complex I is restored to enable optimal proliferation in UOK269 cells. Intriguingly, inducible expression of an alternative complex I worsens cell proliferation and tumor growth of UOK269 cells. These results highlight a potential well-designed benefit for optimal proliferation in cancer cells.

Chapter 6. Summary and Future Directions

6.1 Big Picture Summary

Succinate dehydrogenase (SDH) was discovered as a tumor suppressor in pheochromocytomas in 2000, sparking investigation into mechanisms of tumorigenesis (Baysal et al., 2000). Since then, loss of function mutations in all four subunits of SDH as well as SDH assembly factors have been identified in a number of human cancers including pheochromocytomas, paragangliomas, renal cell carcinomas, gastrointestinal stromal tumors, neuroblastomas, pituitary adenomas, urinary bladder paragangliomas, hemangioblastomas, and possibly others (Aghamir et al., 2019; Amar et al., 2007; Astuti et al., 2004; Gill et al., 2014; Klein et al., 2008; Martucci et al., 2015; Miettinen & Lasota, 2014; Roh et al., 2019). In fact, the majority of these cancers are derived from neuroendocrine cells that play a role in sensing oxygen in the body (Spicer & Millhorn, 2003). For example, chromaffin cells, or pheochromocytes, found in the adrenal medulla, carotid bodies, bladder epithelium, and prostate are responsible for secreting catecholamines, such as epinephrine and norepinephrine in response to hypoxia (Nurse et al., 2018). Interestingly, altitude has been described as a phenotypic modifier in hereditary paragangliomas (Astrom et al., 2003; Saldana et al., 1973). More specifically, people with germline mutations in SDH components are predisposed to paragangliomas were more likely to have multiple tumors living at altitude than those of the same age living at sea-level (Astrom et al., 2003). Therefore, tumor penetrance is exacerbated at

higher altitudes. Researchers studying patients with hereditary paraganglioma postulated that the oxygen deficiency at higher altitudes increased the proliferation of actively dividing heterozygous $SDH^{-/+}$ cells, which possibly increased the likelihood of a second hit somatic mutation, driving cancer (Astrom et al., 2003).

Interestingly, von Hippel-Lindau (VHL) mutations are often observed in these cancers, either with or without an existing SDH mutation, highlighting another association between hypoxia, oxygen sensing, and SDH-driven cancers. VHL is commonly mutated in hemangioblastomas, clear-cell renal cell carcinoma, pancreatic neuroendocrine tumors, and pheochromocytomas (Linehan et al., 2009; Varshney et al., 2017). Molecular consequences of VHL loss include constitutive expression of hypoxia-inducible factors (HIFs), which contribute to cancer progression and metastasis. Stabilization of HIFs leads to transcriptional activation of genes that regulate glycolysis, cell migration and adhesion, and angiogenesis. Together, this information alludes to a strong connection between inactivating SDH mutations, a lack of oxygen utilization, and cancer development.

Although groups have identified that SDH-null cancer cells in culture require respiration deficiency to phenocopy an SDH-mutant tumor cell, no functional benefit of respiration loss had been identified (Lorendeau et al., 2017). This dissertation compares SDH-null cancer cells (arising from respiration-competent osteosarcoma cells) with a patient-derived SDHB-mutant renal cell carcinoma line. I found that the SDHB-mutant renal cell carcinoma line indeed displays a complete loss of respiration, while respiration is slowly and progressively lost over time after SDH is lost in the osteosarcoma cells. Indeed, SDH status (intact or null) corresponds to whether respiration is functional or not. These metabolic adaptations likely occur from selective pressure of the fastest

proliferators which is mediated by aspartate biosynthesis. When SDH is intact, active respiratory capacity is advantageous for the cells, but when SDH is mutated, respiration is deleterious, so the cells adapt to synthesize more aspartate, which is mediated by complex I loss and therefore inhibition of NADH turnover to promote alternative pathways.

6.2 Future Directions

We reveal that SDHB-mutant UOK269 renal cell carcinoma cells are metabolically similar to tissue non-specific late passage (LP) SDHB KO cells. We consider that SDH/CI-inhibited cells resemble an ‘acute’ state, where metabolism is immediately shifted temporarily, yet the intrinsic nature of the cell is unchanged. However, LP SDHB KO cells and WT UOK269 cells are categorized in a ‘chronic’ state, where the cells have selected for loss of complex I and adapted their metabolism to stimulate alternative aspartate synthesis and proliferation. We hypothesize that the mechanisms by which these cells regain proliferative ability differs between acute and chronic states. For example, the fraction of glutamine-derived aspartate in WT UOK269 cells (chronic) is much larger than in EP SDHB KO 143B cells treated with rotenone (acute) (Figures 4.1B, 5.1B). In addition, the fraction of M+3 aspartate from glucose also decreases in LP SDHB KO 143B cells when compared to EP SDHB KO cells treated with rotenone or metformin. These data suggest that aspartate acquisition pathways are changing over time as complex I is lost, which could provide more insight in optimal ways to target SDH-mutant tumors.

The cellular mechanisms of how complex I loss occurs in SDH-null cells, or how complex I loss is regained when SDH is returned are interesting avenues for future studies and will be important to understand oncogenic transformation of SDH-mutant cancer

cells. The lab is currently investigating the mechanisms of how complex I is progressively lost in respiration-intact cells and how complex I activity is regained after SDH re-establishment in WT UOK269 cells.

Another avenue for future research is to further investigate SDHB null tumor xenografts and develop autochthonous mouse models of SDHB null pheochromocytomas or renal cell carcinomas. An interesting observation from the iNDI1 UOK269 xenograft experiment (Figure 5.3G) was that mice that given DOX chow appeared healthier than the control mice towards the end of the experiment. Control mice were noticeably more lethargic and generally appeared sicker than the mice given DOX chow. Even though tumors in control group grew larger, they never surpassed 300 mm^3, leading to the hypothesis that respiration loss in SDHB-null tumors contributes to metastasis or other complications from tumor engraftment. In more long-term, aging related mouse models of SDHB null cancers, it would be interesting to see if impairments to complex I through chronic metformin treatment or mild hypoxia result in earlier formation of tumors.

6.3 Impacts

This work provides insight into how SDH-null tumors manifest and develop in humans despite a major metabolic roadblock in the central, amphibolic TCA cycle. One such impact is that perhaps people with germline mutations in SDH or with a family history of neuroendocrine tumors should not take metformin, the classic anti-diabetes drug that functions in part by suppressing complex I. Interestingly, among cohorts who have taken metformin, there are generally lower rates of cancer, highlighting the true paradoxical nature of SDH-null tumors. Much like high altitude, it's possible that chronic complex I

impairment could exacerbate the chances of the ‘second hit’ mutation, which would lead to tumor development. Additionally, we have discovered mechanisms by which SDH-null cancer cells overcome aspartate limitation once respiration deficiency has occurred. In addition, mitochondrial pyruvate carrier (MPC), which we showed impairs both forms of alternative aspartate synthesis through blocking both PC and GPT2 mediated AKG production for RCQ, could be an applicable avenue for a novel therapeutic target in SDH-mutant tumors.

References

Aghamir, S. M. K., Heshmat, R., Ebrahimi, M., Ketabchi, S. E., Parichehreh Dizaji, S., & Khatami, F. (2019). The Impact Of Succinate Dehydrogenase Gene (SDH) Mutations In Renal Cell Carcinoma (RCC): A Systematic Review. *OncoTargets and Therapy*, *12*, 7929–7940. https://doi.org/10.2147/OTT.S207460

Ahn, C. S., & Metallo, C. M. (2015). Mitochondria as biosynthetic factories for cancer proliferation. *Cancer & Metabolism*, *3*, 1. https://doi.org/10.1186/s40170-015-0128-2

Altea-Manzano, P., Vandekeere, A., Edwards-Hicks, J., Roldan, M., Abraham, E., Lleshi, X., Guerrieri, A. N., Berardi, D., Wills, J., Junior, J. M., Pantazi, A., Acosta, J. C., Sanchez-Martin, R. M., Fendt, S.-M., Martin-Hernandez, M., & Finch, A. J. (2022). Reversal of mitochondrial malate dehydrogenase 2 enables anaplerosis via redox rescue in respiration-deficient cells. *Molecular Cell*, *82*(23), 4537-4547.e7. https://doi.org/10.1016/j.molcel.2022.10.005

Amar, L., Baudin, E., Burnichon, N., Peyrard, S., Silvera, S., Bertherat, J., Bertagna, X., Schlumberger, M., Jeunemaitre, X., Gimenez-Roqueplo, A.-P., & Plouin, P.-F. (2007). Succinate dehydrogenase B gene mutations predict survival in patients with malignant pheochromocytomas or paragangliomas. *The Journal of Clinical Endocrinology and Metabolism*, *92*(10), 3822–3828. https://doi.org/10.1210/jc.2007-0709

Apiz Saab, J. J., Dzierozynski, L. N., Jonker, P. B., AminiTabrizi, R., Shah, H., Menjivar, R. E., Scott, A. J., Nwosu, Z. C., Zhu, Z., Chen, R. N., Oh, M., Sheehan, C., Wahl, D. R., Pasca di Magliano, M., Lyssiotis, C. A., Macleod, K. F., Weber, C. R., & Muir, A. (2023). Pancreatic tumors exhibit myeloid-driven amino acid stress and upregulate arginine biosynthesis. *ELife*, *12*, e81289. https://doi.org/10.7554/eLife.81289

Arnold, P. K., & Finley, L. W. S. (2022). Regulation and function of the mammalian tricarboxylic acid cycle. *Journal of Biological Chemistry*, *0*(0). https://doi.org/10.1016/j.jbc.2022.102838

Arnold, P. K., Jackson, B. T., Paras, K. I., Brunner, J. S., Hart, M. L., Newsom, O. J., Alibeckoff, S. P., Endress, J., Drill, E., Sullivan, L. B., & Finley, L. W. S. (2022). A non-canonical tricarboxylic acid cycle underlies cellular identity. *Nature*, 1–5. https://doi.org/10.1038/s41586-022-04475-w

Astrom, K., Cohen, J. E., Willett-Brozick, J. E., Aston, C. E., & Baysal, B. E. (2003). Altitude is a phenotypic modifier in hereditary paraganglioma type□1: Evidence for an oxygen-sensing defect. *Human Genetics*, *113*(3), 228–237. https://doi.org/10.1007/s00439-003-0969-6

Astuti, D., Latif, F., Dallol, A., Dahia, P. L. M., Douglas, F., George, E., Sköldberg, F., Husebye, E. S., Eng, C., & Maher, E. R. (2001). Gene Mutations in the Succinate Dehydrogenase Subunit SDHB Cause Susceptibility to Familial Pheochromocytoma and to Familial Paraganglioma. *The American Journal of Human Genetics*, *69*(1), 49–54. https://doi.org/10.1086/321282

Astuti, D., Morris, M., Krona, C., Abel, F., Gentle, D., Martinsson, T., Kogner, P., Neumann, H. P. H., Voutilainen, R., Eng, C., Rustin, P., Latif, F., & Maher, E. R. (2004). Investigation of the role of SDHB inactivation in sporadic phaeochromocytoma and neuroblastoma. *British Journal of Cancer*, *91*(10), 1835–1841. https://doi.org/10.1038/sj.bjc.6602202

Baccelli, I., Gareau, Y., Lehnertz, B., Gingras, S., Spinella, J.-F., Corneau, S., Mayotte, N., Girard, S., Frechette, M., Blouin-Chagnon, V., Leveillé, K., Boivin, I., MacRae, T., Krosl, J., Thiollier, C., Lavallée, V.-P., Kanshin, E., Bertomeu, T., Coulombe-Huntington, J., … Sauvageau, G. (2019). Mubritinib Targets the Electron Transport Chain Complex I and Reveals the Landscape of OXPHOS Dependency in Acute Myeloid Leukemia. *Cancer Cell*, *36*(1), 84-99.e8. https://doi.org/10.1016/j.ccell.2019.06.003

Badenhop, R. F., Jansen, J. C., Fagan, P. A., Lord, R. S. A., Wang, Z. G., Foster, W. J., & Schofield, P. R. (2004). The prevalence of SDHB, SDHC, and SDHD mutations in patients with head and neck paraganglioma and association of mutations with clinical features. *Journal of Medical Genetics*, *41*(7), e99–e99. https://doi.org/10.1136/jmg.2003.011551

Bardella, C., Pollard, P. J., & Tomlinson, I. (2011). SDH mutations in cancer. *Biochimica et Biophysica Acta (BBA) - Bioenergetics*, *1807*(11), 1432–1443. https://doi.org/10.1016/j.bbabio.2011.07.003

Baysal, B. E., Ferrell, R. E., Willett-Brozick, J. E., Lawrence, E. C., Myssiorek, D., Bosch, A., Mey, A. van der, Taschner, P. E. M., Rubinstein, W. S., Myers, E. N., Richard, C. W., Cornelisse, C. J., Devilee, P., & Devlin, B. (2000). Mutations in SDHD, a Mitochondrial Complex II Gene, in Hereditary Paraganglioma. *Science*, *287*(5454), 848–851. https://doi.org/10.1126/science.287.5454.848

Birsoy, K., Wang, T., Chen, W. W., Freinkman, E., Abu-Remaileh, M., & Sabatini, D. M. (2015). An Essential Role of the Mitochondrial Electron Transport Chain in Cell Proliferation Is to Enable Aspartate Synthesis. *Cell*, *162*(3), 540–551. https://doi.org/10.1016/j.cell.2015.07.016

Burnichon, N., Brière, J.-J., Libé, R., Vescovo, L., Rivière, J., Tissier, F., Jouanno, E., Jeunemaitre, X., Bénit, P., Tzagoloff, A., Rustin, P., Bertherat, J., Favier, J., & Gimenez-Roqueplo, A.-P. (2010). SDHA is a tumor suppressor gene causing paraganglioma. *Human Molecular Genetics*, *19*(15), 3011–3020. https://doi.org/10.1093/hmg/ddq206

Cantor, J. R., Abu-Remaileh, M., Kanarek, N., Freinkman, E., Gao, X., Louissaint, A., Lewis, C. A., & Sabatini, D. M. (2017). Physiologic Medium Rewires Cellular Metabolism and Reveals Uric Acid as an Endogenous Inhibitor of UMP Synthase. *Cell*, *169*(2), 258-272.e17. https://doi.org/10.1016/j.cell.2017.03.023

Cardaci, S., Zheng, L., MacKay, G., van den Broek, N. J. F., MacKenzie, E. D., Nixon, C., Stevenson, D., Tumanov, S., Bulusu, V., Kamphorst, J. J., Vazquez, A., Fleming, S., Schiavi, F., Kalna, G., Blyth, K., Strathdee, D., & Gottlieb, E. (2015). Pyruvate carboxylation enables growth of SDH-deficient cells by supporting aspartate biosynthesis. *Nature Cell Biology*, *17*(10), 1317–1326. https://doi.org/10.1038/ncb3233

Castro-Vega, L. J., Letouzé, E., Burnichon, N., Buffet, A., Disderot, P.-H., Khalifa, E., Loriot, C., Elarouci, N., Morin, A., Menara, M., Lepoutre-Lussey, C., Badoual, C., Sibony, M., Dousset, B., Libé, R., Zinzindohoue, F., Plouin, P. F., Bertherat, J., Amar, L., … Gimenez-Roqueplo, A.-P. (2015). Multi-omics analysis defines core genomic alterations in pheochromocytomas and paragangliomas. *Nature Communications*, *6*. https://doi.org/10.1038/ncomms7044

Ciccarese, F., & Ciminale, V. (2017). Escaping Death: Mitochondrial Redox Homeostasis in Cancer Cells. *Frontiers in Oncology*, *7*. https://doi.org/10.3389/fonc.2017.00117

Commisso, C., Davidson, S. M., Soydaner-Azeloglu, R. G., Parker, S. J., Kamphorst, J. J., Hackett, S., Grabocka, E., Nofal, M., Drebin, J. A., Thompson, C. B., Rabinowitz, J. D., Metallo, C. M., Vander Heiden, M. G., & Bar-Sagi, D. (2013). Macropinocytosis of protein is an amino acid supply route in Ras-transformed cells. *Nature*, *497*(7451), 633–637. https://doi.org/10.1038/nature12138

Cori, C. F. (1931). Mammalian carbohydrate metabolism. *Physiological Reviews*, *11*(2), 143–275. https://doi.org/10.1152/physrev.1931.11.2.143

Courtney, K. D., Bezwada, D., Mashimo, T., Pichumani, K., Vemireddy, V., Funk, A. M., Wimberly, J., McNeil, S. S., Kapur, P., Lotan, Y., Margulis, V., Cadeddu, J. A., Pedrosa, I., DeBerardinis, R. J., Malloy, C. R., Bachoo, R. M., & Maher, E. A. (2018). Isotope Tracing of Human Clear Cell Renal Cell Carcinomas Demonstrates Suppressed Glucose Oxidation In Vivo. *Cell Metabolism*, *28*(5), 793-800.e2. https://doi.org/10.1016/j.cmet.2018.07.020

Cracan, V., Titov, D. V., Shen, H., Grabarek, Z., & Mootha, V. K. (2017). A genetically encoded tool for manipulation of NADP+/NADPH in living cells. *Nature Chemical Biology*, *13*(10), 1088–1095. https://doi.org/10.1038/nchembio.2454

Crooks, D. R., Maio, N., Lang, M., Ricketts, C. J., Vocke, C. D., Gurram, S., Turan, S., Kim, Y.-Y., Cawthon, G. M., Sohelian, F., De Val, N., Pfeiffer, R. M., Jailwala, P.,

Tandon, M., Tran, B., Fan, T. W.-M., Lane, A. N., Ried, T., Wangsa, D., … Linehan, W. M. (2021). Mitochondrial DNA alterations underlie an irreversible shift to aerobic glycolysis in fumarate hydratase-deficient renal cancer. *Science Signaling*, *14*(664), eabc4436. https://doi.org/10.1126/scisignal.abc4436

Dang, C. V. (2007). The interplay between MYC and HIF in the Warburg effect. *Ernst Schering Foundation Symposium Proceedings*, *4*, 35–53. https://doi.org/10.1007/2789_2008_088

Diehl, F. F., Lewis, C. A., Fiske, B. P., & Vander Heiden, M. G. (2019). Cellular redox state constrains serine synthesis and nucleotide production to impact cell proliferation. *Nature Metabolism*, *1*(9), 861–867. https://doi.org/10.1038/s42255-019-0108-x

Dimauro, S., & Davidzon, G. (2005). Mitochondrial DNA and disease. *Annals of Medicine*, *37*(3), 222–232. https://doi.org/10.1080/07853890510007368

Eagle, H. (1955). Nutrition needs of mammalian cells in tissue culture. *Science (New York, N.Y.)*, *122*(3168), 501–514. https://doi.org/10.1126/science.122.3168.501

Egler, R. A., Ahuja, S. P., & Matloub, Y. (2016). L-asparaginase in the treatment of patients with acute lymphoblastic leukemia. *Journal of Pharmacology & Pharmacotherapeutics*, *7*(2), 62–71. https://doi.org/10.4103/0976-500X.184769

Eijkelenkamp, K., Osinga, T. E., Links, T. P., & van der Horst-Schrivers, A. N. A. (2020). Clinical implications of the oncometabolite succinate in SDHx-mutation carriers. *Clinical Genetics*, *97*(1), 39–53. https://doi.org/10.1111/cge.13553

Garcia-Bermudez, J., Badgley, M. A., Prasad, S., Baudrier, L., Liu, Y., La, K., Soula, M., Williams, R. T., Yamaguchi, N., Hwang, R. F., Taylor, L. J., de Stanchina, E., Rostandy, B., Alwaseem, H., Molina, H., Bar-Sagi, D., & Birsoy, K. (2022). Adaptive stimulation of macropinocytosis overcomes aspartate limitation in cancer cells under hypoxia. *Nature Metabolism*, *4*(6), 724–738. https://doi.org/10.1038/s42255-022-00583-z

Garcia-Bermudez, J., Baudrier, L., La, K., Zhu, X. G., Fidelin, J., Sviderskiy, V. O., Papagiannakopoulos, T., Molina, H., Snuderl, M., Lewis, C. A., Possemato, R. L., & Birsoy, K. (2018). Aspartate is a limiting metabolite for cancer cell proliferation under hypoxia and in tumours. *Nature Cell Biology*, *20*(7), Article 7. https://doi.org/10.1038/s41556-018-0118-z

Gaude, E., Schmidt, C., Gammage, P. A., Dugourd, A., Blacker, T., Chew, S. P., Saez-Rodriguez, J., O'Neill, J. S., Szabadkai, G., Minczuk, M., & Frezza, C. (2018). NADH Shuttling Couples Cytosolic Reductive Carboxylation of Glutamine with Glycolysis in Cells with Mitochondrial Dysfunction. *Molecular Cell*, *69*(4), 581-593.e7. https://doi.org/10.1016/j.molcel.2018.01.034

Gill, A. J., Toon, C. W., Clarkson, A., Sioson, L., Chou, A., Winship, I., Robinson, B. G., Benn, D. E., Clifton-Bligh, R. J., & Dwight, T. (2014). Succinate Dehydrogenase Deficiency Is Rare in Pituitary Adenomas. *The American Journal of Surgical Pathology*, *38*(4), 560–566. https://doi.org/10.1097/PAS.0000000000000149

Gorelick, A. N., Kim, M., Chatila, W. K., La, K., Hakimi, A. A., Berger, M. F., Taylor, B. S., Gammage, P. A., & Reznik, E. (2021). Respiratory complex and tissue lineage drive recurrent mutations in tumour mtDNA. *Nature Metabolism*, *3*(4), 558–570. https://doi.org/10.1038/s42255-021-00378-8

Gray, M. W. (2017). Lynn Margulis and the endosymbiont hypothesis: 50 years later. *Molecular Biology of the Cell*, *28*(10), 1285–1287. https://doi.org/10.1091/mbc.E16-07-0509

Gui, D. Y., Sullivan, L. B., Luengo, A., Hosios, A. M., Bush, L. N., Gitego, N., Davidson, S. M., Freinkman, E., Thomas, C. J., & Vander Heiden, M. G. (2016). Environment Dictates Dependence on Mitochondrial Complex I for NAD+ and Aspartate Production and Determines Cancer Cell Sensitivity to Metformin. *Cell Metabolism*, *24*(5), 716–727. https://doi.org/10.1016/j.cmet.2016.09.006

Hanahan, D., & Weinberg, R. A. (2011). Hallmarks of Cancer: The Next Generation. *Cell*, *144*(5), 646–674. https://doi.org/10.1016/j.cell.2011.02.013

Hao, H.-X., Khalimonchuk, O., Schraders, M., Dephoure, N., Bayley, J.-P., Kunst, H., Devilee, P., Cremers, C. W. R. J., Schiffman, J. D., Bentz, B. G., Gygi, S. P., Winge, D. R., Kremer, H., & Rutter, J. (2009). SDH5, a Gene Required for Flavination of Succinate Dehydrogenase, Is Mutated in Paraganglioma. *Science (New York, N.Y.)*, *325*(5944). https://doi.org/10.1126/science.1175689

Hardie, D. G. (2022). 100 years of the Warburg effect: A historical perspective. *Endocrine-Related Cancer*, *29*(12), T1–T13. https://doi.org/10.1530/ERC-22-0173

Hensley, C. T., Wasti, A. T., & DeBerardinis, R. J. (2013). Glutamine and cancer: Cell biology, physiology, and clinical opportunities. *The Journal of Clinical Investigation*, *123*(9), 3678–3684. https://doi.org/10.1172/JCI69600

Hoellerbauer, P., Kufeld, M., & Paddison, P. J. (2020). Efficient Multi-Allelic Genome Editing of Primary Cell Cultures via CRISPR-Cas9 Ribonucleoprotein Nucleofection. *Current Protocols in Stem Cell Biology*, *54*(1), e126. https://doi.org/10.1002/cpsc.126

Ilter, D., Drapela, S., Schild, T., Ward, N. P., Adhikari, E., Low, V., Asara, J., Oskarsson, T., Lau, E. K., DeNicola, G. M., McReynolds, M. R., & Gomes, A. P. (2023). NADK-mediated de novo NADP(H) synthesis is a metabolic adaptation essential

for breast cancer metastasis. *Redox Biology*, *61*, 102627. https://doi.org/10.1016/j.redox.2023.102627

Janku, F., LoRusso, P., Mansfield, A. S., Nanda, R., Spira, A., Wang, T., Melhem-Bertrandt, A., Sugg, J., & Ball, H. A. (2021). First-in-human evaluation of the novel mitochondrial complex I inhibitor ASP4132 for treatment of cancer. *Investigational New Drugs*, *39*(5), 1348–1356. https://doi.org/10.1007/s10637-021-01112-7

Jiang, J., Batra, S., & Zhang, J. (2021). Asparagine: A Metabolite to Be Targeted in Cancers. *Metabolites*, *11*(6), 402. https://doi.org/10.3390/metabo11060402

Jiang, L., Shestov, A. A., Swain, P., Yang, C., Parker, S. J., Wang, Q. A., Terada, L. S., Adams, N. D., McCabe, M. T., Pietrak, B., Schmidt, S., Metallo, C. M., Dranka, B. P., Schwartz, B., & DeBerardinis, R. J. (2016). Reductive carboxylation supports redox homeostasis during anchorage-independent growth. *Nature*, *532*(7598), 255–258. https://doi.org/10.1038/nature17393

King, M. P., & Attardi, G. (1989). Human cells lacking mtDNA: Repopulation with exogenous mitochondria by complementation. *Science*, *246*(4929), 500–503. https://doi.org/10.1126/science.2814477

Klein, R. D., Jin, L., Rumilla, K., Young, W. F., & Lloyd, R. V. (2008). Germline SDHB mutations are common in patients with apparently sporadic sympathetic paragangliomas. *Diagnostic Molecular Pathology: The American Journal of Surgical Pathology, Part B*, *17*(2), 94–100. https://doi.org/10.1097/PDM.0b013e318150d67c

Kluckova, K., & Tennant, D. A. (2018a). Metabolic implications of hypoxia and pseudohypoxia in pheochromocytoma and paraganglioma. *Cell and Tissue Research*, *372*(2), 367–378. https://doi.org/10.1007/s00441-018-2801-6

Kluckova, K., & Tennant, D. A. (2018b). Metabolic implications of hypoxia and pseudohypoxia in pheochromocytoma and paraganglioma. *Cell and Tissue Research*, *372*(2), 367–378. https://doi.org/10.1007/s00441-018-2801-6

Korotkevich, G., Sukhov, V., Budin, N., Shpak, B., Artyomov, M. N., & Sergushichev, A. (2021). *Fast gene set enrichment analysis* (p. 060012). bioRxiv. https://doi.org/10.1101/060012

Krall, A. S., Mullen, P. J., Surjono, F., Momcilovic, M., Schmid, E. W., Halbrook, C. J., Thambundit, A., Mittelman, S. D., Lyssiotis, C. A., Shackelford, D. B., Knott, S. R. V., & Christofk, H. R. (2021). Asparagine couples mitochondrial respiration to ATF4 activity and tumor growth. *Cell Metabolism*, *33*(5), 1013-1026.e6. https://doi.org/10.1016/j.cmet.2021.02.001

Krebs, H. A. (1972). Otto Heinrich Warburg, 1883-1970. *Biographical Memoirs of Fellows of the Royal Society. Royal Society (Great Britain)*, *18*, 629–699.

Kumari, S., Adewale, R., & Klubo-Gwiezdzinska, J. (2020). The Molecular Landscape of Hürthle Cell Thyroid Cancer Is Associated with Altered Mitochondrial Function-A Comprehensive Review. *Cells*, *9*(7), 1570. https://doi.org/10.3390/cells9071570

Lee, W. D., Mukha, D., Aizenshtein, E., & Shlomi, T. (2019). Spatial-fluxomics provides a subcellular-compartmentalized view of reductive glutamine metabolism in cancer cells. *Nature Communications*, *10*(1), Article 1. https://doi.org/10.1038/s41467-019-09352-1

Letouzé, E., Martinelli, C., Loriot, C., Burnichon, N., Abermil, N., Ottolenghi, C., Janin, M., Menara, M., Nguyen, A. T., Benit, P., Buffet, A., Marcaillou, C., Bertherat, J., Amar, L., Rustin, P., De Reyniès, A., Gimenez-Roqueplo, A.-P., & Favier, J. (2013). SDH Mutations Establish a Hypermethylator Phenotype in Paraganglioma. *Cancer Cell*, *23*(6), 739–752. https://doi.org/10.1016/j.ccr.2013.04.018

Liberti, M. V., & Locasale, J. W. (2016). The Warburg Effect: How Does it Benefit Cancer Cells? *Trends in Biochemical Sciences*, *41*(3), 211–218. https://doi.org/10.1016/j.tibs.2015.12.001

Linehan, W. M., & Ricketts, C. J. (2013). The Metabolic Basis of Kidney Cancer. *Seminars in Cancer Biology*, *23*(1), 46–55. https://doi.org/10.1016/j.semcancer.2012.06.002

Linehan, W. M., Rubin, J. S., & Bottaro, D. P. (2009). VHL Loss of Function and Its Impact on Oncogenic Signaling Networks in Clear Cell Renal Cell Carcinoma. *The International Journal of Biochemistry & Cell Biology*, *41*(4), 753–756. https://doi.org/10.1016/j.biocel.2008.09.024

Locasale, J. W., Grassian, A. R., Melman, T., Lyssiotis, C. A., Mattaini, K. R., Bass, A. J., Heffron, G., Metallo, C. M., Muranen, T., Sharfi, H., Sasaki, A. T., Anastasiou, D., Mullarky, E., Vokes, N. I., Sasaki, M., Beroukhim, R., Stephanopoulos, G., Ligon, A. H., Meyerson, M., … Vander Heiden, M. G. (2011). Phosphoglycerate dehydrogenase diverts glycolytic flux and contributes to oncogenesis. *Nature Genetics*, *43*(9), Article 9. https://doi.org/10.1038/ng.890

Lorendeau, D., Rinaldi, G., Boon, R., Spincemaille, P., Metzger, K., Jäger, C., Christen, S., Dong, X., Kuenen, S., Voordeckers, K., Verstreken, P., Cassiman, D., Vermeersch, P., Verfaillie, C., Hiller, K., & Fendt, S.-M. (2017). Dual loss of succinate dehydrogenase (SDH) and complex I activity is necessary to recapitulate the metabolic phenotype of SDH mutant tumors. *Metabolic Engineering*, *43*, 187–197. https://doi.org/10.1016/j.ymben.2016.11.005

Luengo, A., Li, Z., Gui, D. Y., Sullivan, L. B., Zagorulya, M., Do, B. T., Ferreira, R., Naamati, A., Ali, A., Lewis, C. A., Thomas, C. J., Spranger, S., Matheson, N. J., & Vander Heiden, M. G. (2021). Increased demand for NAD+ relative to ATP drives aerobic glycolysis. *Molecular Cell*, *81*(4), 691-707.e6. https://doi.org/10.1016/j.molcel.2020.12.012

Lussey-Lepoutre, C., Hollinshead, K. E. R., Ludwig, C., Menara, M., Morin, A., Castro-Vega, L.-J., Parker, S. J., Janin, M., Martinelli, C., Ottolenghi, C., Metallo, C., Gimenez-Roqueplo, A.-P., Favier, J., & Tennant, D. A. (2015). Loss of succinate dehydrogenase activity results in dependency on pyruvate carboxylation for cellular anabolism. *Nature Communications*, *6*(1), 1–9. https://doi.org/10.1038/ncomms9784

Maddocks, O. D. K., Athineos, D., Cheung, E. C., Lee, P., Zhang, T., van den Broek, N. J. F., Mackay, G. M., Labuschagne, C. F., Gay, D., Kruiswijk, F., Blagih, J., Vincent, D. F., Campbell, K. J., Ceteci, F., Sansom, O. J., Blyth, K., & Vousden, K. H. (2017). Modulating the therapeutic response of tumours to dietary serine and glycine starvation. *Nature*, *544*(7650), Article 7650. https://doi.org/10.1038/nature22056

Martínez-Reyes, I., Cardona, L. R., Kong, H., Vasan, K., McElroy, G. S., Werner, M., Kihshen, H., Reczek, C. R., Weinberg, S. E., Gao, P., Steinert, E. M., Piseaux, R., Budinger, G. R. S., & Chandel, N. S. (2020). Mitochondrial ubiquinol oxidation is necessary for tumour growth. *Nature*, *585*(7824), Article 7824. https://doi.org/10.1038/s41586-020-2475-6

Martucci, V. L., Lorenzo, Z. G., Weintraub, M., del Rivero, J., Ling, A., Merino, M., Siddiqui, M., Shuch, B., Vourganti, S., Linehan, W. M., Agarwal, P. K., & Pacak, K. (2015). Association of urinary bladder paragangliomas with germline mutations in the SDHB and VHL genes. *Urologic Oncology*, *33*(4), 167.e13-167.e20. https://doi.org/10.1016/j.urolonc.2014.11.017

Mayr, J. A., Meierhofer, D., Zimmermann, F., Feichtinger, R., Kögler, C., Ratschek, M., Schmeller, N., Sperl, W., & Kofler, B. (2008). Loss of Complex I due to Mitochondrial DNA Mutations in Renal Oncocytoma. *Clinical Cancer Research*, *14*(8), 2270–2275. https://doi.org/10.1158/1078-0432.CCR-07-4131

McBride, M.J., Hunter, C.J. and Rabinowitz J.D. (2023). *Glycine homeostasis requires reverse SHMT flux | bioRxiv*. (n.d.). Retrieved February 21, 2023, from https://www.biorxiv.org/content/10.1101/2023.01.11.523668v1

Metallo, C. M., Gameiro, P. A., Bell, E. L., Mattaini, K. R., Yang, J., Hiller, K., Jewell, C. M., Johnson, Z. R., Irvine, D. J., Guarente, L., Kelleher, J. K., Vander Heiden, M. G., Iliopoulos, O., & Stephanopoulos, G. (2011). Reductive glutamine metabolism by IDH1 mediates lipogenesis under hypoxia. *Nature*, *481*(7381), 380–384. https://doi.org/10.1038/nature10602

Miettinen, M., & Lasota, J. (2014). Succinate dehydrogenase deficient gastrointestinal stromal tumors (GISTs)—A review. *The International Journal of Biochemistry & Cell Biology*, *53*, 514–519. https://doi.org/10.1016/j.biocel.2014.05.033

Molina, J. R., Sun, Y., Protopopova, M., Gera, S., Bandi, M., Bristow, C., McAfoos, T., Morlacchi, P., Ackroyd, J., Agip, A.-N. A., Al-Atrash, G., Asara, J., Bardenhagen, J., Carrillo, C. C., Carroll, C., Chang, E., Ciurea, S., Cross, J. B., Czako, B., … Marszalek, J. R. (2018). An inhibitor of oxidative phosphorylation exploits cancer vulnerability. *Nature Medicine*, *24*(7), 1036–1046. https://doi.org/10.1038/s41591-018-0052-4

Momcilovic, M., Jones, A., Bailey, S. T., Waldmann, C. M., Li, R., Lee, J. T., Abdelhady, G., Gomez, A., Holloway, T., Schmid, E., Stout, D., Fishbein, M. C., Stiles, L., Dabir, D. V., Dubinett, S. M., Christofk, H., Shirihai, O., Koehler, C. M., Sadeghi, S., & Shackelford, D. B. (2019). In vivo imaging of mitochondrial membrane potential in non-small cell lung cancer. *Nature*, *575*(7782), 380–384. https://doi.org/10.1038/s41586-019-1715-0

Morrell, J. A., Orme, J., Butlin, R. J., Roche, T. E., Mayers, R. M., & Kilgour, E. (2003). AZD7545 is a selective inhibitor of pyruvate dehydrogenase kinase 2. *Biochemical Society Transactions*, *31*(Pt 6), 1168–1170. https://doi.org/10.1042/bst0311168

Muir, A., Danai, L. V., Gui, D. Y., Waingarten, C. Y., Lewis, C. A., & Vander Heiden, M. G. (2017). Environmental cystine drives glutamine anaplerosis and sensitizes cancer cells to glutaminase inhibition. *ELife*, *6*, e27713. https://doi.org/10.7554/eLife.27713

Mullen, A. R., Hu, Z., Shi, X., Jiang, L., Boroughs, L. K., Kovacs, Z., Boriack, R., Rakheja, D., Sullivan, L. B., Linehan, W. M., Chandel, N. S., & DeBerardinis, R. J. (2014). Oxidation of Alpha-Ketoglutarate Is Required for Reductive Carboxylation in Cancer Cells with Mitochondrial Defects. *Cell Reports*, *7*(5), 1679–1690. https://doi.org/10.1016/j.celrep.2014.04.037

Mullen, A. R., Wheaton, W. W., Jin, E. S., Chen, P.-H., Sullivan, L. B., Cheng, T., Yang, Y., Linehan, W. M., Chandel, N. S., & DeBerardinis, R. J. (2012). Reductive carboxylation supports growth in tumour cells with defective mitochondria. *Nature*, *481*(7381), 385–388. https://doi.org/10.1038/nature10642

Murphy, E., Ardehali, H., Balaban, R. S., DiLisa, F., Dorn, G. W., Kitsis, R. N., Otsu, K., Ping, P., Rizzuto, R., Sack, M. N., Wallace, D., & Youle, R. J. (2016). Mitochondrial Function, Biology, and Role in Disease. *Circulation Research*, *118*(12), 1960–1991. https://doi.org/10.1161/RES.0000000000000104

Niemann, S., & Müller, U. (2000). Mutations in SDHC cause autosomal dominant paraganglioma, type 3. *Nature Genetics*, *26*(3), 268–270. https://doi.org/10.1038/81551

Nurse, C. A., Salman, S., & Scott, A. L. (2018). Hypoxia-regulated catecholamine secretion in chromaffin cells. *Cell and Tissue Research*, *372*(2), 433–441. https://doi.org/10.1007/s00441-017-2703-z

Osellame, L. D., Blacker, T. S., & Duchen, M. R. (2012). Cellular and molecular mechanisms of mitochondrial function. *Best Practice & Research. Clinical Endocrinology & Metabolism*, *26*(6), 711–723. https://doi.org/10.1016/j.beem.2012.05.003

Pagliarini, D. J., Calvo, S. E., Chang, B., Sheth, S. A., Vafai, S. B., Ong, S.-E., Walford, G. A., Sugiana, C., Boneh, A., Chen, W. K., Hill, D. E., Vidal, M., Evans, J. G., Thorburn, D. R., Carr, S. A., & Mootha, V. K. (2008). A Mitochondrial Protein Compendium Elucidates Complex I Disease Biology. *Cell*, *134*(1), 112–123. https://doi.org/10.1016/j.cell.2008.06.016

Pavlova, N. N., Zhu, J., & Thompson, C. B. (2022). The hallmarks of cancer metabolism: Still emerging. *Cell Metabolism*, *34*(3), 355–377. https://doi.org/10.1016/j.cmet.2022.01.007

Potter, M., Newport, E., & Morten, K. J. (2016). The Warburg effect: 80 years on. *Biochemical Society Transactions*, *44*(5), 1499–1505. https://doi.org/10.1042/BST20160094

R Core Team (2020). —European Environment Agency. (n.d.). [Methodology Reference]. Retrieved March 9, 2022, from https://www.eea.europa.eu/data-and-maps/indicators/oxygen-consuming-substances-in-rivers/r-development-core-team-2006

Rabinovich, S., Adler, L., Yizhak, K., Sarver, A., Silberman, A., Agron, S., Stettner, N., Sun, Q., Brandis, A., Helbling, D., Korman, S., Itzkovitz, S., Dimmock, D., Ulitsky, I., Nagamani, S. C., Ruppin, E., & Erez, A. (2015). Diversion of aspartate in ASS1-deficient tumours fosters de novo pyrimidine synthesis. *Nature*, *527*(7578), 379–383. https://doi.org/10.1038/nature15529

Rath, S., Sharma, R., Gupta, R., Ast, T., Chan, C., Durham, T. J., Goodman, R. P., Grabarek, Z., Haas, M. E., Hung, W. H. W., Joshi, P. R., Jourdain, A. A., Kim, S. H., Kotrys, A. V., Lam, S. S., McCoy, J. G., Meisel, J. D., Miranda, M., Panda, A., … Mootha, V. K. (2021). MitoCarta3.0: An updated mitochondrial proteome now with sub-organelle localization and pathway annotations. *Nucleic Acids Research*, *49*(D1), D1541–D1547. https://doi.org/10.1093/nar/gkaa1011

Recouvreux, M. V., & Commisso, C. (2017). Macropinocytosis: A Metabolic Adaptation to Nutrient Stress in Cancer. *Frontiers in Endocrinology*, *8*. https://doi.org/10.3389/fendo.2017.00261

Reznik, E., Wang, Q., La, K., Schultz, N., & Sander, C. (2017). Mitochondrial respiratory gene expression is suppressed in many cancers. *ELife*, *6*, e21592. https://doi.org/10.7554/eLife.21592

Roh, T. H., Yim, H., Roh, J., Lee, K. B., Park, S. H., Jeong, S.-Y., Kim, S.-H., & Kim, J.-H. (2019). The loss of succinate dehydrogenase B expression is frequently identified in hemangioblastoma of the central nervous system. *Scientific Reports*, *9*(1), Article 1. https://doi.org/10.1038/s41598-019-42338-z

Rossiter, N. J., Huggler, K. S., Adelmann, C. H., Keys, H. R., Soens, R. W., Sabatini, D. M., & Cantor, J. R. (2021). CRISPR screens in physiologic medium reveal conditionally essential genes in human cells. *Cell Metabolism*, *33*(6), 1248-1263.e9. https://doi.org/10.1016/j.cmet.2021.02.005

Sa, K., L, L., Al, M., Dj, S., A, A., P, S., L, Z., Y, Z., Ja, J., Bs, N., B, C., A, R., G, T., Sb, K., Ng, S., Mt, H., Hj, W., D, L., Se, A., … Ca, L. (2022). Metabolic requirement for GOT2 in pancreatic cancer depends on environmental context. *ELife*, *11*. https://doi.org/10.7554/eLife.73245

Sagan, L. (1967). On the origin of mitosing cells. *Journal of Theoretical Biology*, *14*(3), 255–274. https://doi.org/10.1016/0022-5193(67)90079-3

Saldana, M. J., Salem, L. E., & Travezan, R. (1973). High altitude hypoxia and chemodectomas. *Human Pathology*, *4*(2), 251–263. https://doi.org/10.1016/S0046-8177(73)80012-7

Saxena, N., Maio, N., Crooks, D. R., Ricketts, C. J., Yang, Y., Wei, M.-H., Fan, T. W.-M., Lane, A. N., Sourbier, C., Singh, A., Killian, J. K., Meltzer, P. S., Vocke, C. D., Rouault, T. A., & Linehan, W. M. (2015). SDHB-Deficient Cancers: The Role of Mutations That Impair Iron Sulfur Cluster Delivery. *JNCI Journal of the National Cancer Institute*, *108*(1). https://doi.org/10.1093/jnci/djv287

Semenza, G. L. (2003). Targeting HIF-1 for cancer therapy. *Nature Reviews Cancer*, *3*(10), Article 10. https://doi.org/10.1038/nrc1187

Seo, B. B., Kitajima-Ihara, T., Chan, E. K. L., Scheffler, I. E., Matsuno-Yagi, A., & Yagi, T. (1998). Molecular remedy of complex I defects: Rotenone-insensitive internal NADH-quinone oxidoreductase of Saccharomyces cerevisiae mitochondria restores the NADH oxidase activity of complex I-deficient mammalian cells. *Proceedings of the National Academy of Sciences*, *95*(16), 9167–9171. https://doi.org/10.1073/pnas.95.16.9167

Sherratt, H. S. (1991). Mitochondria: Structure and function. *Revue Neurologique*, *147*(6–7), 417–430.

Shim, H., Dolde, C., Lewis, B. C., Wu, C. S., Dang, G., Jungmann, R. A., Dalla-Favera, R., & Dang, C. V. (1997). c-Myc transactivation of LDH-A: Implications for tumor metabolism and growth. *Proceedings of the National Academy of Sciences of the United States of America*, *94*(13), 6658–6663. https://doi.org/10.1073/pnas.94.13.6658

Simonnet, H., Demont, J., Pfeiffer, K., Guenaneche, L., Bouvier, R., Brandt, U., Schägger, H., & Godinot, C. (2003). Mitochondrial complex I is deficient in renal oncocytomas. *Carcinogenesis*, *24*(9), 1461–1466. https://doi.org/10.1093/carcin/bgg109

Spicer, Z., & Millhorn, D. E. (2003). Oxygen sensing in neuroendocrine cells and other cell types: Pheochromocytoma (PC12) cells as an experimental model. *Endocrine Pathology*, *14*(4), 277–291. https://doi.org/10.1385/EP:14:4:277

Stine, Z. E., Walton, Z. E., Altman, B. J., Hsieh, A. L., & Dang, C. V. (2015). MYC, Metabolism, and Cancer. *Cancer Discovery*, *5*(10), 1024–1039. https://doi.org/10.1158/2159-8290.CD-15-0507

Subramanian, A., Tamayo, P., Mootha, V. K., Mukherjee, S., Ebert, B. L., Gillette, M. A., Paulovich, A., Pomeroy, S. L., Golub, T. R., Lander, E. S., & Mesirov, J. P. (2005). Gene set enrichment analysis: A knowledge-based approach for interpreting genome-wide expression profiles. *Proceedings of the National Academy of Sciences*, *102*(43), 15545–15550. https://doi.org/10.1073/pnas.0506580102

Sullivan, L. B., Gui, D. Y., Hosios, A. M., Bush, L. N., Freinkman, E., & Vander Heiden, M. G. (2015). Supporting Aspartate Biosynthesis Is an Essential Function of Respiration in Proliferating Cells. *Cell*, *162*(3), 552–563. https://doi.org/10.1016/j.cell.2015.07.017

Sullivan, L. B., Gui, D. Y., & Vander Heiden, M. G. (2016). Altered metabolite levels in cancer: Implications for tumour biology and cancer therapy. *Nature Reviews. Cancer*, *16*(11), 680–693. https://doi.org/10.1038/nrc.2016.85

Sullivan, L. B., Luengo, A., Danai, L. V., Bush, L. N., Diehl, F. F., Hosios, A. M., Lau, A. N., Elmiligy, S., Malstrom, S., Lewis, C. A., & Vander Heiden, M. G. (2018). Aspartate is an endogenous metabolic limitation for tumour growth. *Nature Cell Biology*, *20*(7), 782–788. https://doi.org/10.1038/s41556-018-0125-0

Sullivan, M. R., Mattaini, K. R., Dennstedt, E. A., Nguyen, A. A., Sivanand, S., Reilly, M. F., Meeth, K., Muir, A., Darnell, A. M., Bosenberg, M. W., Lewis, C. A., & Vander Heiden, M. G. (2019). Increased Serine Synthesis Provides an Advantage for

Tumors Arising in Tissues Where Serine Levels Are Limiting. *Cell Metabolism*, *29*(6), 1410-1421.e4. https://doi.org/10.1016/j.cmet.2019.02.015

Titov, D. V., Cracan, V., Goodman, R. P., Peng, J., Grabarek, Z., & Mootha, V. K. (2016). Complementation of mitochondrial electron transport chain by manipulation of the NAD+/NADH ratio. *Science (New York, N.Y.)*, *352*(6282), 231–235. https://doi.org/10.1126/science.aad4017

To, T.-L., Cuadros, A. M., Shah, H., Hung, W. H. W., Li, Y., Kim, S. H., Rubin, D. H. F., Boe, R. H., Rath, S., Eaton, J. K., Piccioni, F., Goodale, A., Kalani, Z., Doench, J. G., Root, D. E., Schreiber, S. L., Vafai, S. B., & Mootha, V. K. (2019). A Compendium of Genetic Modifiers of Mitochondrial Dysfunction Reveals Intra-organelle Buffering. *Cell*, *179*(5), 1222-1238.e17. https://doi.org/10.1016/j.cell.2019.10.032

Tomlinson, I. P. M., Alam, N. A., Rowan, A. J., Barclay, E., Jaeger, E. E. M., Kelsell, D., Leigh, I., Gorman, P., Lamlum, H., Rahman, S., Roylance, R. R., Olpin, S., Bevan, S., Barker, K., Hearle, N., Houlston, R. S., Kiuru, M., Lehtonen, R., Karhu, A., … Multiple Leiomyoma Consortium. (2002). Germline mutations in FH predispose to dominantly inherited uterine fibroids, skin leiomyomata and papillary renal cell cancer. *Nature Genetics*, *30*(4), 406–410. https://doi.org/10.1038/ng849

Vander Heiden, M. G., & DeBerardinis, R. J. (2017). Understanding the Intersections between Metabolism and Cancer Biology. *Cell*, *168*(4), 657–669. https://doi.org/10.1016/j.cell.2016.12.039

Varshney, N., Kebede, A. A., Owusu-Dapaah, H., Lather, J., Kaushik, M., & Bhullar, J. S. (2017). A Review of Von Hippel-Lindau Syndrome. *Journal of Kidney Cancer and VHL*, *4*(3), 20–29. https://doi.org/10.15586/jkcvhl.2017.88

Warburg, O. (1925a). Iron, the Oxygen-Carrier of Respiration-Ferment. *Science*, *61*(1588), 575–582. https://doi.org/10.1126/science.61.1588.575

Warburg, O. (1925b). The Metabolism of Carcinoma Cells. *The Journal of Cancer Research*, *9*(1), 148–163. https://doi.org/10.1158/jcr.1925.148

Warburg, O. (1928). The Chemical Constitution of Respiration Ferment. *Science*, *68*(1767), 437–443. https://doi.org/10.1126/science.68.1767.437

Wei, P., Bott, A. J., Cluntun, A. A., Morgan, J. T., Cunningham, C. N., Schell, J. C., Ouyang, Y., Ficarro, S. B., Marto, J. A., Danial, N. N., DeBerardinis, R. J., & Rutter, J. (2022). Mitochondrial pyruvate supports lymphoma proliferation by fueling a glutamate pyruvate transaminase 2–dependent glutaminolysis pathway. *Science Advances*, *8*(39), eabq0117. https://doi.org/10.1126/sciadv.abq0117

Weinberg, F., Hamanaka, R., Wheaton, W. W., Weinberg, S., Joseph, J., Lopez, M., Kalyanaraman, B., Mutlu, G. M., Budinger, G. R. S., & Chandel, N. S. (2010). Mitochondrial metabolism and ROS generation are essential for Kras-mediated tumorigenicity. *Proceedings of the National Academy of Sciences*, *107*(19), 8788–8793. https://doi.org/10.1073/pnas.1003428107

Weinhouse, S. (1956). On Respiratory Impairment in Cancer Cells. *Science*, *124*(3215), 267–269. https://doi.org/10.1126/science.124.3215.267

Wheaton, W. W., Weinberg, S. E., Hamanaka, R. B., Soberanes, S., Sullivan, L. B., Anso, E., Glasauer, A., Dufour, E., Mutlu, G. M., Budigner, G. S., & Chandel, N. S. (2014). Metformin inhibits mitochondrial complex I of cancer cells to reduce tumorigenesis. *ELife*, *3*, e02242. https://doi.org/10.7554/eLife.02242

Williamson, D. H., Lund, P., & Krebs, H. A. (1967). The redox state of free nicotinamide-adenine dinucleotide in the cytoplasm and mitochondria of rat liver. *Biochemical Journal*, *103*(2), 514–527.

Wise, D. R., DeBerardinis, R. J., Mancuso, A., Sayed, N., Zhang, X.-Y., Pfeiffer, H. K., Nissim, I., Daikhin, E., Yudkoff, M., McMahon, S. B., & Thompson, C. B. (2008). Myc regulates a transcriptional program that stimulates mitochondrial glutaminolysis and leads to glutamine addiction. *Proceedings of the National Academy of Sciences of the United States of America*, *105*(48), 18782–18787. https://doi.org/10.1073/pnas.0810199105

Wise, D. R., Ward, P. S., Shay, J. E. S., Cross, J. R., Gruber, J. J., Sachdeva, U. M., Platt, J. M., DeMatteo, R. G., Simon, M. C., & Thompson, C. B. (2011). Hypoxia promotes isocitrate dehydrogenase-dependent carboxylation of α-ketoglutarate to citrate to support cell growth and viability. *Proceedings of the National Academy of Sciences of the United States of America*, *108*(49), 19611–19616. https://doi.org/10.1073/pnas.1117773108

Yancopoulos, G. D., Nisen, P. D., Tesfaye, A., Kohl, N. E., Goldfarb, M. P., & Alt, F. W. (1985). N-myc can cooperate with ras to transform normal cells in culture. *Proceedings of the National Academy of Sciences of the United States of America*, *82*(16), 5455–5459. https://doi.org/10.1073/pnas.82.16.5455

Yang, M., & Vousden, K. H. (2016). Serine and one-carbon metabolism in cancer. *Nature Reviews Cancer*, *16*(10), Article 10. https://doi.org/10.1038/nrc.2016.81

Yap, T. A., Daver, N., Mahendra, M., Zhang, J., Kamiya-Matsuoka, C., Meric-Bernstam, F., Kantarjian, H. M., Ravandi, F., Collins, M. E., Francesco, M. E. D., Dumbrava, E. E., Fu, S., Gao, S., Gay, J. P., Gera, S., Han, J., Hong, D. S., Jabbour, E. J., Ju, Z., … Konopleva, M. (2023). Complex I inhibitor of oxidative phosphorylation in advanced solid tumors and acute myeloid leukemia: Phase I trials. *Nature Medicine*, *29*(1), Article 1. https://doi.org/10.1038/s41591-022-02103-8

Yap, T. A., Rodon Ahnert, J., Piha-Paul, S. A., Fu, S., Janku, F., Karp, D. D., Naing, A., Ileana Dumbrava, E. E., Pant, S., Subbiah, V., Tsimberidou, A. M., Hong, D. S., Rose, K. M., Xu, Q., Vellano, C. P., Mahendra, M., Jones, P., Di Francesco, M. E., Marszalek, J. R., & Meric-Bernstam, F. (2019). Phase I trial of IACS-010759 (IACS), a potent, selective inhibitor of complex I of the mitochondrial electron transport chain, in patients (pts) with advanced solid tumors. *Journal of Clinical Oncology*, *37*(15_suppl), 3014–3014. https://doi.org/10.1200/JCO.2019.37.15_suppl.3014

Zhao, X., & Sandelin, A. (2012). GMD: Measuring the distance between histograms with applications on high-throughput sequencing reads. *Bioinformatics (Oxford, England)*, *28*(8), 1164–1165. https://doi.org/10.1093/bioinformatics/bts087

Zimorski, V., Mentel, M., Tielens, A. G. M., & Martin, W. F. (2019). Energy metabolism in anaerobic eukaryotes and Earth's late oxygenation. *Free Radical Biology & Medicine*, *140*, 279–294. https://doi.org/10.1016/j.freeradbiomed.2019.03.030